STATE ESTIMATION AND TRANSIENT STABILITY ANALYSIS IN POWER SYSTEMS USING ARTIFICIAL NEURAL NETWORKS

by

Mahta Boozari

A THESIS SUBMITTED IN PARTIAL FULFILLMENT
OF THE REQUIREMENTS FOR THE DEGREE OF
MASTER OF APPLIED SCIENCE
in the School
of
Engineering Science

SIMON FRASER UNIVERSITY

Fall 2004

APPROVAL

Name: Mahta Boozari

Degree: Master of Applied Science

Title of Thesis: State estimation and transient stability analysis in power systems using artificial neural networks

Examining Committee: Dr. Glenn H. Chapman, Chair
Professor, School of Engineering Science
Simon Fraser University

Dr. Mehrdad Saif, Senior Supervisor
Professor, School of Engineering Science
Simon Fraser University

Dr. Andrew H. Rawicz, Supervisor
Professor, School of Engineering Science
Simon Fraser University

Dr. John D. Jones, Examiner
Associate Professor, School of Engineering Science
Simon Fraser University

Date Approved: December 7th, 2004

SIMON FRASER UNIVERSITY

PARTIAL COPYRIGHT LICENCE

Abstract

Power system state estimation and security assessment have recently become two major issues in the operation of power systems due to the increasing stress on power system networks.

Utility operators must be properly informed of the operating condition or state of the power system in order to achieve a more secure and economical operation of today's complicated power systems. The state of a power system is described by a collection of voltage vectors for a given network topology and parameters. In this work, we applied Artificial Neural Networks (ANN) to estimate the state of a power system. State filtering and forecasting techniques were used to build Time Delay Neural Network (TDNN) and Functional Link Network (FLN) to capture the dynamic of a power system.

Security assessment is the evaluation of a power system's ability to withstand disturbances while maintaining the quality of service. Many different techniques have been proposed for stability analysis in power systems. We focused on using neural networks as a fast and accurate alternative to security assessment. We developed an ANN-based tool to identify stable and unstable conditions of a power system after fault clearing. The hybrid method employing neural networks was used to successfully evaluate the Transient Energy Function (TEF) as a security index.

Dedication

To my dear parents.

Acknowledgements

I am deeply indebted to my supervisor, Dr. Saif, whose help, suggestions, and guidance made this work possible. Thank you for all your feedbacks and support through my studies at Simon Fraser University.

I would like to thank my defense committee members, Glenn Chapman, Andrew Rawicz, and specially John Jones for taking the time to review my work. Also my special thanks to Susan Stevenson for her valuable comments on editing my thesis.

My sincere thanks goes to all my friends at Simon Fraser University specially Maryam Samiei for always being there for me.

Finally, I extend my thanks to my beloved family, my parents, my sister, and my husband for their enduring love and support.

Table of Contents

List of Figures

List of Tables

Table of Acronyms

AGC:	Automatic Generation Control
ANN:	Artificial Neural Network
BPN:	Back Propagation Network
COI:	Center Of Inertia
CPN:	Counter Propagation Network
DSA:	Dynamic Security Assessment
EMS:	Energy Management System
EKF:	Extended Kalman Filter
FLN:	Functional Link Network
GPE:	Generalized Potential Energy
KE:	Kinetic Energy
LMS:	Least Mean Square
NN:	Neural Network
PE:	Potential Energy
PEBS:	Potential Energy Boundary Surface
PSS:	Power System Stabilizer
PST:	Power System Toolbox
SCADA:	Supervisory Control And Data Acquisition
TDNN:	Time Delay Neural Network
TEF:	Transient Energy Function
UEP:	Unstable Equilibrium Point

Chapter 1

Introduction

1.1 State Estimation

State Estimation is becoming increasingly important in modern energy management of power systems. Especially, with world-wide deregulation of the power industry, power system state estimation has gained an even greater importance as a real-time monitoring tool. In regard to new possibilities associated with open access and the operation of transmission networks, the patterns of power flow in a deregulated power system have become less predictable compared to the integrated systems of the past. In order to achieve a more secure and economic operation of such a complicated system, it is vital for utility operators to be properly informed of the operating condition or state of the power system.

The state of the power system is described by a collection of voltage vectors for a given network topology and parameters. The set of measurements used for state estimation are collected through the Supervisory Control And Data Acquisition (SCADA) system. To gain more time and accurate information in making control decisions such

as economic dispatch, stability assessment, and other related functions [22], the system operator inputs the previous estimate of the system state and measurements transmitted through SCADA into the power system state estimator.

This estimation process can be carried out through two functions that include state forecasting and state filtering. State forecasting uses the past information while state filtering determines the optimal estimate by considering all available measurements and predicted states. Several algorithms have been proposed to achieve this estimation function. The most commonly used method for state estimation in power systems has been the Extended Kalman Filter (EKF) [30, 4, 7, 5]. In this method, when the system is operating normally, the EKF scheme provides an optimal state estimate.

Most of the Extended Kalman Filter equations seen in the literature are divided into forecasting and filtering steps, formulated as follows :

- The State Forecasting consists of a dynamic model using a state transition equation of the form [8]

$$X(k+1) = F(k)X(k) + G(k) + w(k); \qquad w \sim N(0, Q), \tag{1.1}$$

  where $X(k)$ is the state vector, $F(k)$ is the dynamic model parameter matrix, $G(k)$ is the control vector of the system, and $w(k)$ is white noise with normal probability distribution and covariance matrix, Q.

- The State Filtering consists of the measurement model of the form

$$Z(k) = h(X(k)) + v(k); \qquad v \sim N(0, R), \tag{1.2}$$

  where $Z(k)$ is the measurement vector, $h(.)$ is the nonlinear measurement function and $v(k)$ is the measurement noise vector with normal probability distribution and covariance matrix, R. With $\hat{X}$ being the estimate of state vector and

$\tilde{X}(k)$ being the predicted value, Extended Kalman Filter (EKF) provides the minimum variance estimate of the state at time sample k as

$$\hat{X}(k) = \tilde{X}(k) + K(k)[Z(k) - h(\tilde{X}(k))], \tag{1.3}$$

With the predicted state vector obtained from Equation 1.1

$$\tilde{X}(k+1) = F(k)\hat{X}(k) + G(k), \tag{1.4}$$

where

$$\begin{aligned} K(k) &= P_0(k)H^T(k)M^{-1}(k), \\ M(k) &= [H(k)P_0(k)H^T(k) + R(k)], \\ R(k) &= W^{-1}(k), \\ P_0(k+1) &= F(k)P_+(k)F^T(k) + Q(k), \\ P_+(k) &= [1 - K(k)H(k)]P_0(k)[I - K(k)H(k)]^T + K(k)R(k)K^T(k). \end{aligned} \tag{1.5}$$

Note that $P_+$is the covariance matrix of error, $e_+ = \hat{X} - X$ and H is the Jacobian matrix of h ($H = \frac{\partial h}{\partial X}$).

All the approaches based on the above method have a common difficulty which is using the diagonal transition matrix, F. Using diagonal transition is physically unacceptable because the time evolution of the voltages of topologically close nodes is strongly related and dependent upon nodal power injections [33].

Two other major problems specific to the EKF method are that EKF is computationally very demanding specially combined with the multidimensional aspects of real-world power systems [24] and that once the system encounters large load changes, the performance is significantly affected due to linearization of nonlinear equations.

To overcome the dimensionality problem, the hierarchical state estimation method was proposed. "In the hierarchical model, the overall physical system is decomposed

into subsystems. "Dynamic Hierarchical State Estimation" is used for each subsystem independently and then the various estimations are coordinated on a higher level" [34].

To address the problem of sudden load changes, the nonlinearities of measurement functions were taken into account, but the computational burden became significant [25]. Because of their fast response and efficient learning, neural networks have become a suitable candidate in the study of state estimation. Neural networks can achieve high computational speed by employing a massive number of simple processing elements arranged in parallel with a high degree of connectivity between elements.

This thesis project applies a dynamic neural network model to solve the state estimation problem using the two estimation steps explained above.

Most real-world problems of power systems are time-varying in nature. Hence, dynamic neural networks should be used for such time varying systems rather than static neural networks. To capture the dynamics of the power system states, a nonlinear temporal dynamic model of Artificial Neural Network (ANN) is required for the state forecasting.

There are two ways of incorporating time information into ANNs [21]. "The first technique is to use a spatial representation of time, such as in Time Delay Neural Networks (TDNNs). In these ANNs, time information is represented spatially across the network input, and the ANNs compute a static mapping from the input to output. In the second technique, time is represented implicitly by using a recurrent ANN architecture, that is, the effect of temporal evolution are captured in the state of the network. In this research, TDNN has been used for the forecasting step because the structure is straightforward with a satisfactory speed and precision" [17].

To solve the state filtering problem, four different ANN models based on multilayer perceptron, Functional Link Network (FLN), counter propagation network (CPN), and Hopfield network were developed [18]. Out of these four models, FLN was found to be most suitable for state estimation. Moreover, [18] established that compared with other neural network models, the FLN model has superior inherent filtering capability for bad data in the measurement set. Also, the FLN-based static state estimator provides system states in one forward pass and does not involve any iterative process. Hence, the FLN has been used in the present work for the state filtering step.

1.2 Transient Stability

Another important problem in power systems is stability. Many major recent blackouts, caused by power system instability, show the importance of this phenomenon [38]. Transient stability has been the dominant stability problem on most systems, and has been the focus of much of the industry's attention concerning system stability assessment. Transient stability assessment is concerned with the behavior of the synchronous machines after they have been perturbed following a large disturbance in a system.

Power system stability is defined as "The ability of an electric power system, for a given initial operating condition, to regain a state of operating equilibrium after being subjected to a physical disturbance, with most system variables bounded so that practically the entire system remains intact" [20].

A variety of transient stability assessment methods have been reported in the literature [27]. These methods include time domain solutions [31, 37], extended equal area criteria [40], and direct stability methods such as transient energy function [13, 2],

pattern recognition and expert systems/neural networks [9, 31, 16].

In the time domain simulation method, the initial system state is obtained from the pre-fault system. This is the starting point used for the integration of the fault-on dynamic equations. After the fault is cleared, the post-fault dynamic equations are numerically integrated. The machine angles may be plotted versus time and analyzed. If these angles are bounded, the system is stable, otherwise it is unstable.

On the one hand, time domain simulation provides the most accurate approach for determining the transient stability of the system. This method allows flexible modeling of components. However, it is computationally intensive and not suitable for on-line application. On the other hand, a direct method in transient stability analysis offers the opportunity of assessing the transient stability of power systems without explicitly solving differential equations. Therefore, they are computationally fast and suitable for real-time transient stability analysis [39]. However, they require significant approximations which limit modeling accuracy.

To overcome such problems, pattern-matching methods have been proposed [26]. "These methods are driven by a large database of examples from off-line studies. Among these methods artificial neural networks have been frequently proposed since they offer certain features such as fast execution and excellent generalization capability" [11].

This thesis project was also concerned with the use of ANNs in transient stability analysis. A method based on ANNs is used to estimate the transient energy function as a security index. The distance between the current operating point and the security limit for a given power system is the security index that is obtained by applying standard operation criteria for transient response to off-line simulations. These simulations form a database that can be used later on to train ANNs. Further investigation

was undertaken by constructing an ANN-based tool to identify stable and unstable conditions of a given power system using the transient energy function.

The remainder of this thesis is organized as follows. In Chapter Two, all the power system benchmarks used in this thesis are explained. It includes sample simulations of each case with related plots. Chapter Three describes the ANN-based state estimation methods and explains the architecture of Time Delay Neural Network (TDNN) and Functional Link Networks. Chapter Four represents the results of the proposed ANN design for state estimation. It contains input selection and validation results and discussion of each test system. Transient stability analysis starts from Chapter Five which reviews background information on stability assessment and discusses different methods including transient energy function. Chapter Six presents the ANN structure, feature selection, and error analogy. Finally, conclusions are drawn in Chapter Seven and possible future research directions are discussed.

Chapter 2

Power Systems Model Description

Four test power systems were employed in this thesis project as benchmarks. In this chapter the structure of each test power system with the mathematical model of their elements is presented. These models are coded as MATLAB functions in Power System Toolbox (PST) [6]. These benchmarks were used to perform transient stability simulations and to build data patterns which were used later for training and testing neural networks.

For each test system, the one-line diagram following a description of all the equipment characteristics is presented. Sample simulations were conducted for each benchmark to give a better understanding of them. Later, the simulation algorithm and the process of data generating are explained.

2.1 Power System Structure

Every power system is basically divided into three subsystems which are Generation, transmission, and distribution. The generation unit usually consist of all prime movers

and electric generators and their associated control units. Transmission system interconnects all the generating and load units. Distribution system is the final destination of a power system where the power is transferred to consumers. To illustrate a power system and its interconnected elements, the following test system which is one of the test systems provided by PST [6] is explained.

2.2 Single-machine-infinite-bus System

The smallest and simplest system used in this study is a single-machine system with three buses. In this power system, bus 1 is the slack bus, bus 2 is the generation bus, and bus 3 is the load bus. Figure 2.1 shows the one-line diagram of the system. Generator 2 is presented as an infinite bus, therefore, the voltage of bus 2 is maintained

Figure 2.1: Machine connected to an infinite bus

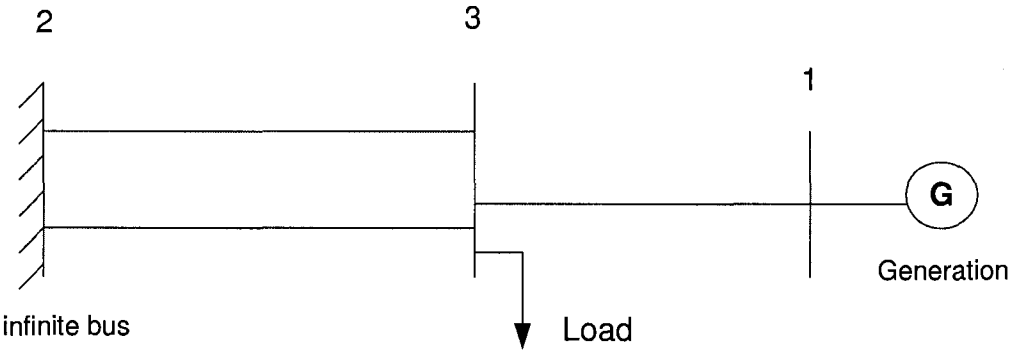

constant, i.e., the internal voltage behind either transient or subtransient impedance is fixed. Transient and subtransient parameters are explained later in the synchronous machine section. The following is a list of basic element in the single-machine-infinite-bus test system:

1. Bus and Line specifications

   There are three types of bus in a power system: 1- Load buses which all loads

Figure 2.2: Approximate equivalent circuit for a transmission line [19]

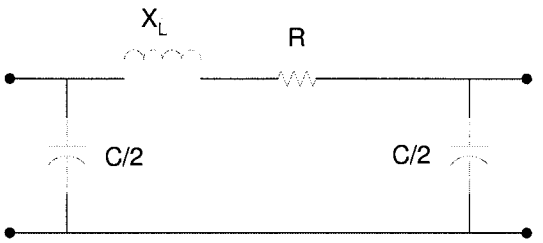

(active and reactive powers) are connected to them. 2- Generator buses which all generators are connected to these buses. 3- Slack or swing bus which has a generator connected to this bus where it's voltage magnitude and phase angle are fixed for power flow calculation.

A transmission line in a power system is characterized by three main parameters: series resistance R due to the conductor resistivity, line reactance which is mostly series inductance L due to the magnetic field between conductors, and line charging or shunt capacitance C due to the electric field between conductors. A simplified "π" model of a transmission line is shown in Figure 2.2.

2. Synchronous Machines

Synchronous generators form the principal source of electric energy in power system. Many large loads are driven by synchronous motors. "A synchronous machine has two essential elements: the field and the armature. The field is on the rotor and the armature is on the stator. The field winding is excited by direct current. When the rotor is driven by a prime mover (turbine), the rotating magnetic field of the winding induces alternative voltages in the three phase armature windings of the stator.

Following a disturbance, currents are induced in the synchronous machine rotor

Figure 2.3: Simple synchronous machine model based on [19]

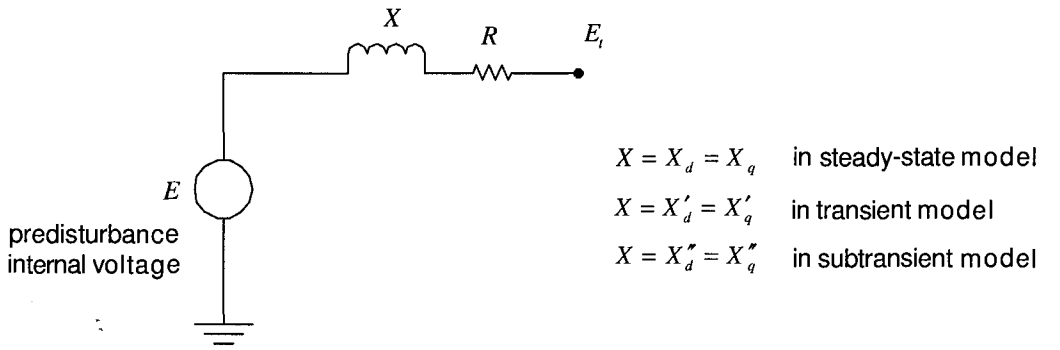

circuits. Some of these induced rotor currents decay more rapidly than others. Machine parameters that influence rapidly decaying components are called *sub-transient* parameters, while those influencing the slowly decaying components are called the *transient* parameters, and those influencing sustained components are the *synchronous* parameters" [19].

The synchronous machine characteristics of interest are the effective inductance (or reactance) as seen from the terminals of the machine and associated with the fundamental frequency currents during sustained, transient, and subtransient conditions. A simplified model of a synchronous machine, under conditions mentioned above, is shown in Figure 2.3.

3. Exciter data specification

The basic function of an excitation system is to provide direct current to the synchronous machine field winding. "The excitation system performs control and protective functions essential to the satisfactory performance of the power system by controlling the field voltage and thereby the field current. The control functions include the control of voltage and reactive power flow, and the

Table 2.1: Bus specification matrix in PST for the single machine case

Bus no.	voltage (pu)	angle (deg)	P gen	Q gen	P load	Q load	G shunt	B shunt	bus type	max V	min V
1	1.05	0.0	0.9	0.0	0.0	0.0	0.0	0.0	2	999	-999
2	1.08103	0.0	0.0	0.0	0.0	0.0	0.0	0.0	1	0	0
3	1.0	0	0	0	0	0	0	0	3	0	0

enhancement of system stability. The excitation system supplies and automatically adjusts the field current of the synchronous generator to maintain the terminal voltage as the output varies within continuous capability of the generator.

4. Governor Specifications

   The prime sources of electrical energy supplied by utilities are the kinetic energy of water, the thermal energy derived from fossil fuels, and nuclear fission. The prime movers convert these sources of energy into mechanical energy that is, in turn, converted to electrical energy by synchronous generators. The prime mover governing systems provide a means of controlling power and frequency also known as load-frequency control. Governors vary prime mover output(torque) automatically for changes in system speed (frequency)" [19]. Figure 2.4 depicts the relation of prime movers and excitation controls in the generation unit. The prime movers are concerned with speed regulation and control of energy supply while excitation control is to regulate generator voltage and reactive power output.

In Power System Toolbox, the power system structure is defined by bus and line specification matrices. Table 2.1 shows the matrix of bus specifications of the single-machine system. The same specification format is used for all bus matrices.

Figure 2.4: Generation system with associated control unit based on [12]

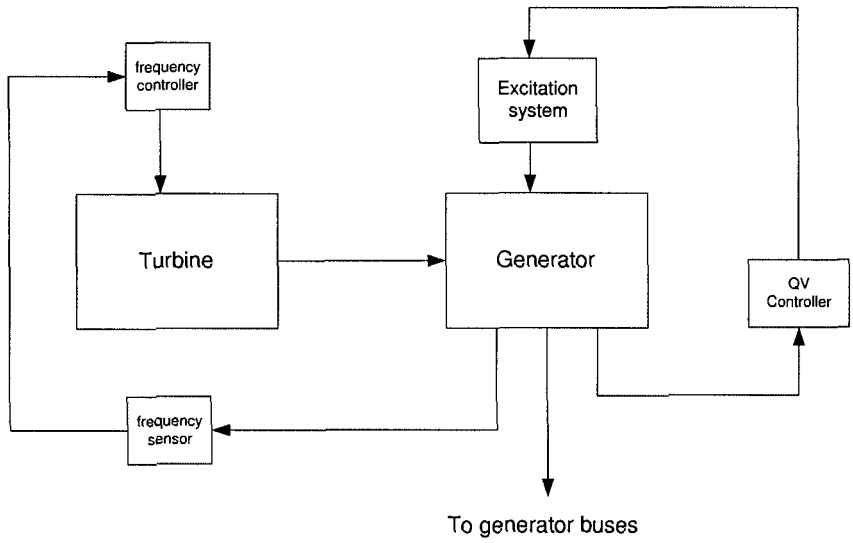

Table 2.2: Line specification matrix in PST for the single machine case

from bus	to bus	resistance	reactance	line charging	tap ratio	phase shifter angle
1	3	0.0	0.1	0.0	1.0	0.0
2	3	0.0	0.3999	0.0	1.0	0.0
2	3	0.0	0.3999	0.0	1.0	0.0

Bus 2 is the swing bus with voltage magnitude fixed at 1.05pu based on Table 2.1. Active power generation on this bus is 0.9 (pu). It has zero real power generation and acts as a reactive power source to hold the voltage at the center of the interconnecting transmission lines. The swing bus generator at bus two has limits of -999 (pu) to 999 (pu) for voltage magnitude. Table 2.2 shows the line format and the line matrix for the single-machine case in PST.

There are three types of synchronous machine models used in PST, the electromechanical or classical model, the transient model, and the subtransient model. In Power System Toolbox, the machine specification matrix is called *mac_con*. Table B.1 shows

the machine data format in PST.

$$mac\_con = \begin{bmatrix} 1 & 1 & 991 & 0.15 & 0 & 2 & 0.245 & 0.2 & 5.0 & 0.031 \\ 2 & 2 & 100000 & 0.00 & 0 & 0 & 0.01 & 0 & 0 & 0 \\ 1.91 & 0.42 & 0.2 & 0.66 & 0.061 & 2.8756 & 0.0 & 0 & 1 & 0 & 0 \\ 0 & 0 & 0 & 0 & 0 & 3 & 2 & 0 & 2 & 0 & 0 \end{bmatrix}$$

The first generator data set is for a subtransient model and the second data set is for an electromechanical generator model used to represent the infinite bus. Time constants $T'_{do}, T''_{do}, T'_{qo}$, and T''_{qo} are the four principal $d-$ and $q-$ axis open circuit time constants. These time constants determine the rate of decay of currents and voltages from the *standard parameters* used in specifying synchronous machine electrical characteristics.

The algorithm of modeling the generators in PST is as follows: "The initialization uses the solved load flow bus voltages and angles to compute the internal voltage and the rotor angle. The d-axis voltage is identically zero for all time. The network interface computation generates the voltage behind the transient reactance on the system reference frame. In the dynamics calculation, the rotor torque imbalance and the speed deviation are used to compute the rates of change of the two state variables, machine angle, and machine speed.

The data set for ST3 exciters in the single-machine-infinite-bus system is:

$$exc\_con = \begin{bmatrix} 3 & 1 & 0 & 7.04 & 0.4 & 6.67 & 1.0 & 7.57 & 0 & 0.2 \\ -0.2 & 200 & 4.365 & 20 & 4.83 & 0.091 & 1.096 & 6.53 & 1 & 6.53 \end{bmatrix}$$

The exciter is initialized using the generator field voltage to compute the state variables. Then the exciter output voltage is converted to the field voltage of the synchronous machine. In the dynamics calculation, generator terminal voltage, and the external signal is used to calculate the rates of change of the excitation system states"[6]. Table B.2 shows the data format of IEEE ST3 exciter used in Power

System Toolbox and Figure A.2 shows the exciter control diagram.

Table B.3 shows the data format of governor specification in Power System Toolbox. The control diagram of the governor is also represented in Figure A.3. The following (*tg_con*)is the parameter matrix of single machine governor.

$$tg\_con = \begin{bmatrix} 1 & 1 & 1.0 & 25.5 & 1.0 & 0.1 & 0.4 & 0.0 & 1.25 & 5.0 \end{bmatrix}$$

No time constant is allowed to be set to zero in this model. This data specification can be used to model a steam unit or a hydro unit.

There is another data specification matrix called switching file, *sw_con*, which defines the simulation control times. This matrix provides the control of simulation start time, initial time step, fault application time, fault location bus number, type of fault, duration of fault, fault clearing time, and finishing time.

2.2.1 Transient Stability Simulation

A power system transient stability simulation model consists of a set of differential equations determined by the dynamic models and a set of algebraic equations determined by the power system network. Figure 2.5 shows the general structure of the power system model applicable to transient stability analysis.

First in transient simulation, a load flow study is performed to obtain a set of feasible steady-state system conditions to be used as initial condition. Power System Toolbox [6] calculates system bus voltage magnitudes and angles (unknown variables) by solving the nonlinear algebraic network equations using the Newton-Raphson algorithm in polar coordinates so that the specified loads are supplied. A Jacobian in terms of these variables is generated at each iteration and is used to update the magnitude and angle variables. As the solution progresses, if the voltages at the load buses are found to be out-of-limits then the corresponding adjustments are made to

Figure 2.5: Structure of the complete power system model for transient stability analysis based on [19]

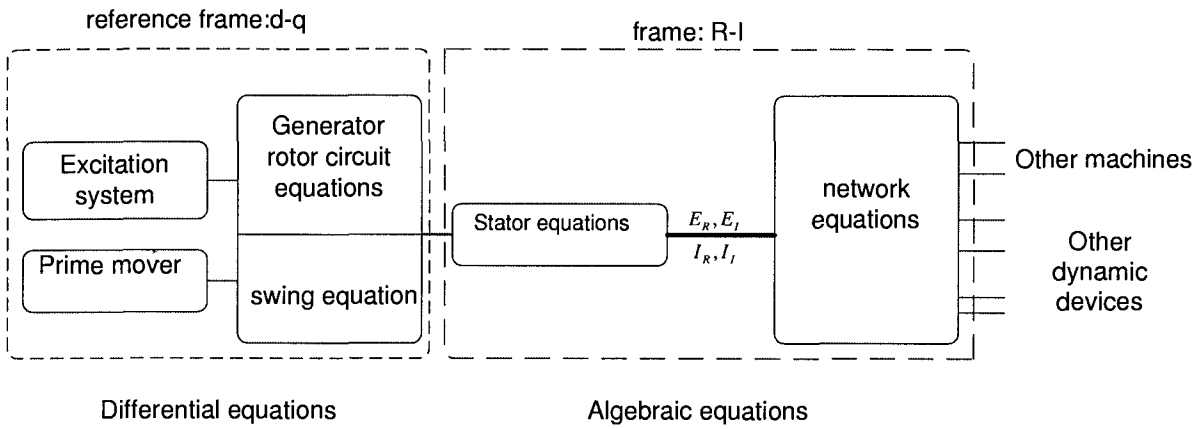

bring their voltages back in range. At the end of the solution process, either the solution has converged, or the number of allowed iterations has been exceeded. A solved load flow case is required to set the operating condition used to initialize the dynamic device models.

In Power System Toolbox [6], the dynamic generator models calculate the generator internal node voltages, i.e., the voltage behind transient impedance for the electromechanical generator, transient generator, and the voltage behind subtransient impedance for the subtransient generator. These internal voltages are used with a system admittance matrix reduced to the internal nodes to compute the current injections into the generators and motors. A MATLAB script file, *s_simu*, calls the models of the Power System Toolbox to:

1. select a data file (In this work it is either the single-machine, 3-machine, 7-machine or 19-machine test system)

2. perform a load flow

3. initialize the non-linear simulation models

4. do a step-by-step integration of the non-linear dynamic equations to give the response to a specified system fault

Simulation

A predictor-corrector algorithm is used for the step-by-step integration of the system equations. At each time step:

1. The non-linear equations for the load at load buses are solved to give the voltage at these buses. The current injected by the generators and absorbed by the motors is calculated from the reduced admittance matrix appropriate to the specified fault condition at that time step based on the machine internal voltages and the load bus voltages.

2. The rates of change of the state variables are calculated.

3. A predictor integration step is performed which gives an estimate of the states at the next time step.

4. A second network interface step is performed.

5. The rates of change of the state variables are recalculated.

6. A corrector integration step is performed to obtain the final value of the states at the next time step.

All calculations are performed using MATLAB's vector calculation facility. This results in a simulation time which is largely a function of the number of time steps. In most simulations there are at least 500 time steps which are adjustable.

A menu of plots is presented at the completion of the simulation. These plots include all dynamic states, induction motor active and reactive powers, generator

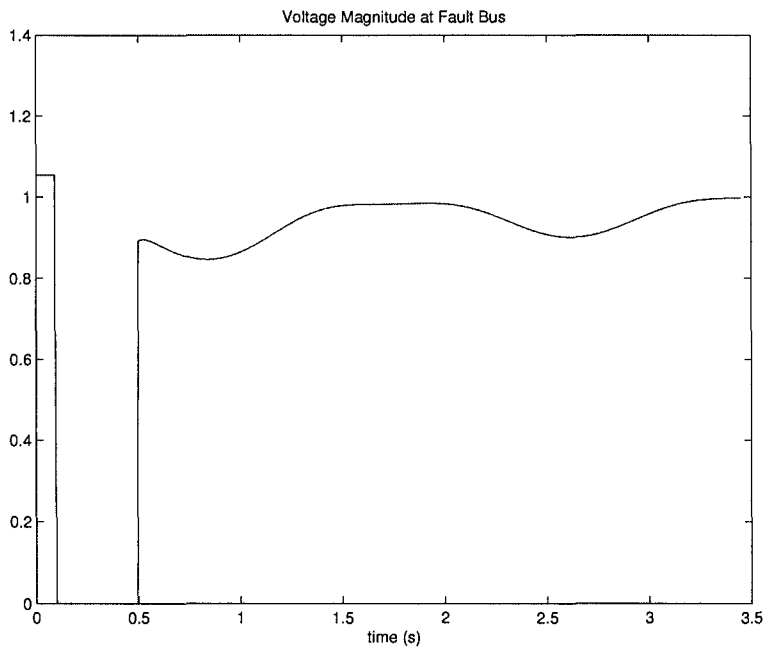

Figure 2.6: Voltage magnitude(pu) at the faulty bus (3)

terminal voltage magnitudes, and bus voltages (magnitude and angle). Figures 2.6-2.8 are sample simulations of the single-machine system for 3.5 seconds. At 0.1 second, a three-phase fault was applied at bus 3 on line 3-2. At 0.5 second the line was disconnected at bus 3. The fault persists for 1.0 second when the line was disconnected from bus 2. The time step is 0.005 second.

Figure 2.6 shows voltage magnitude of the faulty bus (bus 3). Plots in Figure 2.7 show the speed deviation of each machine and plots in Figure 2.8 illustrate all machine angles.

Before applying the fault, the system has a satisfactory and stable initial condition. Voltage magnitude is fixed at 1.05pu and there is no oscillation during this period. During the fault application, voltage vector is set to zero (three phase fault) and machine speed deviation and angle start to increase until fault cleared at 1.0

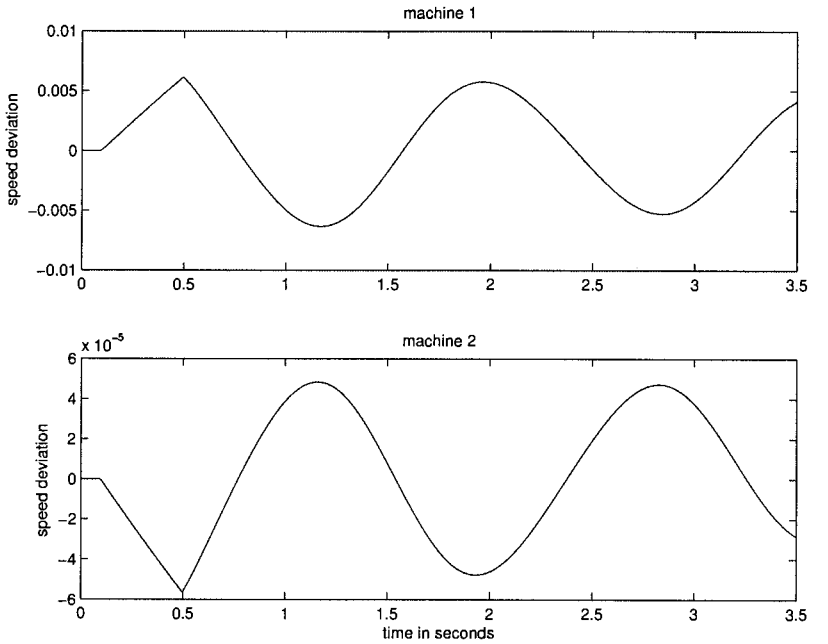

Figure 2.7: Speed deviation of all machines

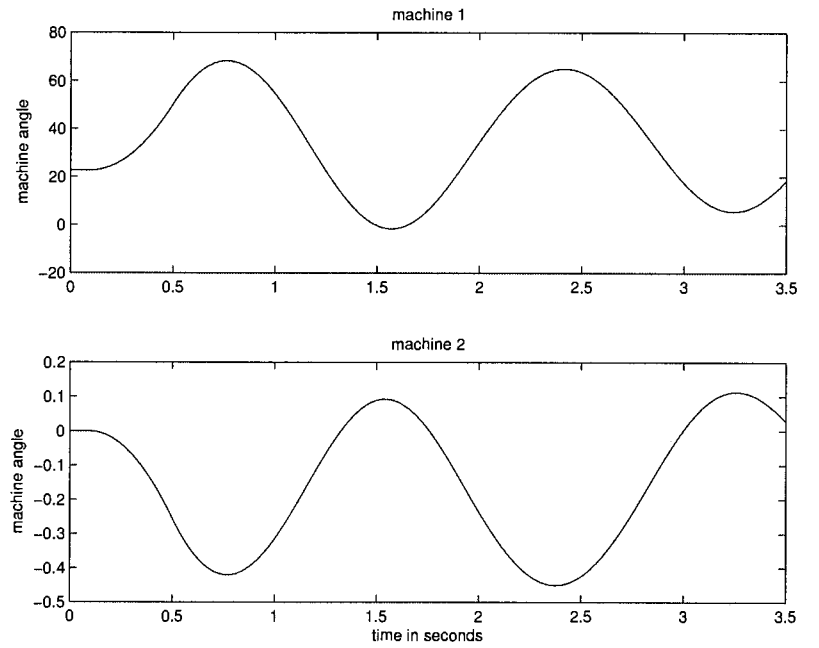

Figure 2.8: Machine angles

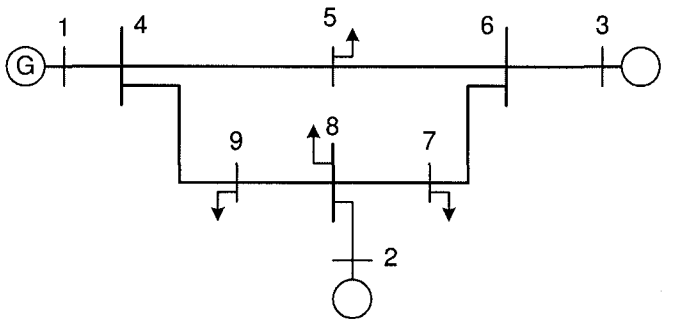

Figure 2.9: One-line diagram of 3-machine system

second. After removing the fault, both speed deviation and angle of machine 2 start to oscillate. Machine 2 does not lose synchronism with the rest of the system since angle oscillation does not go over 90 degrees. Note that in Figure 2.7 and 2.8, machine 2 does not show that much variation in speed and angle compared to machine 1 since it is modeled as the infinite bus.

2.3 3-machine-9-bus System

Figure 2.9 shows the one-line diagram of the second test power system used in this work. The power system consists of 9 buses, i.e., one slack or swing bus, 2 generator buses and 6 load buses. The bus and line data format is the same as explained in the previous case. Matrices *Bus* and *Line* are bus and line specifications for the

3-machine system.

$$Bus = \begin{bmatrix} 1 & 1.04 & 0.00 & 0.00 & 0.00 & 0.00 & 0.00 & 0.00 & 0.00 & 1 \\ 2 & 1.02533 & 0.00 & 1.63 & 0.00 & 0.00 & 0.00 & 0.00 & 0.00 & 2 \\ 3 & 1.02536 & 0.00 & 0.85 & 0.00 & 0.00 & 0.00 & 0.00 & 0.00 & 2 \\ 4 & 1.00 & 0.00 & 0.00 & 0.00 & 0.00 & 0.00 & 0.00 & 0.00 & 3 \\ 5 & 1.00 & 0.00 & 0.00 & 0.00 & 0.90 & 0.30 & 0.00 & 0.00 & 3 \\ 6 & 1.00 & 0.00 & 0.00 & 0.00 & 0.00 & 0.00 & 0.00 & 0.00 & 3 \\ 7 & 1.00 & 0.00 & 0.00 & 0.00 & 1.00 & 0.35 & 0.00 & 0.00 & 3 \\ 8 & 1.00 & 0.00 & 0.00 & 0.00 & -0.5 & 0.35 & 0.00 & 0.00 & 3 \\ 9 & 1.00 & 0.00 & 0.00 & 0.00 & 1.25 & 0.50 & 0.00 & 0.00 & 3 \end{bmatrix}$$

$$Line = \begin{bmatrix} 1 & 4 & 0.0 & 0.0576 & 0. & 1. & 0. \\ 4 & 5 & 0.017 & 0.092 & 0.158 & 1. & 0. \\ 5 & 6 & 0.039 & 0.17 & 0.358 & 1. & 0. \\ 3 & 6 & 0.0 & 0.0586 & 0. & 1. & 0. \\ 6 & 7 & 0.0119 & 0.1008 & 0.209 & 1. & 0. \\ 7 & 8 & 0.0085 & 0.072 & 0.149 & 1. & 0. \\ 8 & 2 & 0.0 & 0.0625 & 0. & 1. & 0. \\ 8 & 9 & 0.032 & 0.161 & 0.306 & 1. & 0. \\ 9 & 4 & 0.01 & 0.085 & 0.176 & 1. & 0. \end{bmatrix}$$

The system has 2 generator buses at buses 2 and 3. There is an induction generator at bus 8 which is modeled as a negative load in the load flow.

As indicated before, motors form a major portion of the system loads. "Induction motors in particular form the workhorse of the electric power industry. An induction machine carries alternating currents in both the stator and rotor windings. In a three-phase induction machine, the stator windings are connected to a balanced three-phase supply. The rotor windings are either short-circuited internally or connected through slip rings to a passive external circuit. The distinctive feature of the induction machine is that the rotor currents are induced by electromagnetic induction from the stator.

Figure 2.10: Equivalent circuit of a three-phase induction machine [19]

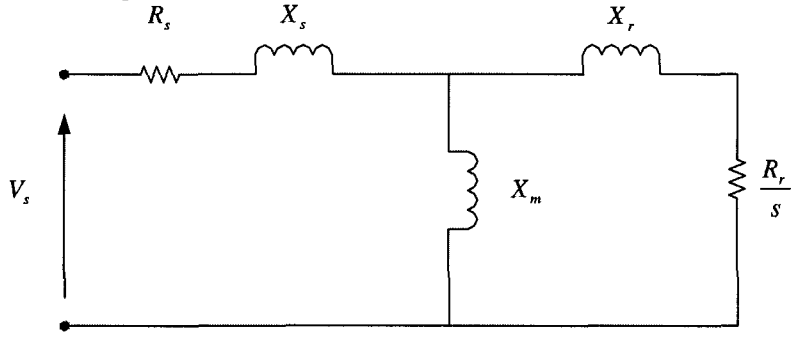

This is the reason they are called *induction machine*" [19]. Figure 2.10 represents the steady-state equivalent circuit of the induction machine. Data format for induction generator in Power System Toolbox is presented in Table B.1. Matrix *igen_con* shows the parameters of the induction generator in the 3-machine case.

$$igen\_con = \begin{bmatrix} 1 & 8 & 60. & .001 & .01 & 3 & .009 & .01 & 2. & 0 & 0 & 0 & 0 & 0 & 1 \end{bmatrix}$$

In PST, the dynamic model for an induction machine is formulated by Brereton, Lewis and Young [3]. In this model the three states are the d and q voltages behind transient reactance and the slip.

Generator and machine specifications are the same as in Table B.1. According to the specification matrix, all the machines at buses 1, 2, and 3 are modeled as electro-mechanical machines because their transient and subtransient parameters are set to zero.

$$mac\_con = \begin{bmatrix} 1 & 1 & 100 & 0.000 & 0.000 & 0. & 0.0608 & 0 \\ 2 & 2 & 100 & 0.000 & 0.000 & 0. & 0.1198 & 0 \\ 3 & 3 & 100 & 0.000 & 0.000 & 0. & 0.1813 & 0 \end{bmatrix}$$

$$\begin{bmatrix} 0 & 0 & 0 & 0 & 0 & 0 & 0 & 13.64 & 9.6 & 0 & 1 \\ 0 & 0 & 0 & 0 & 0 & 0 & 0 & 6.4 & 2.5 & 0 & 2 \\ 0 & 0 & 0 & 0 & 0 & 0 & 0 & 3.01 & 1.0 & 0 & 3 \end{bmatrix}$$

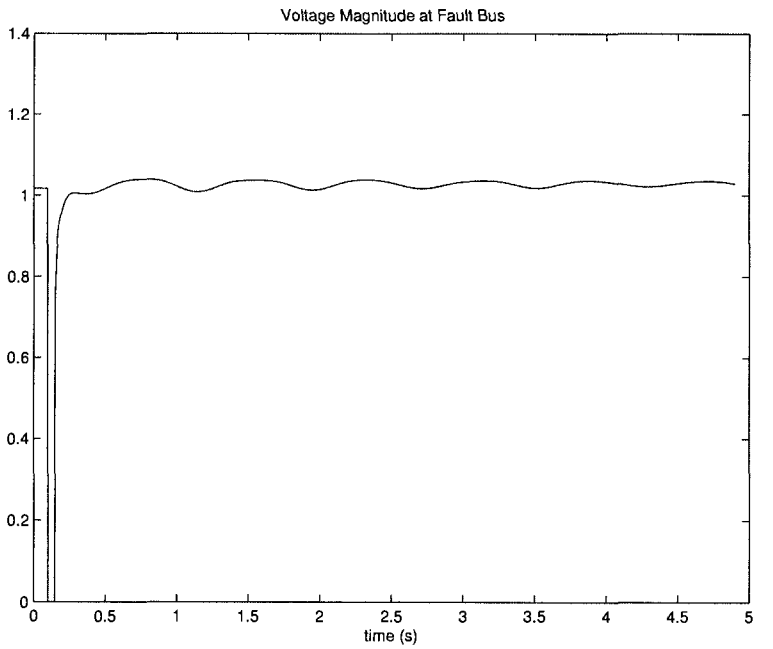

Figure 2.11: Voltage magnitude (pu) at the faulty bus (4-5)

The following plots 2.11, 2.12, and 2.13 are some simulation samples of the system for 5 seconds.

1. Voltage magnitude at faulty bus is shown in Figure 2.11
2. All machines' speed deviations are illustrated in separate plots in Figure 2.12
3. Line power flows is shown in Figure 2.13

At 0.1 second, a three-phase fault was applied at bus 4 on line 4-5. At 0.15 second the line was disconnected at bus 4. The fault persisted until 0.2 second when the line was disconnected from bus 5. The time step was 0.0025 second.

As Figure 2.11 shows, after removing the fault, voltage recovered within 3 to 4 seconds to 1.0(pu). Machine 3 showed more oscillation compared to machine 2 due to

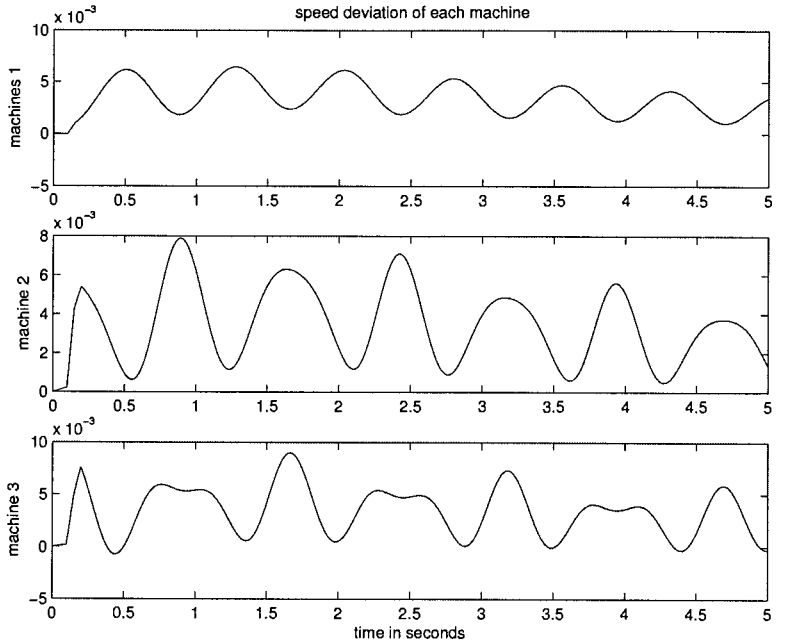

Figure 2.12: Speed deviation of all machines

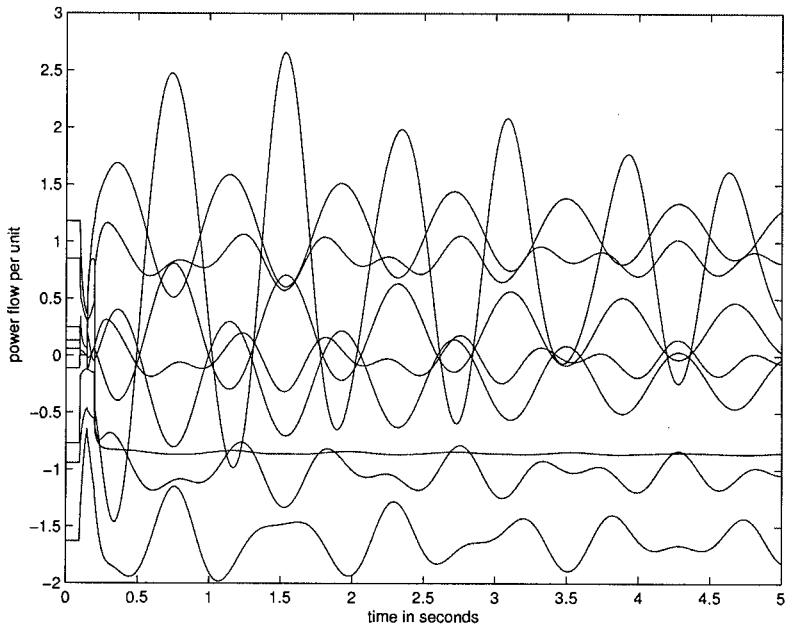

Figure 2.13: Line power flows

Figure 2.14: One-line diagram of the 7-machine system

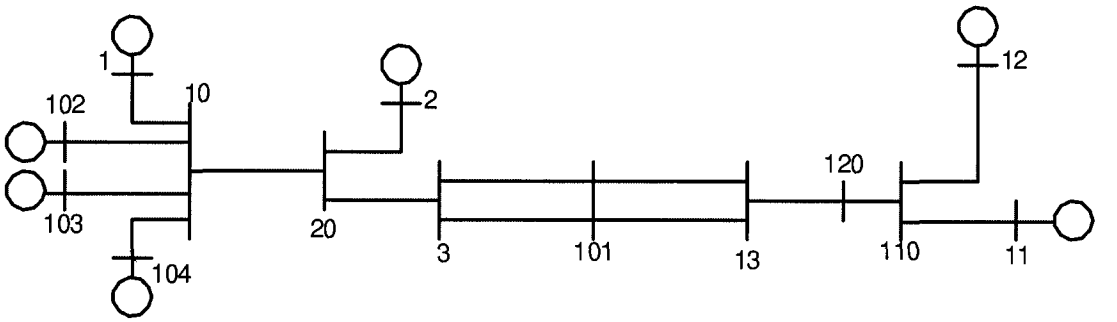

the fault location being closer to it. According to Plot 2.13, variation of power flows for all lines stayed in range of ±1pu except bus 4-5 which was the faulty line.

2.4 7-machine-14-bus System

Figure 2.14 shows the one-line diagram of the 7-machine test power system used in this work. The power system consists of 15 buses, i.e., one slack or swing bus, 7 generator buses, and 7 load buses. The bus and line data format is the same as explained for previous cases. *Bus* and *Line* matrix specifications for the 7-machine system are given in C.1 and C.2. In this system, there are 7 generators at buses 1, 102, 103, 104, 2, and 12. There are simple exciters and turbine governors on all generators and power system stabilizers on generators 1 to 4.

The basic function of a power system stabilizer (PSS) is to add damping to the generator rotor oscillation by controlling its excitation using auxiliary signals. These auxiliary signals are usually shaft speed, terminal frequency, and power. Power system dynamic performance is improved by the damping of system oscillation.

Figure A.1 presents the block diagram of the PSS used in the 7-machine system

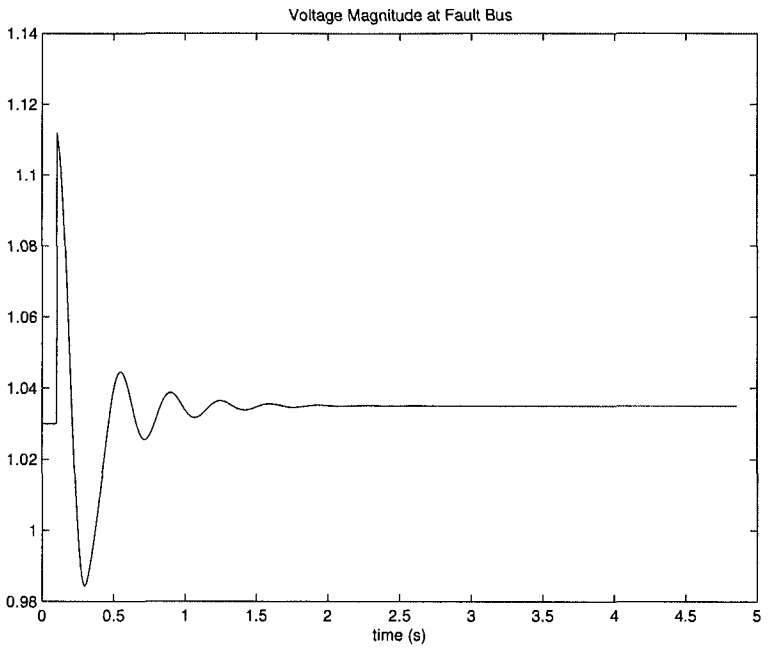

Figure 2.15: Voltage magnitude (pu) at the faulty bus (11-110)

in Power System Toolbox. Data format for PSS in Power System Toolbox is shown in Table B.2. Matrix *pss_con* shows the parameters of the PSS in 7-machine system.

$$pss\_con = \begin{bmatrix} 1 & 1 & 100.0 & 10.0 & 0.05 & 0.01 & 0.00 & 0.00 & 0.2 & -0.05 \\ 1 & 2 & 100.0 & 10.0 & 0.05 & 0.01 & 0.05 & 0.01 & 0.2 & -0.05 \\ 1 & 3 & 100.0 & 10.0 & 0.05 & 0.01 & 0.05 & 0.01 & 0.2 & -0.05 \\ 1 & 4 & 100.0 & 10.0 & 0.05 & 0.01 & 0.05 & 0.01 & 0.2 & -0.05 \end{bmatrix}$$

Generator and machine data format are the same as in Table B.1. The machine specification matrix, provided in C.3, shows that all machines are modeled as sub-transient models.

The following plots 2.15, 2.16, and 2.17 are some simulation samples of the system for 5 seconds.

1. Voltage magnitude at the faulty bus is shown in Figure 2.15

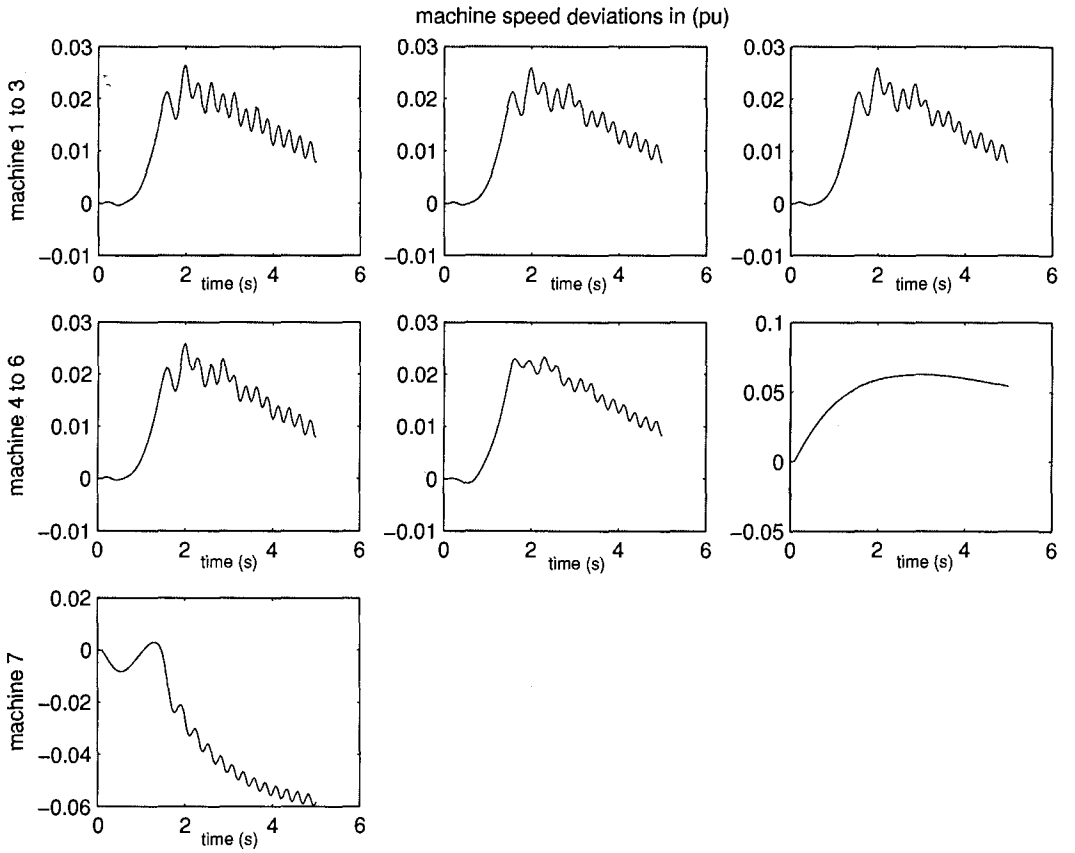

Figure 2.16: Speed deviation of all machines

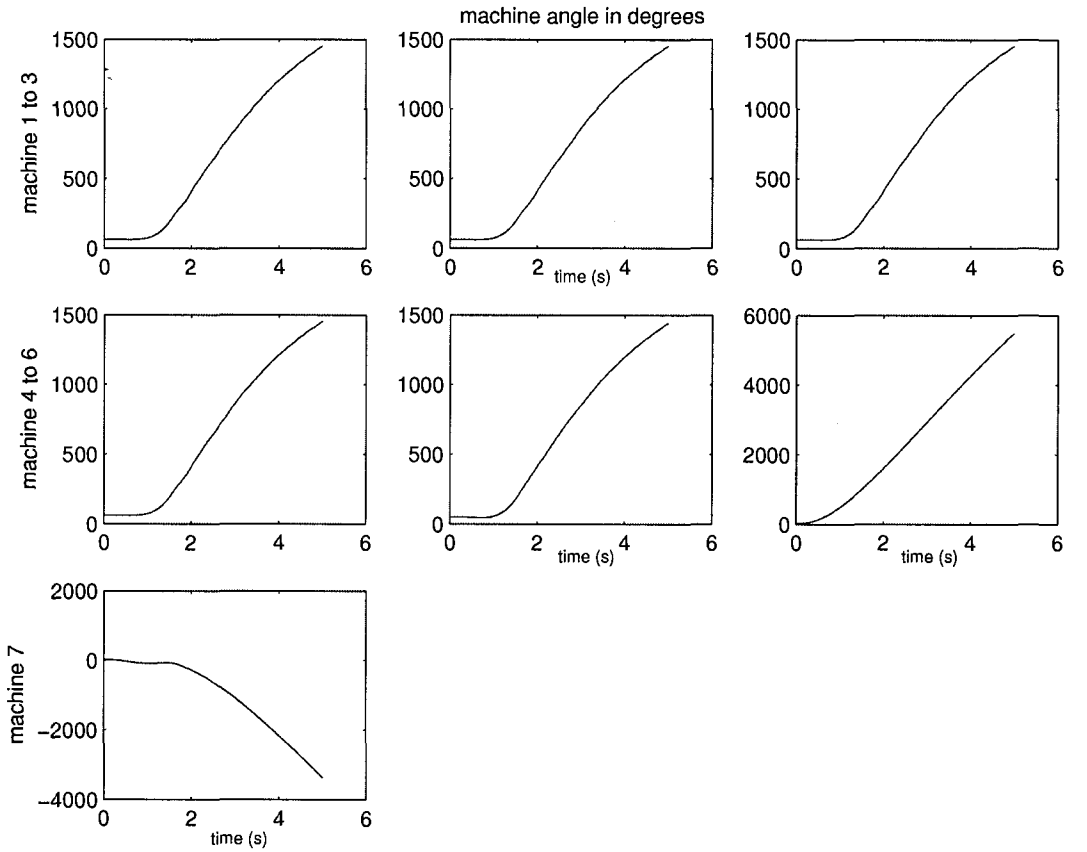

Figure 2.17: Machine angle of all machines

2. All machines' speed deviations are illustrated in separate plots in Figure 2.16

3. All machines' angles are illustrated in Figure 2.17

At 0.1 second, a line-to-ground fault was applied at bus 11 on line 11-110. At 0.15 second the line was disconnected at bus 11. The fault persisted until 0.18 second when the line was disconnected from bus 110. The time step was 0.0055 second.

The speed of machine 6, which is connected to bus 11, has the most oscillation compared to other machines, which is due to the closeness of fault to this machine. According to Figure 2.17, all machine angles go beyond the stability boundary within a few seconds of fault occurrence. This indicates the instability of system after fault removal.

2.5 19-machine-42-bus System

The biggest model under investigation was a 19-machine test power system. Figure 2.18 shows the one-line diagram of this system. The power system consists of 42 buses, one slack or swing bus, 19 generator buses, and 22 load buses. The system has 19 generator buses at buses 1, 2, 3, ..., 18, and 19. All machines are modeled as a classical model except the one at bus 15 which is represented by its subtransient parameters. Loads are constant impedances. Table B.2 shows the value of parameters used for the exciter in the 19-machine case. All the other component characteristics are given in D.1, D.3, and D.5. The same process as explained for the single-machine was used for this case. Bus, line, and machine specification data format are the same as explained before. Figures 2.19, 2.20, and 2.22 are some simulation samples of the system for 5 seconds.

1. Voltage magnitude at the faulty bus is shown in Figure 2.19

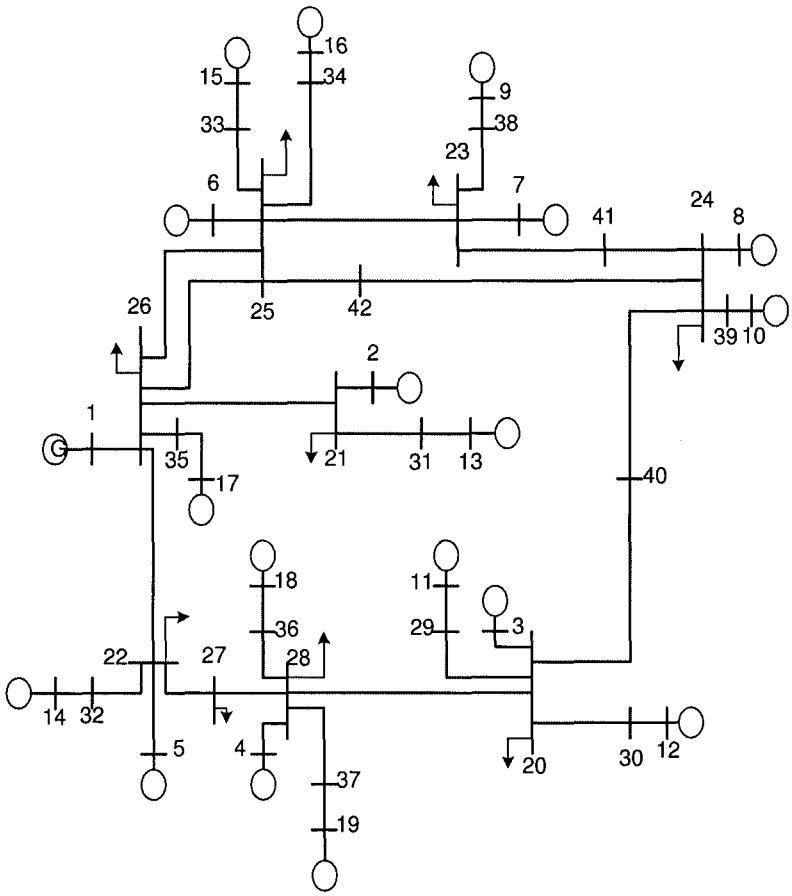

Figure 2.18: One-line diagram of 19-machine system

Table 2.3: Simple exciter data for 19-machine case

voltage regulator gain (K_A)	100 pu
voltage regulator time constant (T_A)	0.02 sec
transient gain reduction time constant (T_C)	0 sec
maximum voltage regulator output (V_{Rmax})	6 pu
minimum voltage regulator output (V_{Rmin})	-3 pu

2. All machines' speed deviation are shown in plots of Figures 2.20 and 2.21

3. Exciter output voltage is shown in Figure 2.22

The simulation ran for 5 seconds with the time step of 0.005 second. At 0.1 sec, a three phase fault was applied at bus 15 on line 15-33. At 0.15 sec the line was disconnected at bus 15. The fault persisted for 0.2 second when the line was disconnected from bus 33. Figure 2.20 and 2.21 show that the speed deviation of machine 15 is much higher than other machines due to the three-phase fault occurring on line 15-33.

These simulations were sources of data generating which were used to train and test neural networks in next chapters. The condition under which these simulations were run, and the process of data pattern generating are explained later for each case.

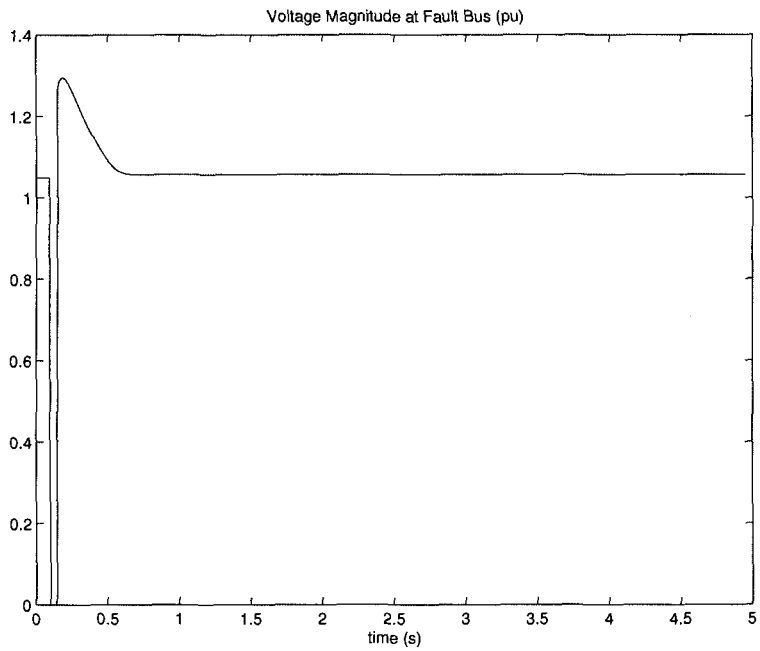

Figure 2.19: Voltage magnitude at the faulty bus (15-33)

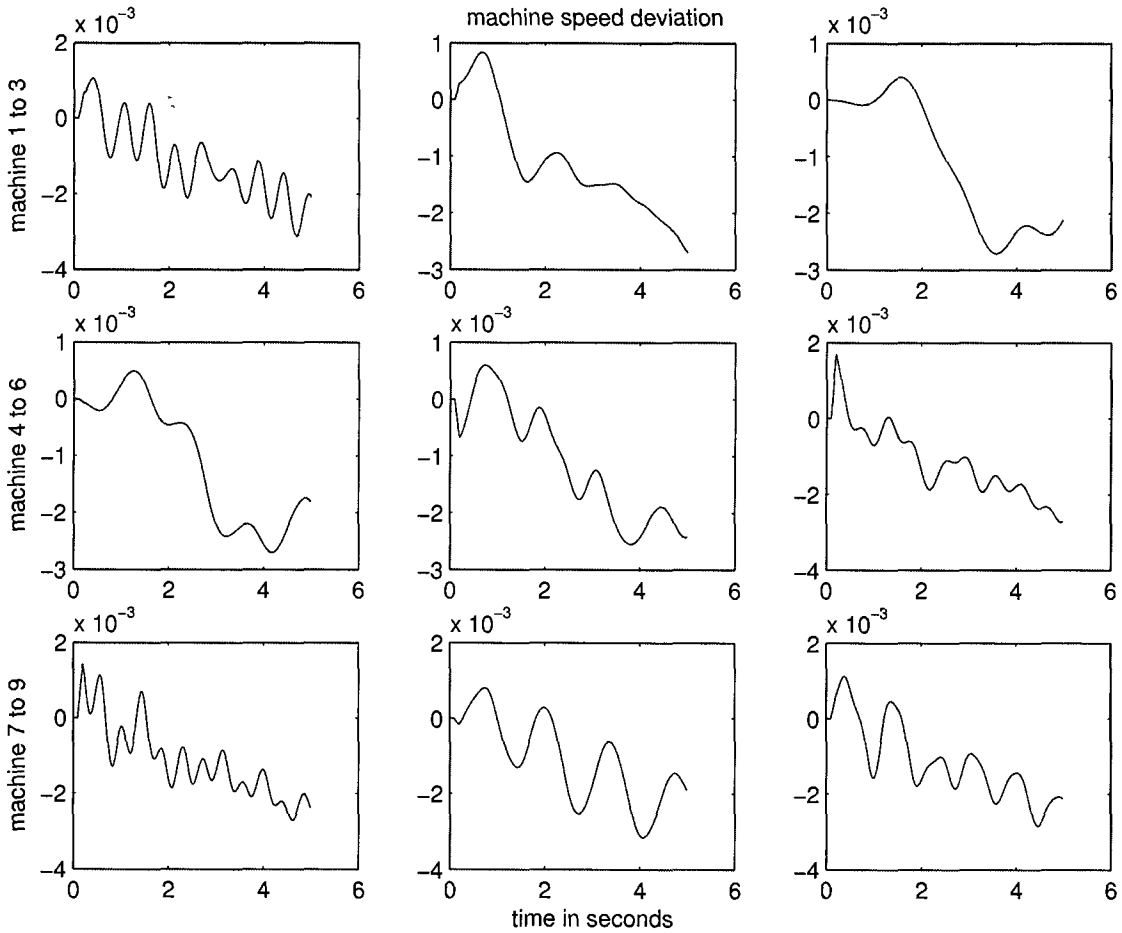

Figure 2.20: Speed deviation of machines 1 to 9

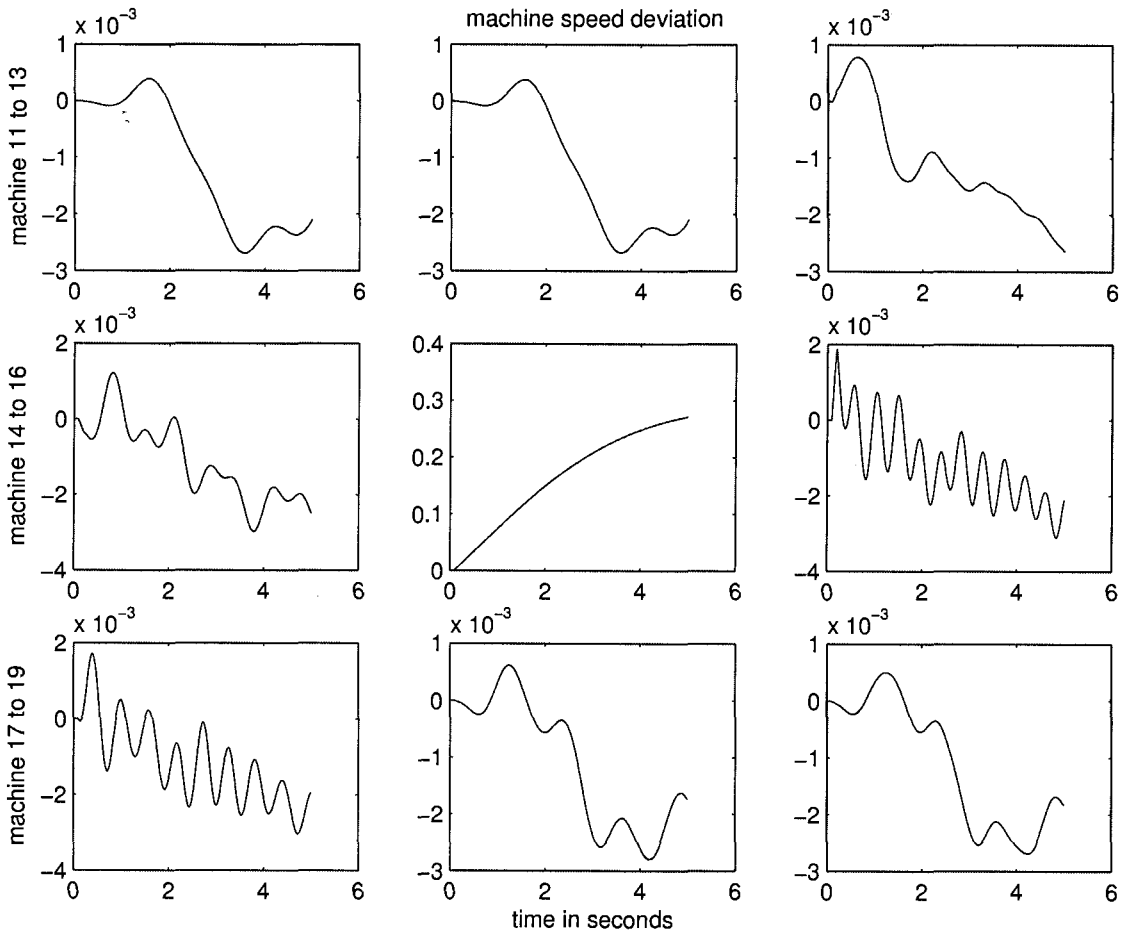

Figure 2.21: Speed deviation of machines 11 to 19

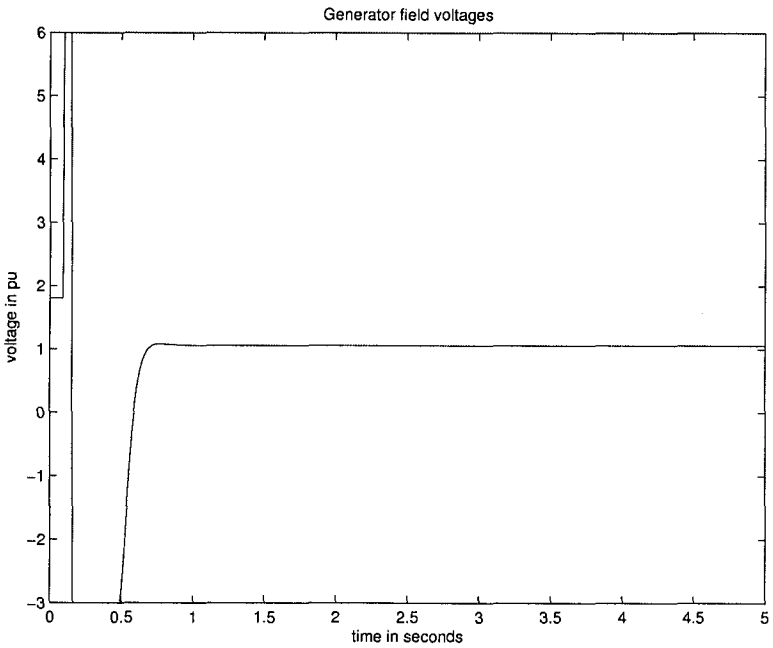

Figure 2.22: Generator field voltage

Chapter 3

ANN-Based State Estimation

This chapter discusses the application of neural networks in state estimation of power systems. Two basic steps of power system state estimation, state filtering and state forecasting, are discussed in this chapter. Two neural networks (FLN and TDNN) were developed for filtering and forecasting process. The architecture of each neural network is explained in detail at the end of this chapter.

3.1 Modeling of System Dynamics

Although, power systems rarely gain a true steady state operation, the magnitude of oscillations due to load variation is generally small. So, it is justifiable to consider it a quasi-static operation, in which change in loads take place at the beginning of each time sample and are instantaneously met by adjusting generated power.

Considering that the system is operating under quasi-static conditions, its state of operation is perfectly characterized by the set of all complex nodal voltages as in Equation 3.1. "The conventional state vector of an N bus power system is composed of $n = 2N - 1$ variables:

$$x = [V_1, \Theta_1, V_2, \Theta_2, ..., V_N]^T, \tag{3.1}$$

where V_i is the voltage magnitude of bus i, and Θ_i is the phase angle of bus i.

For a given network configuration, a unique way of assessing the system state is through the measurements gathered from around the system. The most available measurements used for real-time monitoring consist of:

1. active and reactive power bus injections
2. active and reactive line power flows
3. bus voltage magnitudes

These measurements are related to the state vector by the nonlinear equation:

$$z(k) = h(x(k)) + v(k), \tag{3.2}$$

where m is the number of measurements, $z(k)$ is the m-dimensional measurement vector, $h(\bullet)$ is the m-dimensional nonlinear vector function relating measurement vector (z) to state vector x, and $v(k)$ is the m-dimensional measurement error vector which is normal error affecting the measurements, for example, from the limited accuracy of meter devices.

In addition to Equation 3.2 the dynamic model of a power system is of the following general form:

$$x(k+1) = f(x(k), w(k), k), \tag{3.3}$$

where n is the number of state variables, x is the n-dimensional state vector, f is the n-dimensional nonlinear state transition function, and $w(k)$ is the system noise vector" [17]. Typically, the total number of measurements m, ranges from 1.5 to 3 times the number of state variables n, [8].

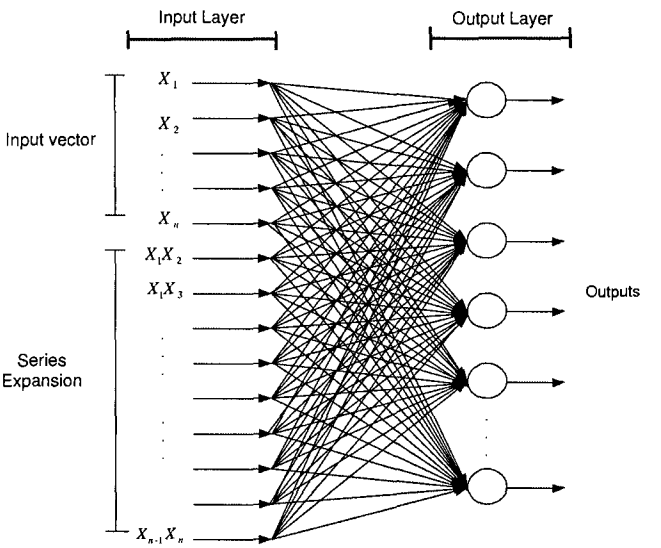

Figure 3.1: Functional link network

Equations 3.1 to 3.3 show the process of power system state estimation based on the forecasting and filtering process. We tried to employ neural networks to estimate the state of a power system by relating to this process. In order to capture the dynamics of the power system states, a nonlinear temporal dynamic model of ANN was required for the state estimation while for the filtering step, a flat delta rule network was developed. The following section discusses this matter in detail.

3.1.1 Functional Link Network

In this study, state filtering was achieved by using Functional Link Network (FLN) [17]. "This static network provides the output, which are state variables, in one forward pass and does not involve any iterative process. Figure 3.1 illustrates a scheme for Functional Link Network.

In FLN, the input patterns are enhanced by means of functional transformations before feeding them into the input layer of the actual network. In enhanced input

pattern representation, each component of the input pattern multiplies the entire input pattern vector [17]. If $x_1, x_2, ..., x_n$ represents a set of original inputs or features, the enhanced inputs along with these original inputs are obtained through a sequence of transformation, such as

$$\{x_i\} \Rightarrow \{x_i, x_i x_j\} \Rightarrow \{x_i, x_i x_j, x_i x_j x_k\} \Rightarrow ... \tag{3.4}$$

The idea of enhanced representation is very close to that of series expansion. Problems that might be difficult in the original pattern space generally become quite straightforward in the enhanced representation space. In the present work, only second-order products of inputs $(x_1 x_2, x_2 x_3, ..., x_{n-1} x_n)$ have been considered as enhanced inputs since the number of inputs were high and the result from the second-order was satisfactory.

An enhanced input/output pair is learned by a flat net, that is, a net with no hidden layer. Previous research indicated that supervised learning can be achieved very well with a flat net and delta rule if the enhancements are done correctly [41]. The flat architecture of the FLN exhibits highly desirable learning capabilities and, in some applications, drastically reduces the convergence time. The delta rule, also known as the Least-Mean-Square (LMS) learning rule, is a method of finding the desired weight vector that can successfully associate each input vector with its desired output [35].

The benefit of the FLN, when applied to mathematical modeling, is the increased accuracy of mapping through the expansion of the basic set.

3.1.2 Time-Delay Neural Network

The most common feedforward networks are static networks, which have no internal time delays. They respond to a particular input by immediately generating a specific output. However, static networks can respond to temporal patterns if the network

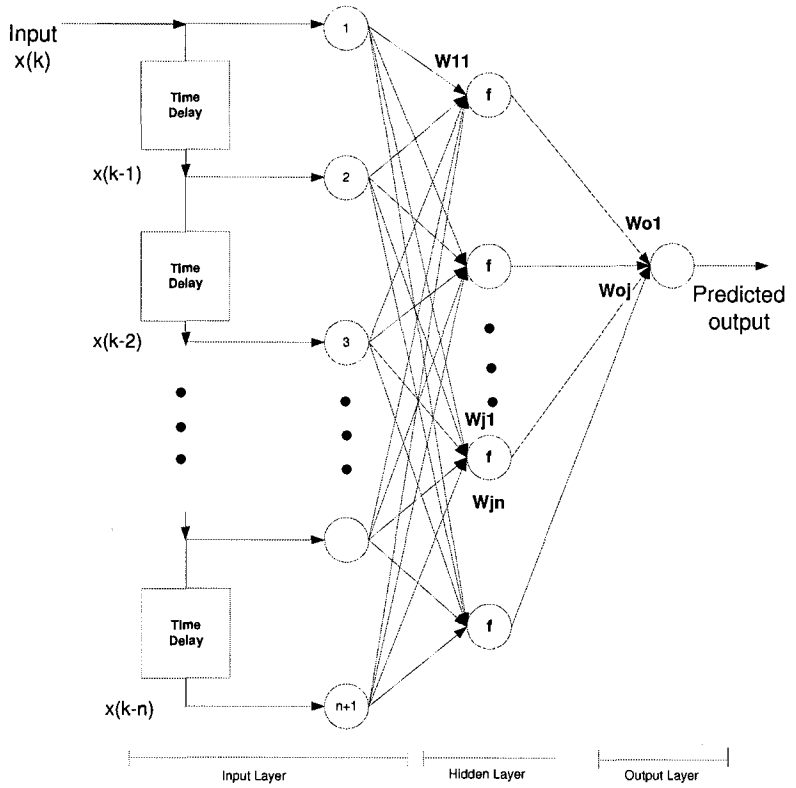

Figure 3.2: Time-delay neural network

inputs are delayed samples of the input signals, i.e., time is treated as another dimension in the problem [17]. Incorporating time as another dimension in neural networks is often referred to as Time Delay Neural Network (TDNN). These networks, trained with the standard back propagation algorithm, have been used as adaptive filters for noise reduction and echo canceling and for chaotic time series prediction [15].

Our TDNN consists of an input layer with delay units, the hidden layer, and the output layer. In TDNN the basic units are modified by introducing delays as shown in Figure 3.2. This structure incorporates time alignment by delaying the input with a fixed time span.

The inputs to such a unit are multiplied by several weights, one for each delay and one for the undelayed unit input. In this way, a TDNN unit has the ability to relate

and compare current input to the past history of events" [17].

TDNN is capable of modeling dynamic systems where the output has a finite temporal dependence on the input, that is

$$x(k+1) = F[x(k), x(k-1), ..., x(k-n)], \tag{3.5}$$

where $F(\bullet)$ is the nonlinear function [17].

The back propagation algorithm has been used as the learning procedure, which works well for classification, prediction, function estimation, and time series tasks [14, 35]. The following is a brief explanation of the back propagation algorithm.

The Back Propagation Algorithm

This algorithm is derived based on the concept of the gradient descent search to minimize the error through the adjustment of weights. For a three-layer ANN with I inputs, one hidden layer with J neurons, and K output neurons, the error function is defined as follows

$$E_p = \frac{1}{2}\sum_{k=1}^{K}(d_{pk} - o_{pk})^2, \tag{3.6}$$

where d_{pk} and o_{pk} are the desired and actual outputs of the ANN for pattern p, for $p = 1, 2, ..., P$ with P being the number of training patterns. Individual weight adjustments are computed by

$$\triangle w_{kj} = -\eta \frac{\partial E_p}{\partial w_{kj}}, \tag{3.7}$$

where η is a learning rate constant. Through some derivations, the following recursive formula for adjustment of weights with the momentum term are obtained.

For the output layer

$$w_{kj}^{l+1} \leftarrow w_{kj}^{l} + \eta \triangle w_{kj}^{l} + \alpha \triangle w_{kj}^{l-1}, \tag{3.8}$$

where $\triangle w_{kj}^{l} = \delta_{ok} y_j$; and $\delta_{ok} = (d_k - o_k) o_k (1 - o_k)$, y_j is the output of the jth hidden neuron, and α is a momentum constant between 0.1 and 0.8.

For the hidden layer

$$v_{ji}^{l+1} \leftarrow v_{ji}^{l} + \eta \triangle v_{ji}^{l} + \alpha \triangle v_{ji}^{l-1}, \tag{3.9}$$

where $\triangle v_{ji}^{l} = y_j (1 - y_j) x_i \sum_{k=1}^{K} \delta_{ok} w_{kj}^{l}$ for $i = 1, 2, ..., I$, and x_i is the value of the ith input variable.

For a given error tolerance E_{max}, learning rate η, momentum α and maximum learning cycle, the ANN with randomly initialized weights is trained through repeated presentation of the training patterns until the error goal or maximum training cycle is reached.

3.2 Development of ANN-Based State Estimation Model

The state forecasting and filtering steps have been attempted by using FLN and TDNN, respectively. Past history of state variables up to time (k) has been used to forecast the states at time $(k+1)$.

The inputs to the FLN are real-time measurements consisting of real and reactive power bus injections and line flows, whereas the desired outputs are the state variables. The output of the FLN computed for time (k) has been used as the input to the TDNN. The Time Delay Neural Network (TDNN) takes these state variables from FLN at time (k) and forecasts the system states for time $(k+1)$.

Two neural networks proposed for state estimation were explained in this chapter. To validate the results taken from the proposed networks, three different test power systems were investigated. In the next chapter the result of each case is represented.

Chapter 4

The Proposed Neural Network Design

Chapter Three demonstrated the notion of two neural networks built for state estimation of power systems. The first step is filtering, which is accomplished by Functional Link Networks (FLN). The second step is forecasting, which is achieved by Time Delay Neural Networks (TDNN). This chapter consists of a description of each NN structure. In Chapter Two, four power systems were explained in detail. Three of them were used as testing benchmarks in state estimation study in this chapter. All three systems were simulated by MATLAB Power System Toolbox to generate input/output pair patterns for training and testing neural networks.

Each test system was simulated under different loading conditions in order to obtain the training data set. The pair of input/output, $(p, q)/(v, \theta)$, of each bus was collected after each simulation to build the data base. The obtained data set contained the necessary information to help NNs generalize the estimation problem since all the possible loading conditions were considered.

This chapter presents the process and also the condition under which the data is

generated. Each network was tested by a novel pattern to examine its performance. The result is presented at the end of each section.

4.1 The Neural Network Structure

4.1.1 Data Selection

Most of the necessary information for determining the state of a power system is usually contained in the voltage and power waveforms. Therefore, real and reactive power of buses, which are also the most available measurements, were selected as inputs to the Functional Link Network. Voltage magnitude and phase angle of the corresponding buses were used as targets (desired outputs) of the FLN.

In the forecasting step, the output of the FLN at time instant (k) plus two or three time delay units were used as inputs to the Time Delay Neural Network (TDNN). Adding delay units would increase the time of training process. The number of time delays was determined depending on the complexity of the system. The forecasted value of voltage vector at time instant $(k+1)$ was considered as the output of the TDNN.

4.1.2 Data Preparation

As explained in Chapter Three, the input data to Functional Link Network were enhanced before feeding them to the NN. Each component of the input (real and reactive power of each bus) multiplied the entire input vector. Figure 4.1 illustrates this process. Outputs of FLN were voltage magnitudes and phase angles.

"Neural network training can be done more efficiently if certain preprocessing steps are performed on the network inputs and targets" [17]. It is often useful to scale the

Figure 4.1: Functional Link Network

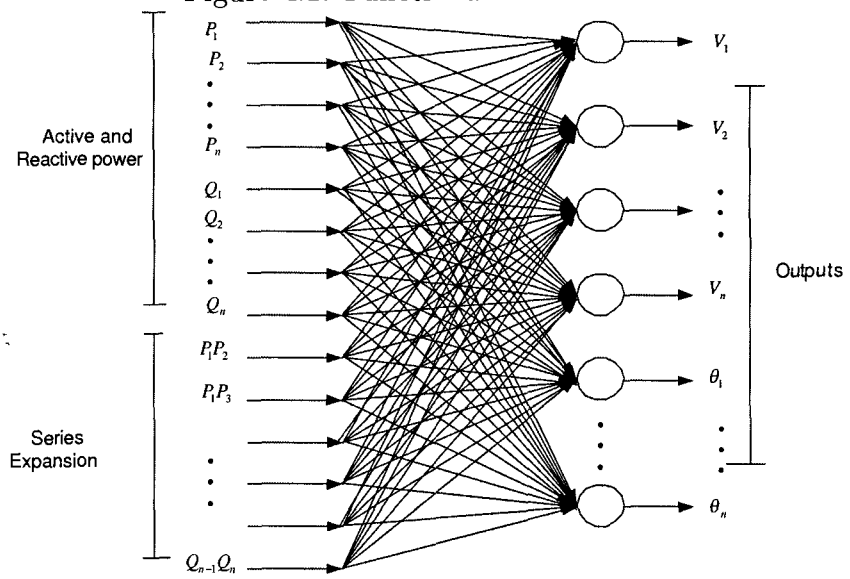

inputs and targets before training, so that they always fall within a specified range. The function "premnmx" in MATLAB was used to scale inputs and targets so that they would fall in the range [-1,1].

The following explains the structure of FLN and TDNN for each test system;

4.2 Single-machine-infinite-bus Test System

The first test power system was the single-machine-infinite-bus system. Training patterns for this case were generated using the load flow program of MATLAB Power System Toolbox. They were generated by varying the active and reactive load at $(P-V)$/generation buses linearly by 100% and for $(P-Q)$/load buses by 50%, thus covering a wide range of operating conditions. "The load curve at each bus was composed of a linear trend plus a random fluctuation (jitter)" [17]. The jitter was represented by a normal distribution random process. Figure 4.2 is a sample of this random fluctuation for the generation bus. As can be seen, the range of

power generation vary between 1(pu) and 3(pu) which is considered a wide range of operation.

Figure 4.2: Power generation variation of bus 1 in the single machine system

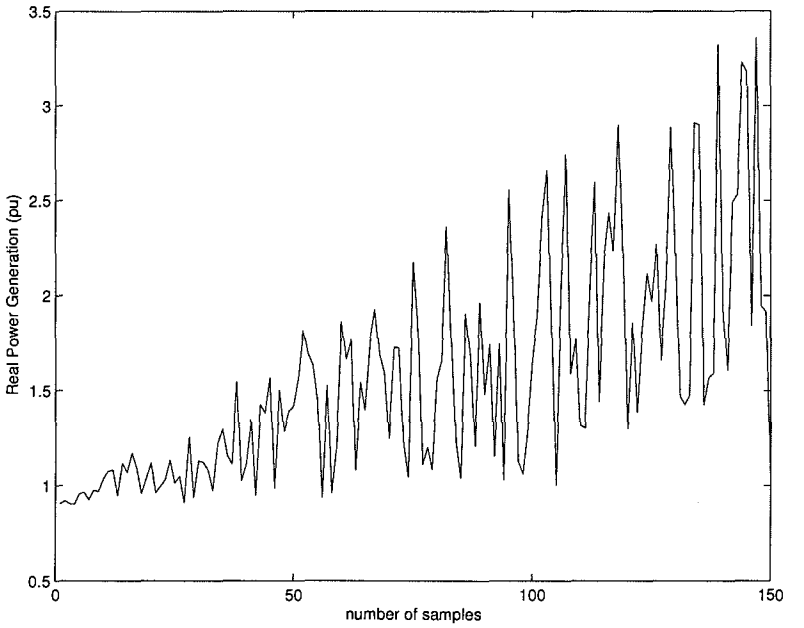

The training patterns, which consisted of real and reactive power of each bus at different load level, were inputs to the FLN. The corresponding voltage magnitude and phase angle were the outputs (targets) of the NN. Initially one neural network was considered for both voltage and angle. This network architecture did not have a satisfactory performance, hence, two separate neural networks were considered. Two FLN-TDNN sets were created. The purpose of one set was to evaluate the bus voltage and the other to evaluate the phase angle.

The following discusses the structure of each set with related results. Note that, MATLAB's Neural Network Toolbox was used to build neural networks in this study. The functions indicated by quotations are MATLAB's functions

4.2.1 Topology of FLN

As explained in Chapter Three, the Functional Link Network was built using a flat net. This network consisted of a single layer, no hidden layer, with the "DOT Product" weight function and a linear transfer function.

1. Input layer

   The number of inputs for this system was 21 which was consisted of real and reactive power of all buses and their second-order outer product. In the single machine system, there are three buses where each has one real and one reactive power value. Therefore, $3 \times 2 = 6$ is the original number of inputs according to Figure 4.1. Considering only second order outer product of these inputs, the sum of arithmetic progression formula gives $6/2(2 \times 1 + (6-1) \times 1) = 21$, which is the total number of inputs.

2. Output layer

   As mentioned before, two FLNs were developed to evaluate voltage and angle of each bus. Each networks had 3 outputs, which was the number of buses in the single-machine system.

3. Widrow-Hoff learning algorithm

   The learning in a neural network means finding an appropriate set of weights to produce the desired outputs when presented with novel inputs. "The learning algorithm used in this part for both networks is Widrow-Hoff weight/bias learning, also known as delta or least-mean-squared (LMS) rule. It is a method of finding the desired weight vector that can successfully associate each input vector with its desired output" [35]. The LMS algorithm can be expressed by

Equation 4.1

$$w(t+1) = w(t) + 2\mu\varepsilon_k x_k, \tag{4.1}$$

where $w(t)$ is the weight vector, ε_k is the error, and μ is the parameter that determines the stability and speed of convergence of the weight vector toward the minimum-error value. The learning rate or (μ) was taken as 1e-4 for the voltage-FLN and 1e-3 for the angle-FLN.

4. FLN training

For training the FLNs, 200 data patterns were generated by varying the loads at each bus covering a wide operating range of the base case load curve. In order to empower the generalization property of neural networks, these generated training data patterns were shuffled several times. The voltage-FLN was trained for 5000 epochs (one epoch is a single training pass through all training patterns), and the angle-FLN for 4000 epochs. Then they were tested with novel input patterns.

Out of 200 patterns, 180 of them were used for training and 20 patterns were used for testing. Figure 4.3 compares the output of FLN with the true value for 7 randomly selected testing points. Table 4.1 shows the exact value of each point in Figure 4.3.

Table 4.1: Voltage values corresponding to Figure 4.3

Voltage of bus 3	7 samples of testing points						
FLN	1.0342	1.0339	1.0335	1.0332	1.0329	1.0325	1.0322
True value	1.0344	1.0341	1.0338	1.0335	1.0332	1.0329	1.0326

Figure 4.3: Voltage comparison between the FLN output and the real value for bus 3

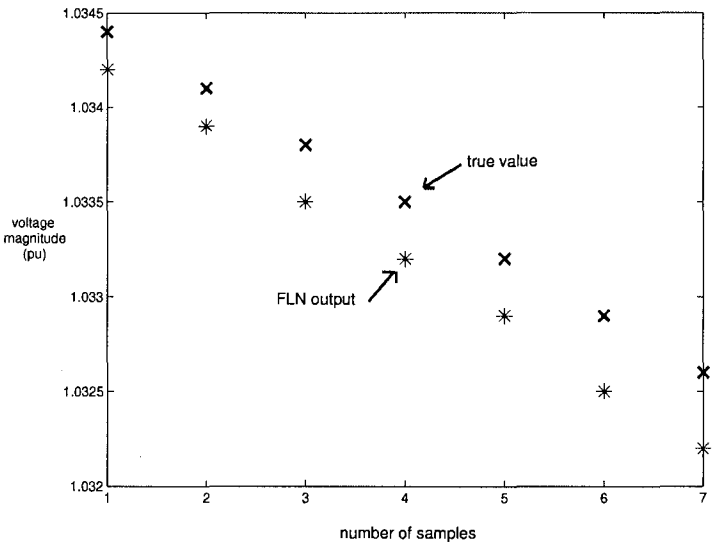

5. Validation Results

Table 4.2 also represents the result of the Functional Link Network compared with those obtained from the MATLAB load flow program (true values) and the corresponding maximum absolute error. Note that only the voltage of bus 3 is presented in the table because two other buses are voltage controlled or (P-V) buses and their voltage is fixed for all loading conditions. It can be seen that, both FLNs can solve state estimation with less than 2% error.

The demand for electricity is continuously changing with various daily, weekly and seasonal influences. A testing pattern was built to model a typical daily

Table 4.2: Voltage comparison between FLN outputs and true values

	True value	FLN output	Absolute error
Bus 3 voltage	1.0358	1.0358	0
Bus 1 angle	26.6966	26.1028	0.5937
Bus 2 angle	0	0	0
Bus 3 angle	17.6876	17.2967	0.3909

load variation of a power system. The performance of two FLNs were tested using the data pattern. Figures 4.4 and 4.5 show the result and compares them with actual values.

The voltage variation due to load drop in bus 1 in the single-machine system is presented in Figures 4.4 and 4.5. Both Figures show how closely FLN output follows the real value.

4.2.2 Topology of TDNN

A feed-forward back propagation network with one hidden layer and one output layer was used for the state forecasting step. Two time-delay neural networks were developed to serve our purpose. One to forecast the voltage magnitude, called voltage-TDNN, and angle-TDNN to forecast the phase angle.

In both TDNN, the output had a finite temporal dependence on the input, that is $\hat{v}(k+1)$ is evaluated using $v(k), v(k-1), v(k-2)$ and also $\hat{\theta}(k+1)$ is evaluated using $\theta(k), \theta(k-1), \theta(k-2)$ where $\hat{v}(k+1)$ and $\hat{\theta}(k+1)$ were the estimate of voltage magnitude and phase angle respectively, $[v(k), v(k-1), v(k-2)]$, and $[\theta(k), \theta(k-1), \theta(k-2)]$ were the sliding window which consisted of three time delay units for voltage and angle input respectively.

In case of single-machine system only the voltage of bus 3 was considered because other buses had a fixed voltage magnitude. Therefore, TDNN for single-machine system has one input with three time delay units and one corresponding output.

1. Hidden layer

   Determining the number of hidden nodes in the hidden layer was based on trial and error since it is not always straightforward. The goal is to use as few neurons as possible because adding one neuron increases the training time substantially.

Figure 4.4: Voltage variation of bus 3 due to load drop

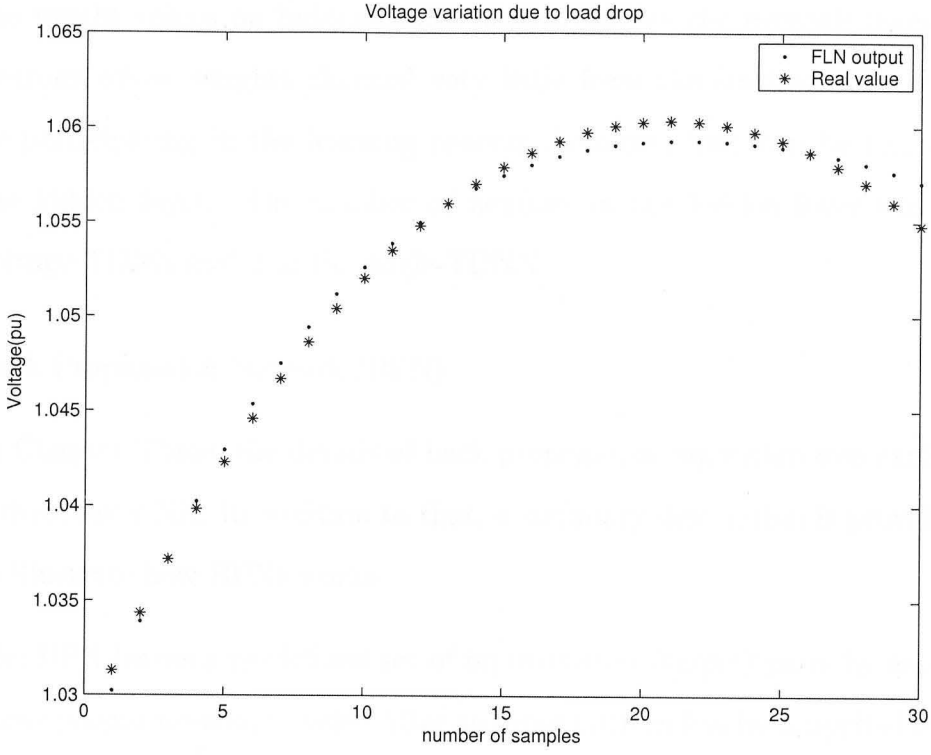

Figure 4.5: Angle variation of bus 3 due to load drop

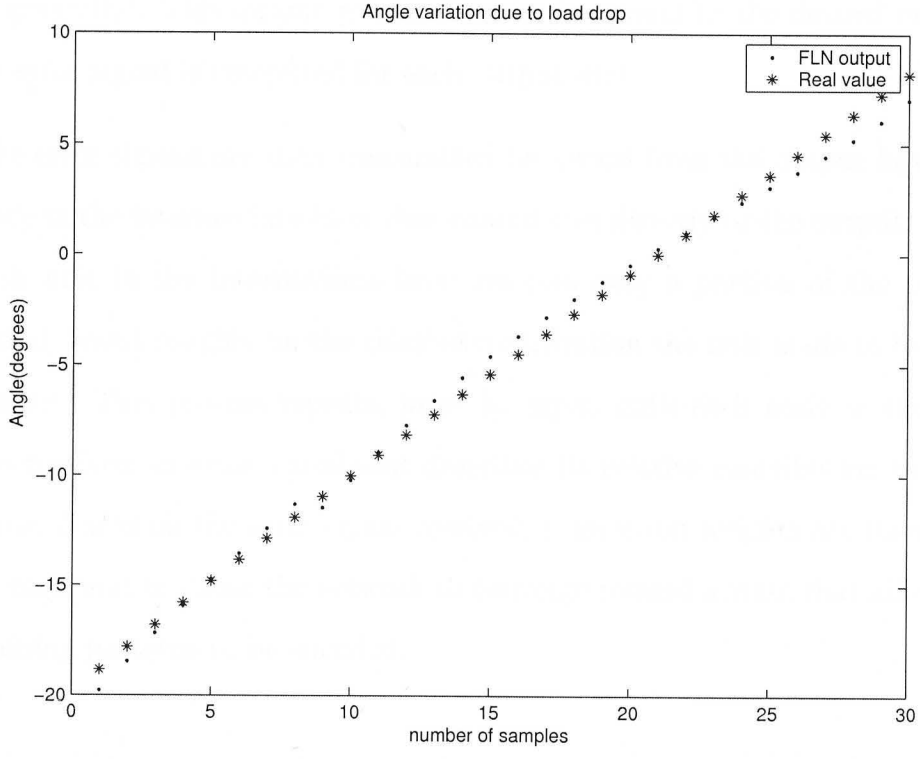

Another way was also tried to determine the number of neurons by examining the weight values on hidden nodes periodically as the network trains. Those neurons whose weights changed very little from the starting value might not be participating in the learning process therefore, they can be removed from the hidden layer. The number of neurons in the hidden layer was 1 in the voltage-TDNN and 2 in the angle-TDNN.

2. Back Propagation Network (BPN)

In Chapter Three, the details of back propagation algorithm was explained for a three-layer NN. In addition to that, a summary description is provided below to illustrate how BPNs works.

The BPN learns a predefined set of input-output (target) pairs by using a two-phase propagate-adapt cycle. After an input pattern has been applied to the first layer of the network, it is propagated through each upper layer until an output is generated. This output pattern is then compared to the desired output and an error signal is computed for each output unit.

The error signals are then transmitted backward from the output layer to each node in the intermediate layer that contributes directly to the output. However, each unit in the intermediate layer receives only a portion of the total error signal, based roughly on the relative contribution the unit made to the original output. This process repeats, layer by layer, until each node in the network has received an error signal that describes its relative contribution to the total error. Based on the error signal received, connection weights are then updated by each unit to cause the network to converge toward a state that allows all the training patterns to be encoded.

Figure 4.6: Voltage comparison between TDNN outputs and true values for bus 3

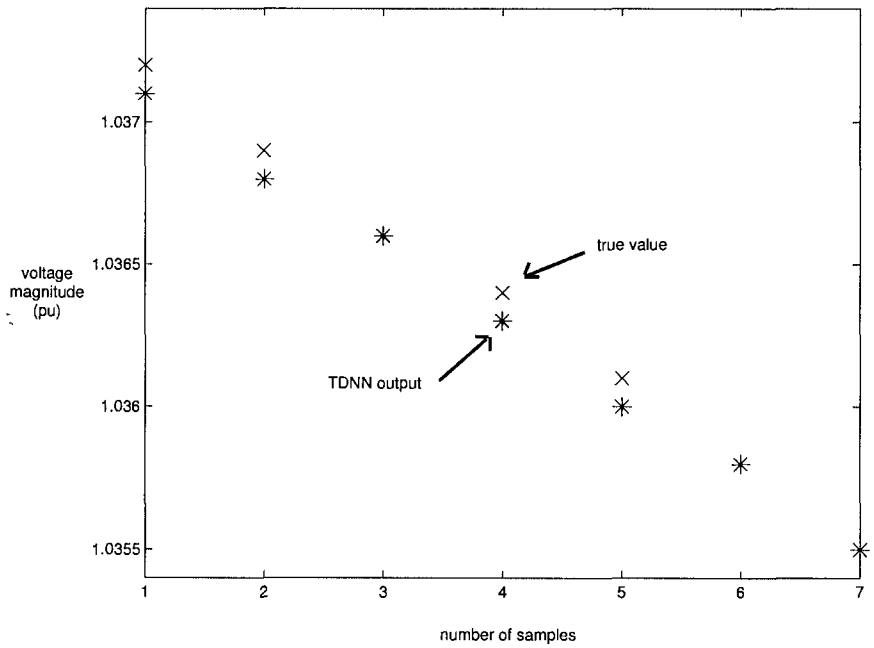

3. TDNN training

The same 200 data patterns, used in FLN section, were used to train and test TDNNs. Out of these, 180 patterns were used to train the neural network, and the remaining 20 patterns were used to test the accuracy and robustness of the ANN. The input to the voltage-TDNN is the voltage of bus 3 plus three time delay units. In case of angle-TDNN, the angle of all three buses with three time delay units were considered as inputs and the forecasted angle of each bus was the output.

The learning rate (μ) of 1e-3 was used because with larger values convergence did not take place. The state forecasting results are given in Table 4.3 and Figure 4.6 for 7 randomly selected testing points.

Table 4.3 shows the value of each point in the Figure 4.6 to clarify the precision

Table 4.3: Voltage comparison between TDNN outputs and true values for bus 3

Voltage magnitude	7 samples of testing patterns						
TDNN	1.0371	1.0368	1.0366	1.0363	1.0360	1.0358	1.0355
True value	1.0372	1.0369	1.0366	1.0364	1.0361	1.0358	1.0355

Table 4.4: Angle comparison between angle-TDNN and true values

	True value	TDNN output	Absolute error
Bus angle 1	21.3308	21.3385	0.0078
Bus angle 2	0	0	0
Bus angle 3	14.1205	14.1216	0.0011

of TDNN.

4. Validation Results

   For training and testing the angle TDNN, another 200 patterns were generated using the same method described before. Out of these, 180 patterns were used to train the neural network and the remaining 20 patterns were used to test the accuracy and robustness of the ANN. Table 4.4 presents the result of the angle-TDNN compared with those obtained from the MATLAB load flow program and the corresponding maximum absolute error. Table 4.4 also shows that the designed neural network can forecast the angle of all buses with absolute error less than 1e-2.

4.3 3-machine Test System

The 3-machine-9-bus system was another test system considered in our study. The one-line diagram and a description of each element of the system are explained in Chapter Two. The same topology and training/learning algorithm as explained in previous section were also used for three-machine system. To avoid the repetitive

explanation of each neural network, only those parts which are different from the single-machine system is described here.

4.3.1 FLN Structure

The number of inputs of FLN for the 3-machine system was 171 which consisted of real and reactive power of load buses and their second-order outer product. There are 9 buses in the 3-machine system with active and reactive powers designated to each bus. Therefore, the original number of inputs were $9 \times 2 = 18$. The enhanced representation of these inputs consisted of their second order outer product, which made the total number of inputs $18/2(2 \times 1 + (18 - 1) \times 1) = 171$.

Voltage of each bus, 9 in total, were considered as voltage-FLN outputs. After monitoring the change of weight value for each node as the network was trained, we realized that the first three outputs, which are the (P-V) buses, did not participate in the learning process. The reason is that they are voltage controlled buses and their voltage magnitudes are fixed for all loading conditions. Therefore, only the voltage of load buses, bus 4 to 9, were considered. For angle-FLN the phase angles of all 9 buses were considered.

The learning rate (μ) was taken as 1e-4 for the voltage-FLN network and 1e-3 for the angle-FLN. The same training/learning algorithm (as explained before) was used for both NNs.

The training patterns were generated for base case using the MATLAB load flow program by varying the load at (P-V) buses linearly by 100%, and (P-Q) buses by 50% covering a wide range of operation. Any operating condition beyond or below this range is unacceptable since the load flow algorithm does not converge.

- FLN results

  For training both FLNs, 250 patterns were generated by varying the loads at each bus covering a wide operating range of the base case load curve. Out of 250 patterns, 200 were used for training and 50 patterns were used for testing. After training for 4000 epochs, the voltage-FLN was tested for a novel input pattern. Figure 4.7 shows the result for 8 randomly data points. Tables in 4.5 are the corresponding values of each point in Figure 4.7.

Figure 4.7: Voltage comparison between FLN outputs and true values for load buses

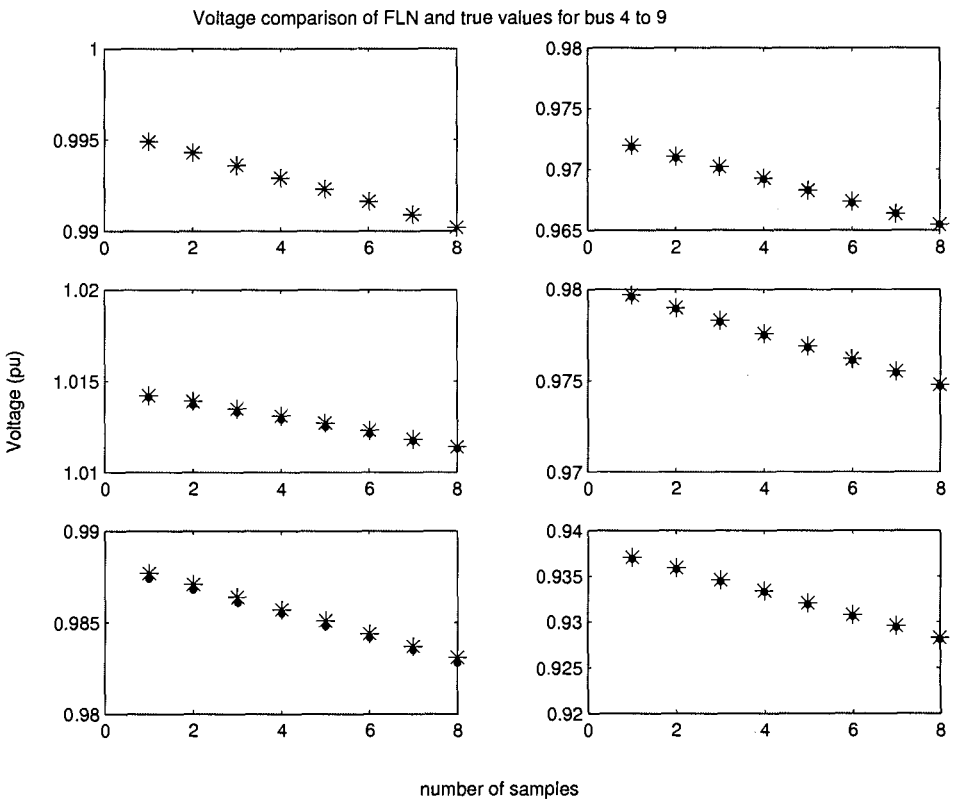

The FLN was able to estimate state variables with less than 0.1% error. The results of the FLN and those obtained from the load flow program with the

Table 4.5: Voltage values corresponding to Figure 4.7

Bus no.	8 samples of testing patterns for FLN							
4	0.9949	0.9942	0.9936	0.9929	0.9923	0.9916	0.9909	0.9902
5	0.9719	0.9710	0.9701	0.9692	0.9683	0.9673	0.9664	0.9655
6	1.0141	1.0137	1.0133	1.0129	1.0125	1.0121	1.0117	1.0113
7	0.9796	0.9789	0.9782	0.9775	0.9768	0.9761	0.9754	0.9747
8	0.9874	0.9868	0.9861	0.9855	0.9848	0.9842	0.9835	0.9828
9	0.9369	0.9357	0.9344	0.9332	0.9319	0.9306	0.9294	0.9281
Bus no.	corresponding true values							
4	0.9949	0.9943	0.9936	0.9929	0.9923	0.9916	0.9909	0.9902
5	0.9720	0.9711	0.9702	0.9693	0.9683	0.9674	0.9664	0.9655
6	1.0142	1.0139	1.0135	1.0131	1.0127	1.0123	1.0118	1.0114
7	0.9797	0.9790	0.9783	0.9776	0.9769	0.9762	0.9755	0.9748
8	0.9877	0.9871	0.9864	0.9857	0.9851	0.9844	0.9837	0.9831
9	0.9371	0.9359	0.9346	0.9334	0.9321	0.9308	0.9296	0.9283

corresponding maximum absolute error are presented in Table 4.6.

4.3.2 TDNN Structure

There were two time-delay neural networks created to estimate the voltage magnitude, called voltage-TDNN, and angle-TDNN to estimate the phase angle. The output variable, voltage magnitude and phase angle, were estimated using the past values of the variable. The sliding window consisted of two time delay units for each input.

The number of hidden nodes was 3, which was obtained based on trial and error. The learning rate (μ) of 1e-5 was used to make sure that the network would settle to a proper solution.

For training and testing the voltage-TDNN, 200 patterns were generated. The same data generating process as used in FLN was used for TDNN. Out of these 200 patterns, 180 patterns were used to train the neural network, and the remaining 20 patterns were used to test the accuracy and robustness of the NN.

Table 4.6: Voltage comparison between FLN outputs and true values

Voltage	FLN output	True value	Absolute error
Bus 4	0.9980	0.9981	0.0001
Bus 5	0.9763	0.9765	0.0002
Bus 6	1.0159	1.0161	0.0002
Bus 7	0.9829	0.9831	0.0002
Bus 8	0.9905	0.9908	0.0003
Bus 9	0.9429	0.9431	0.0002
Angle	**FLN output**	**True value**	**Absolute error**
Bus 1	0	0	0
Bus 2	24.3748	24.4965	0.1217
Bus 3	15.2248	15.3184	0.0936
Bus 4	0.2351	0.2571	0.0220
Bus 5	0.5956	0.6300	0.0344
Bus 6	11.5412	11.6180	0.0768
Bus 7	11.6750	11.7535	0.0785
Bus 8	16.6271	16.7161	0.0890
Bus 9	0.9056	0.9451	0.0395

- TDNN Results

The output of voltage-TDNN consisted of forecasted voltage of load buses and the output of angle-TDNN consisted of forecasted angle of all buses. The result of voltage forecasting is given in Figure 4.8 and Table 4.8. Figure 4.8 compares the output of voltage-TDNN with true values and Table 4.8 presents the value of corresponding points in Figure 4.8.

As it can be seen in Figure 4.8, the first three plots are the (P-V) buses with fixed voltage; therefore the neural network was not able to estimate their voltage properly. The result of angle-TDNN is shown in Figure 4.9. Table 4.8 shows the value of each point in Figure 4.9.

Table 4.9 also shows the result of both TDNNs compared with those obtained from the load flow program and the maximum absolute error.

Figure 4.8: Voltage comparison between TDNN outputs and true values for all buses

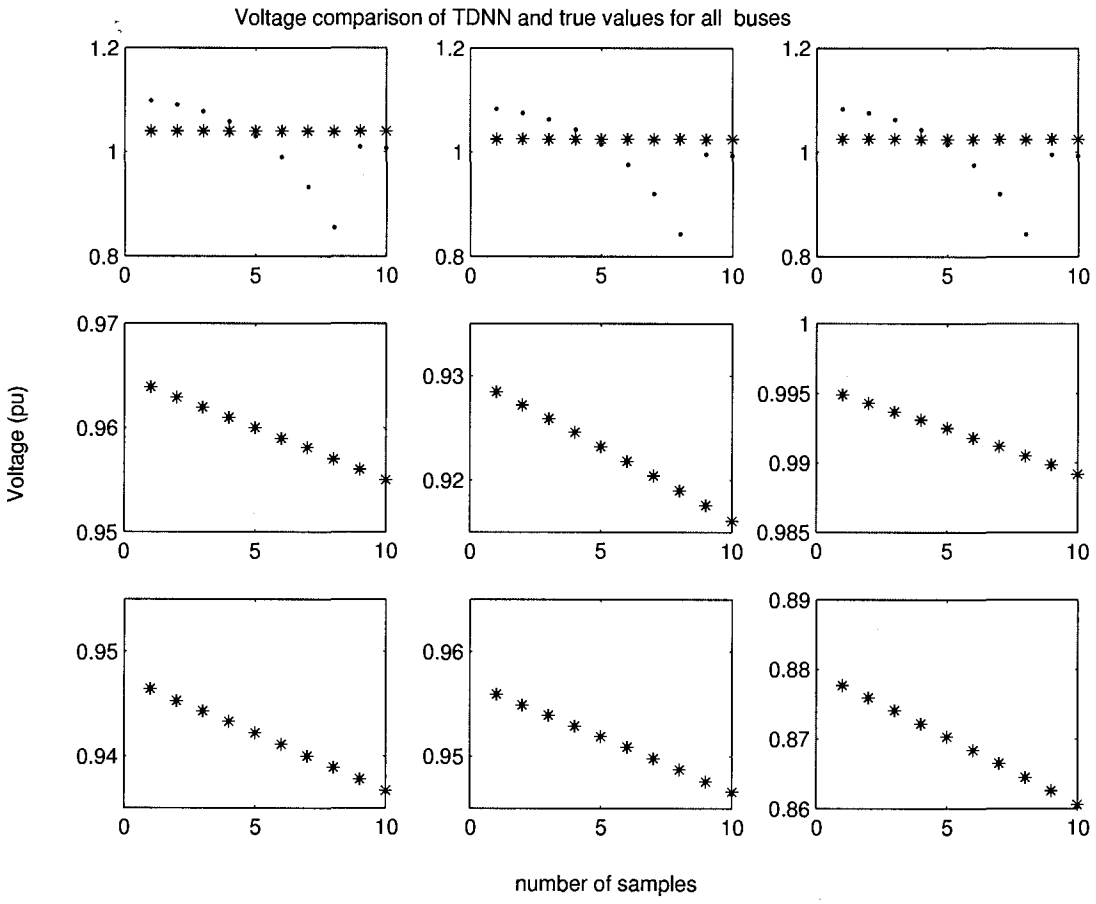

Table 4.7: Voltage values corresponding to Figure 4.8

Bus no.	8 samples of testing patterns for TDNN							
1	1.0988	1.0910	1.0782	1.0588	1.0304	0.9900	0.9334	0.8553
2	1.0833	1.0756	1.0630	1.0438	1.0158	0.9760	0.9202	0.8432
3	1.0834	1.0756	1.0630	1.0439	1.0159	0.9760	0.9203	0.8432
4	0.9638	0.9629	0.9619	0.9610	0.9601	0.9591	0.9582	0.9572
5	0.9284	0.9271	0.9258	0.9245	0.9232	0.9219	0.9206	0.9192
6	0.9949	0.9943	0.9937	0.9931	0.9925	0.9918	0.9912	0.9905
7	0.9463	0.9453	0.9443	0.9433	0.9422	0.9412	0.9401	0.9391
8	0.9559	0.9550	0.9540	0.9530	0.9520	0.9509	0.9498	0.9487
9	0.8776	0.8758	0.8740	0.8722	0.8704	0.8686	0.8668	0.8649
Bus no.	Corresponding true values to TDNN outputs							
1	1.0400	1.0400	1.0400	1.0400	1.0400	1.0400	1.0400	1.0400
2	1.0253	1.0253	1.0253	1.0253	1.0253	1.0253	1.0253	1.0253
3	1.0254	1.0254	1.0254	1.0254	1.0254	1.0254	1.0254	1.0254
4	0.9639	0.9629	0.9620	0.9610	0.9600	0.9590	0.9581	0.9570
5	0.9285	0.9272	0.9259	0.9246	0.9232	0.9218	0.9204	0.9190
6	0.9949	0.9943	0.9937	0.9931	0.9925	0.9918	0.9912	0.9905
7	0.9464	0.9453	0.9443	0.9433	0.9422	0.9411	0.9400	0.9389
8	0.9559	0.9549	0.9539	0.9529	0.9519	0.9509	0.9498	0.9487
9	0.8777	0.8759	0.8741	0.8722	0.8703	0.8684	0.8665	0.8645

Figure 4.9: Angle comparison between TDNN outputs and true values for all buses

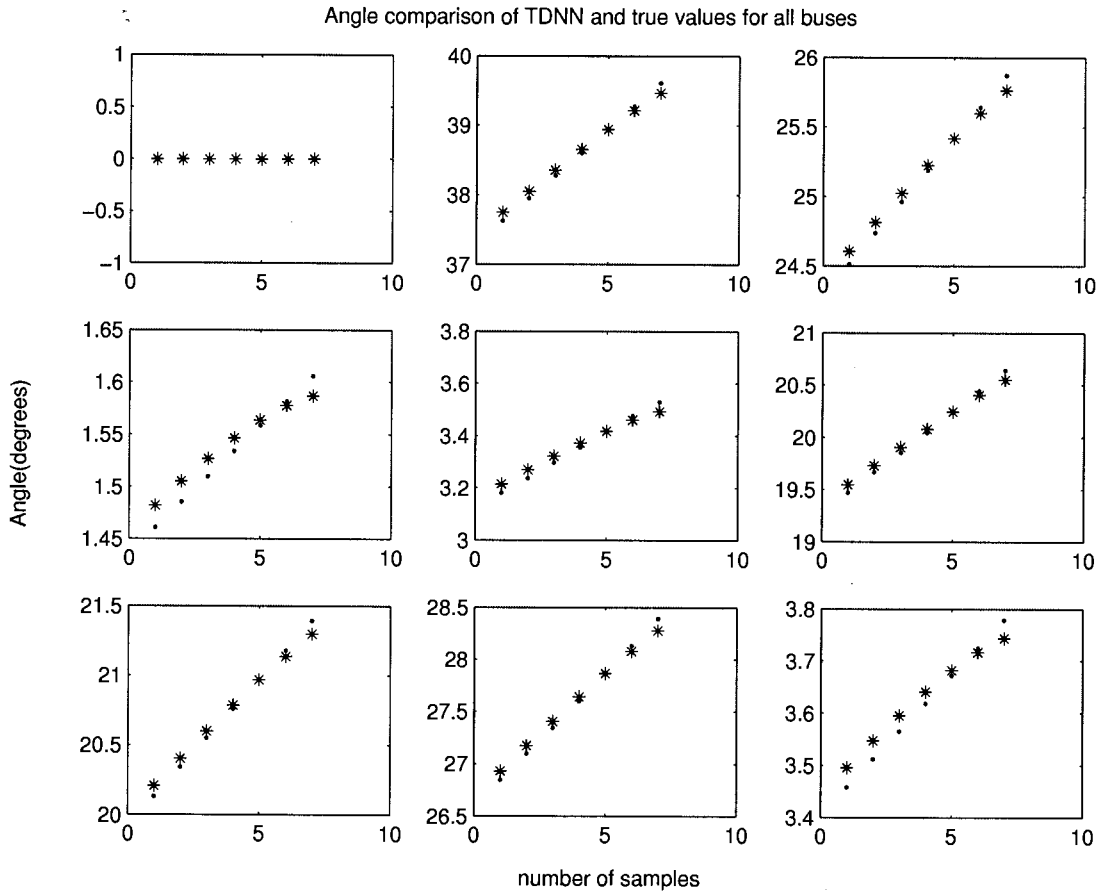

Table 4.8: Phase angle values corresponding to Figure 4.9

Bus no.	7 samples of testing patterns for TDNN						
1	0	0	0	0	0	0	0
2	37.7454	38.0548	38.3589	38.6556	38.9419	39.2141	39.4671
3	24.6041	24.8166	25.0246	25.2264	25.4196	25.6013	25.7671
4	1.4820	1.5051	1.5267	1.5465	1.5637	1.5775	1.5867
5	3.2152	3.2699	3.3226	3.3725	3.4188	3.4601	3.4948
6	19.5469	19.7295	19.9085	20.0824	20.2494	20.4069	20.5516
7	20.2094	20.4058	20.5986	20.7864	20.9673	21.1389	21.2976
8	26.9325	27.1729	27.4096	27.6410	27.8649	28.0788	28.2788
9	3.4960	3.5472	3.5960	3.6414	3.6824	3.7172	3.7439
Bus no.	Corresponding true values to TDNN outputs						
1	0	0	0	0	0	0	0
2	37.6274	37.9530	38.2806	38.6104	38.9423	39.2764	39.6129
3	24.5133	24.7370	24.9619	25.1881	25.4154	25.6441	25.8740
4	1.4609	1.4854	1.5098	1.5341	1.5582	1.5822	1.6060
5	3.1815	3.2395	3.2975	3.3556	3.4137	3.4720	3.5304
6	19.4713	19.6638	19.8575	20.0523	20.2482	20.4454	20.6438
7	20.1316	20.3389	20.5474	20.7573	20.9685	21.1811	21.3952
8	26.8444	27.0980	27.3533	27.6105	27.8694	28.1303	28.3931
9	3.4582	3.5119	3.5655	3.6189	3.6722	3.7253	3.7783

Table 4.9: Voltage and angle comparison of TDNNs with true values

Voltage	TDNN output	True value	Absolute error
Bus 4	1.0494	1.0494	0
Bus 5	1.0486	1.0486	0
Bus 6	1.0407	1.0407	0
Bus 7	1.0347	1.0347	0
Bus 8	1.0338	1.0338	0
Bus 9	1.0400	1.0400	0
Angle	TDNN output	True value	Absolute error
Bus 1	0	0	0
Bus 2	-7.9873	-7.9873	0
Bus 3	-8.4946	-8.4946	0
Bus 4	-4.0498	-4.0498	0
Bus 5	-7.0846	-7.0846	0
Bus 6	-8.4946	-8.4946	0
Bus 7	-9.3257	-9.3257	0
Bus 8	-7.9873	-7.9873	0
Bus 9	-7.2418	-7.2418	0

4.4 19-machine Test System

The 19-machine system was the largest test system used for our study. Due to the complexity of this system, the operating range was tighter than two previous cases. Data patterns were generated by varying the load at each bus, from 70% to 110% of the base case, to cover an acceptable range of operating conditions. The load flow algorithm did not converge for loading levels beyond the mentioned range.

1. FLN Results

   The number of inputs to FLN was 3570 for the 19-machine system. The input consisted of real and reactive power of each bus and their second-order outer products. In enhanced representation by considering the second order product of the original inputs, we arrived at $84/2(2 \times 1 + (84 - 1) \times 1) = 3570$. Like other test systems, only voltage of load buses were considered as outputs of

Figure 4.10: Voltage-FLN response to generation increase at bus 15

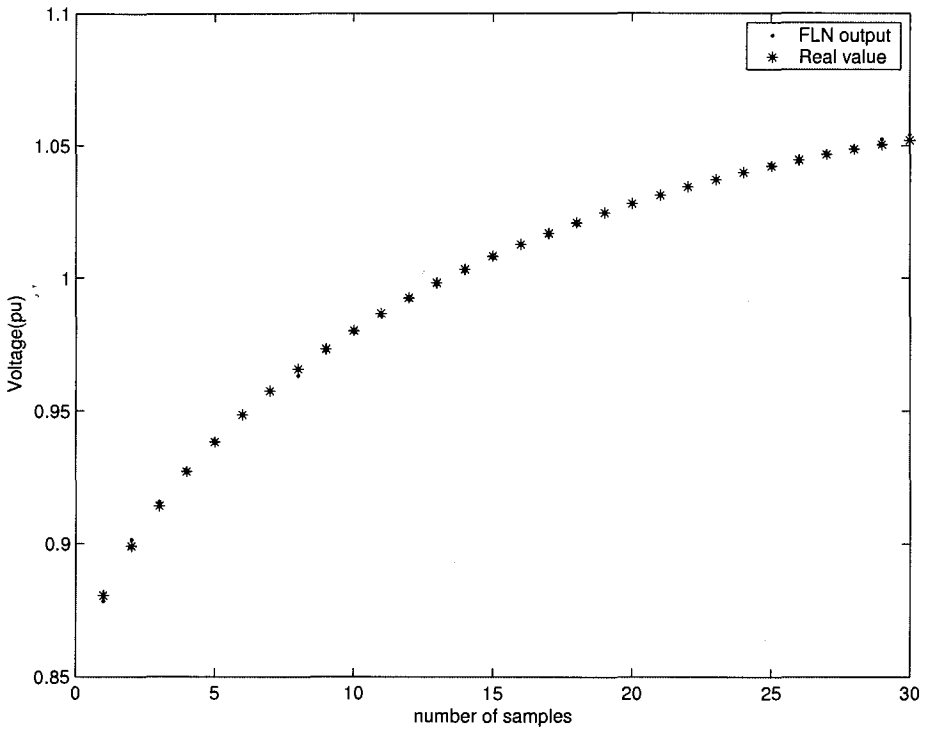

voltage-FLN. The training/learning functions were the same as previous cases. The learning rate (μ) was taken as 1e-5 .

For training FLNs, 800 data patterns were generated where, 700 patterns were used for training and 100 patterns were used for testing. The FLN was able to estimate state variables with less than 1% error.

The results of FLNs compared with those obtained from the load flow program and their maximum absolute error are presented in Tables 4.10 and 4.11.

After training, both FLNs were tested for a novel input pattern. Figure 4.10 shows a sample voltage variation of bus 15, due to generation increase. The response of FLN to the mentioned pattern is shown in Figure 4.10.

Table 4.10: Voltage comparison between voltage-FLN outputs and true values

Voltage	FLN output	True value	Absolute error
Bus 20	1.0084	1.0078	0.0006
Bus 21	0.9985	0.9985	0
Bus 22	1	0.9997	0.0003
Bus 23	1.0434	1.0433	0
Bus 24	1.0431	1.0431	0
Bus 25	1.0128	1.0128	0
Bus 26	1.011	1.0109	0.0001
Bus 27	1.0137	1.0137	0
Bus 28	1.0141	1.0141	0
Bus 29	1.0262	1.0259	0.0003
Bus 30	1.0247	1.0243	0.0004
Bus 31	1.0171	1.0171	0
Bus 32	1.0272	1.0272	0.0001
Bus 33	1.0254	1.0254	0
Bus 34	1.0236	1.0236	0
Bus 35	1.033	1.033	0
Bus 36	1.0211	1.0209	0.0002
Bus 37	1.03	1.03	0
Bus 38	1.0351	1.0351	0
Bus 39	1.0387	1.0386	0
Bus 40	0.979	0.9777	0.0013
Bus 41	1.0349	1.0346	0.0003
Bus 42	1.0189	1.0185	0.0003

Table 4.11: Angle comparison between angle-FLN outputs and true values

Angle	FLN output	True value	Absolute error
Bus 1	0	0	0
Bus 2	27.0654	26.9928	0.0726
Bus 3	-49.8562	-50.4979	0.6417
Bus 4	-88.2939	-89.0819	0.7881
Bus 5	-55.9147	-56.4634	0.5487
Bus 6	8.8534	8.8121	0.0413
Bus 7	15.9695	15.9064	0.063
Bus 8	-13.5285	-13.7597	0.2312
Bus 9	22.1734	22.1014	0.072
Bus 10	-5.7947	-6.0091	0.2144
Bus 11	-48.2982	-48.9397	0.6415
Bus 12	-50.3828	-51.0298	0.647
Bus 13	24.4519	24.3829	0.069
Bus 14	-48.3997	-48.9417	0.542
Bus 15	5.7682	5.7312	0.037
Bus 16	7.4332	7.3938	0.0393
Bus 17	-2.0202	-2.0588	0.0387
Bus 18	-76.826	-77.594	0.768
Bus 19	-77.7801	-78.5588	0.7786
Bus 20	-53.857	-54.5141	0.6571
Bus 21	20.687	20.6235	0.0635
Bus 22	-58.7886	-59.3308	0.5421
Bus 23	15.2758	15.2138	0.062
Bus 24	-14.3232	-14.5561	0.2329
Bus 25	2.9126	2.8797	0.033
Bus 26	-2.6931	-2.7332	0.04
Bus 27	-94.4218	-95.1909	0.7691
Bus 28	-91.394	-92.1741	0.7801
Bus 29	-50.9967	-51.644	0.6473
Bus 30	-52.3709	-53.0228	0.6519
Bus 31	22.3145	22.2487	0.0658
Bus 32	-51.952	-52.5018	0.5498
Bus 33	3.9748	3.9404	0.0344
Bus 34	4.4101	4.3751	0.035
Bus 35	-2.2743	-2.3133	0.039
Bus 36	-84.6295	-85.4221	0.7926
Bus 37	-82.1877	-82.9761	0.7884
Bus 38	18.3862	18.3198	0.0665
Bus 39	-10.9206	-11.1459	0.2254
Bus 40	-47.955	-48.5599	0.6049
Bus 41	10.3876	10.3173	0.0702
Bus 42	-0.4407	-0.5101	0.0694

2. TDNN Results

Like previous cases, two TDNNs were developed to estimate the voltage and phase angle. For training and testing the voltage-TDNN, 800 patterns were generated with using the same process explained before. Out of these, 700 patterns were used to train the neural network, and the remaining 100 patterns were used to test the accuracy and robustness of the ANN.

The inputs to the voltage-TDNN were the voltage of load buses at time instant (k) plus two time delay units. For the angle-TDNN, phase angles of all buses were considered. The outputs of TDNNs were predicted values of the state variables at time $(k+1)$. The result for both TDNNs are given in Tables 4.12 and 4.13.

Table 4.12: Voltage comparison between voltage-TDNN output and true values

Voltage	TDNN output	True value	Absolute error
Bus 20	1.0187	1.0188	0.0001
Bus 21	1.0103	1.0104	0.0001
Bus 22	1.0193	1.0194	0.0001
Bus 23	1.0448	1.0448	0
Bus 24	1.0464	1.0464	0
Bus 25	1.0231	1.0232	0.0001
Bus 26	1.0252	1.0253	0.0001
Bus 27	1.0467	1.047	0.0017
Bus 28	1.035	1.0351	0.0001
Bus 29	1.0321	1.0321	0
Bus 30	1.0309	1.031	0.0001
Bus 31	1.0246	1.0246	0
Bus 32	1.0356	1.0356	0
Bus 33	1.0321	1.0322	0.0001
Bus 34	1.0309	1.0309	0
Bus 35	1.039	1.039	0
Bus 36	1.0355	1.0356	0.0001
Bus 37	1.0395	1.0395	0
Bus 38	1.0366	1.0366	0
Bus 39	1.0417	1.0417	0
Bus 40	1.0079	1.008	0.0001
Bus 41	1.0437	1.0437	0
Bus 42	1.0301	1.0302	0.0001

Table 4.13: Angle comparison between angle-TDNN outputs and true values

Angle	TDNN output	True value	Absolute error
Bus 1	-0.0001	0	0.0001
Bus 2	21.7352	21.7372	0.0019
Bus 3	-31.9332	-31.9384	0.0052
Bus 4	-61.3504	-61.3555	0.0051
Bus 5	-37.7305	-37.7351	0.0046
Bus 6	7.5424	7.5428	0.0004
Bus 7	13.5049	13.5061	0.0012
Bus 8	-8.1892	-8.1898	0.0006
Bus 9	18.5223	18.5233	0.001
Bus 10	-1.9267	-1.9272	0.0005
Bus 11	-30.682	-30.6836	0.0015
Bus 12	-32.3617	-32.3639	0.0022
Bus 13	19.6531	19.6546	0.0015
Bus 14	-31.7596	-31.7622	0.0027
Bus 15	5.0727	5.0728	0.0001
Bus 16	6.4067	6.407	0.0003
Bus 17	-1.1982	-1.1984	0.0002
Bus 18	-52.2579	-52.2614	0.0035
Bus 19	-53.0178	-53.0205	0.0027
Bus 20	-35.1596	-35.1614	0.0018
Bus 21	16.6328	16.6331	0.0003
Bus 22	-40.0119	-40.0167	0.0048
Bus 23	12.9439	12.9448	0.0009
Bus 24	-8.8332	-8.834	0.0008
Bus 25	2.7806	2.7807	0.0001
Bus 26	-1.7444	-1.7446	0.0002
Bus 27	-66.2281	-66.2337	0.0056
Bus 28	-63.8087	-63.8134	0.0047
Bus 29	-32.8662	-32.8701	0.0039
Bus 30	-33.9671	-33.9718	0.0047
Bus 31	17.9266	17.9283	0.0017
Bus 32	-34.6274	-34.6302	0.0028
Bus 33	3.6271	3.6272	0.0002
Bus 34	3.9734	3.9735	0.0001
Bus 35	-1.4101	-1.4103	0.0001
Bus 36	-58.5183	-58.524	0.0057
Bus 37	-56.5731	-56.5772	0.0041
Bus 38	15.4571	15.458	0.0009
Bus 39	-6.0828	-6.0836	0.0008
Bus 40	-31.1247	-31.1253	0.0006
Bus 41	9.3269	9.3271	0.0002
Bus 42	0.5328	0.5326	0.0001

Chapter 5

The Transient Energy Function

This Chapter presents a general introduction to the power system transient stability problem. The objective is to provide an overview of the power system stability phenomena and the analytical techniques applicable to transient stability analysis. The basic concept of direct methods such as transient energy function is presented.

5.1 Transient Stability

"Power system stability may be broadly defined as the ability of a power system to remain in a state of operating equilibrium under normal operating conditions and to regain an acceptable state of equilibrium after being subjected to a disturbance.

Since power systems rely on synchronous machines for generating electrical power, a necessary condition for satisfactory system operation is that all synchronous machines remain in synchronicity. Transient stability is the ability of the power system to maintain synchronism when subjected to a severe transient disturbance. A disturbance may be a small one in the form of load changes or a severe form such as

short-circuit on a transmission line or loss of a large generator, etc. The system response to such disturbances involves excursion of rotor angles, machine speed, bus voltages and other system variables" [19]. If the resulting variation between machines remains within certain bounds then the system is stable. The loss of synchronism will usually be evident within 2 to 3 seconds of the initial disturbance and it is influenced by the nonlinear characteristics of the power system. The following is a brief illustration of transient stability problem, identification of factors influencing it and a description of analytical techniques applicable to transient stability analysis.

5.1.1 The Swing Equation

For the purpose of analyzing the system response to large disturbances, simple models of power systems are used. All resistances are neglected. Generators are represented by the classical model as a constant voltage behind the direct-axis transient reactance, $X_{d'}$. The loads are modeled as constant admittances, and the input power from the prime mover, P_m, is assumed constant . These parameters constitute the classical representation of a power system which is derived from [23, 39]. The equation of motion or the swing equation in (pu) for machine i in a power system is of the form:

$$\frac{2H_i}{\omega_0}\frac{d^2\delta_i}{dt^2} = P_{mi} - P_{max_i}\sin\delta_i \tag{5.1}$$

Where

P_m=mechanical power input in (pu)

P_{max_i}=maximum electrical power output in (pu)

H=inertia constant in (MW.s/MVA)

ω_0=synchronous speed in (elec.rad/s)

δ=rotor angle in (elec.rad)

t=time in (s)

For an n-machine system, we can write n swing equations namely for $i = 1, ..., n$. Practical power systems have complex network structures. Accurate analysis of their transient stability requires detailed models for generating units and other equipment. "The most practical method of transient stability analysis is time-domain simulation in which the nonlinear differential equations are solved by using step-by-step numerical integration techniques to examine the behavior of the rotor angles. The most common numerical integration methods used in transient stability are Euler method, Runge-Kutta method and implicit integration methods. Solving second order differential equations for every single machine in the system is extremely time consuming and computationally intensive specially for large complex power system. To overcome this difficulty, direct methods were proposed" [19]. Direct methods determine stability without explicitly solving the system's differential equations. This approach is academically appealing and has received considerable attention. The next section describes the basic concepts on which the direct methods are based.

5.2 The Transient Energy

The transient energy approach can be described by considering a ball rolling on the inner surface of a bowl. "The area inside the bowl represents the region of stability, and the area outside, is the region of instability. The rim of the bowl has an irregular shape so different points on the rim have different heights. When the ball is sitting at the bottom of the bowl this state is referred to as the Stable Equilibrium Point (SEP). When the ball is pushed to one side (kinetic energy is injected into the system), it will roll up on the surface in the direction of the force. The point that ball will stop depends on the amount of energy injected to it. When the ball rolls up the kinetic energy is converted to the potential energy. If the ball converts all the kinetic

energy into potential energy before reaching the rim of the bowl then it will roll back and eventually will settle down at the stable equilibrium point due to friction forces. However, if the amount of injected kinetic energy is high enough to cause the ball to go over the rim then the ball will go to the instable region.

Power system stability has a similar concept to the rolling ball. Initially the system is operating at the stable equilibrium point. When a disturbance happens, the system gains kinetic energy and this energy causes the synchronous machines to accelerate. After removing the disturbance this kinetic energy is converted to potential energy. The stability of the power system is the ability of the system to absorb the potential energy of the post disturbance system" [19]. There is a maximum amount of energy that a power system can absorb which is called the critical energy. Assessment of transient stability requires:

1. Functions that describe the transient energy responsible for separation of one or more synchronous machines from the rest of the system.

2. An estimate of the critical energy required for the machines to lose synchronism

The energy function V describes the total system transient energy for the post disturbance system. "It is defined as

$$\begin{aligned} V &= \frac{1}{2}\sum_{i=1}^{n} J_i\omega_i^2 - \sum_{i=1}^{n} P'_{mi}\left(\theta_i - \theta_i^s\right) - \sum_{i=1}^{n-1}\sum_{j=i+1}^{n} E_iE_jB_{ij}\left(\cos\theta_{ij} - \cos\theta_{ij}^s\right) \\ &+ \sum_{i=1}^{n-1}\sum_{j=i+1}^{n}\left[\int_{\theta_i^s+\theta_j^s}^{\theta_i+\theta_j} E_iE_jG_{ij}\cos\theta_{ij}d\left(\theta_i+\theta_j\right)\right] \end{aligned} \tag{5.2}$$

where

θ_i^s=angle of bus i at the post disturbance SEP

$J_i = 2H_i\omega_0$=per unit moment of inertia of the i^{th}generator

E_i=voltage magnitude of the i^{th} generator

$P'_{mi} = P_{mi} - E_i^2 G_{ii}$ and $G_{ij} + jB_{ij}$ is the ij^{th} element of the admittance matrix.

The transient energy function consists of three terms, which can be physically interpreted as follows:

1. The first term is the transient kinetic energy: $V_{ke} = \frac{1}{2}\sum_{i=1}^{n} J_i\omega_i^2$

2. The remainder is the transient potential energy, which may be decomposed in the following two terms:

$$\begin{aligned} V_p &= -\sum_{i=1}^{n} P'_{mi}\left(\theta_i - \theta_i^s\right) - \sum_{i=1}^{n-1}\sum_{j=i+1}^{n} E_i E_j B_{ij}\left(\cos\theta_{ij} - \cos\theta_{ij}^s\right) \\ V_d &= +\sum_{i=1}^{n-1}\sum_{j=i+1}^{n}\left[\int_{\theta_i^s+\theta_j^s}^{\theta_i+\theta_j} E_i E_j G_{ij}\cos\theta_{ij}\, d\left(\theta_i + \theta_j\right)\right] \end{aligned} \tag{5.3}$$

First term in V_p is the change in rotor potential energy of all generators relative to Center of Inertia (COI) and the second term in V_p is the change in stored magnetic energy of all branches. V_d represents the change in dissipated energy of all branches.

For the application of the Transient Energy Function (TEF) method, it is convenient to describe the transient behavior of the system with the generator angles expressed with respect to the inertial center of all generators. The position of the Center of Inertia (COI) is defined as

$$\delta_{COI} \triangleq \frac{1}{H_T}\sum_{i=1}^{n} H_i\delta_i \tag{5.4}$$

where H_T is the sum of the inertia constants of all n generators in the system. The motion of the generators with respect to the COI reference frame can be expressed by defining

$$\theta_i = \delta_i - \delta_{COI}, \tag{5.5}$$

where δ_i is the angle of machine i and δ_{COI} is the position of the center of inertia" [19].

In the Center of Inertia (COI)representation, the physical meaning of the angles has not changed. "The difference between this notation and the original notation is that COI notation measures angles relative to a rotating reference frame whereas the original notation measures angles in reference to a stationary frame. Moreover, the transformation of the former equations into the center of Inertia coordinates provides a concise framework for the analysis of systems with transfer conductances" [10].

The transient stability assessment involves the following steps:

1. Calculation of the critical energy V_{cr}, which is the transient energy of the post fault system at the unstable clearing point.

2. Calculation of the total system energy at the instant of fault-clearing V_{cl}, which is the total energy of system at the fault clearing time.

3. Calculation of stability index: $V_{cr} - V_{cl}$. The system is stable if the stability index is positive.

The most difficult step in applying the TEF method is the calculation of V_{cr}. The above formulation is explained for the single-machine-infinite-bus in the following section.

5.2.1 One-machine-infinite-bus System

Consider a machine connected to an infinite bus through two parallel lines. Assume

Figure 5.1: Machine connected to an infinite bus

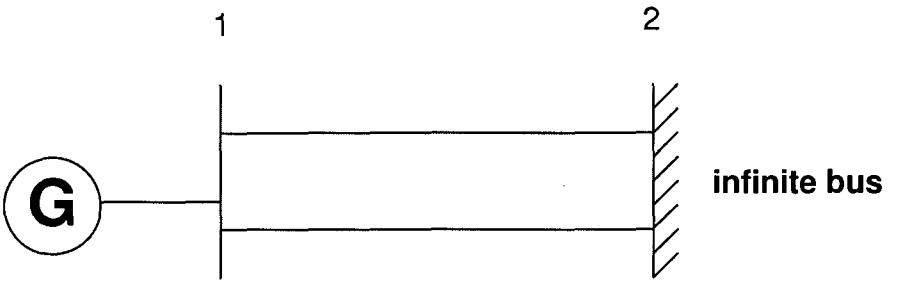

that a fault occurs at the middle of one of these lines. "Using the expression in the Equation 5.2, the total energy is defined by

$$\begin{aligned} V(\delta,\omega) &= V_{ke}(\omega) + V_{pe}(\delta) \\ V(\delta,\omega) &= \frac{1}{2}J\omega^2 - P_m(\delta - \delta_s) - P_{max}(\cos\delta - \cos\delta_s) \end{aligned} \tag{5.6}$$

Since the provided model is ideal and damping is neglected, the total energy is constant along the post-fault trajectory and it is equal to the total energy level at the clearing time. In other words, the only form of energy in the system are either kinetic energy or potential energy or the sum of these two energies, called the total energy. The latter is always constant at any time in the post-fault period. From the expression of the total energy, the transient energy method can easily be explained. Referring to the rolling ball case as depicted in Figure 5.2, an additional energy is injected into the system during the fault-on period, in the same way as the ball in the bowl is given energy when it is initially pushed. During the post-fault period, the total energy remains constant. In Figure 5.2, $A1$ represents the excess of kinetic energy injected into the system during the time period where the fault is on and $A2$ represents the transient energy margin. The stability of the system is determined by the ability of the post-fault system to convert the excess of kinetic energy $V_{ke}(\omega_c)$ [32]. If the kinetic energy at the clearing time exceeds the difference between the potential energy

Figure 5.2: TEF approach

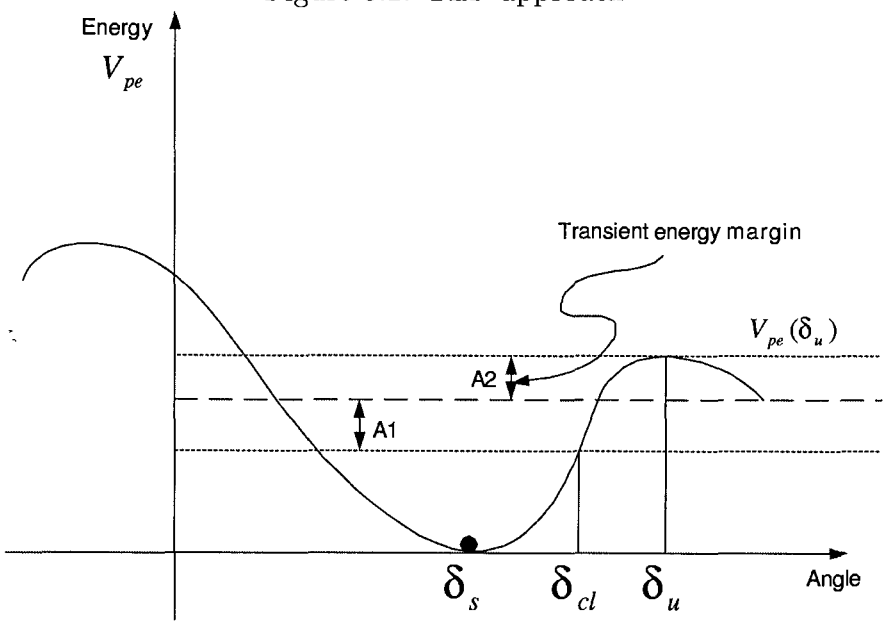

at clearing time and that at the unstable equilibrium point then the system will be unstable. Then we have

$$V_{ke}(\omega_{cl}) + V_{pe}(\delta_{cl}) < V_{pe}(\delta_u) \tag{5.7}$$

This inequality is the mathematical way of stating the Energy Approach. The above inequality, must hold not only at clearing time, but also during the post-fault time" [23].

$$V_{ke}(\omega) + V_{pe}(\delta) < V_{pe}(\delta_u) \tag{5.8}$$

According to the inequality 5.8 a transient stability criterion can be defined and extended to a multi machine system as follows: *Following a disturbance, the system is transiently stable if the total energy is less than the potential energy evaluated at the closest Unstable Equilibrium Point (UEP)* [39]. "The calculation of $V_{pe}(\delta_u)$ or V_{cr} in general, is the most difficult step in applying the TEF method. Three different

approaches are briefly described below.

5.3 The Closest Unstable Equilibrium Point (UEP) Approach

Unstable equilibrium point is one of the early TEF methods for transient stability analysis used to determine the smallest V_{cr}. UEPs are determined by solving the post-disturbance system steady-state equations with different initial values of bus angles. Then the system potential energy at each point is evaluated. The minimum potential energy is considered as the V_{cr}. For a power system this approach calculates the critical energy by implicitly assuming the worst fault; hence, the results are very conservative and usually of little practical value.

5.4 The Controlling UEP Approach

This method removes much of the above mentioned problem by computing the critical energy dependent on the fault location. This approach is based on the system trajectories for all critically stable cases that are closely related to the boundary of system separation. These points are called controlling unstable equilibrium points. Numerical problems are usually encountered when solving for the controlling UEP. The problem is formulated as a computationally intensive multi-dimensional optimization problem which may suffer from non-convergence under stressed conditions.

5.5 Sustained-fault Approach

To avoid the time-consuming controlling-UEP computation, the sustained fault method was developed" [19].

The critical energy is determined as follows:

1. A time domain simulation with a sustained fault is run until the system crosses the Potential Energy Boundary Surface (PEBS). The crossing of the PEBS is indicated by the potential energy reaching its maximum.

2. The potential energy at the crossing of the PEBS is taken as the critical energy for that particular fault location.

5.6 Limitation of Direct Methods

In spite of the many significant accomplishments in the direct methods, modeling limitations and the unreliability of computation techniques are major obstacles to their widespread practical use. On the other hand, time-domain method has an unlimited modeling capability but due to the step-by-step integration of differential equations, it is very slow and not suitable for on-line applications.

The best way appears to be the use of a hybrid approach in which the transient energy calculation is incorporated into the conventional time-domain simulation. This enhances the capability of simulations by computing the stability margin and minimizing the effort required in determining the stability limits. Chapter Six discusses this approach in detail.

Chapter 6

Stability Analysis with Hybrid Methods

Chapter Five introduces the concept of transient stability analysis, also known as Dynamic Security Assessment (DSA). It also presents different methods of transient stability assessment and their shortcomings. Recent research has shown interest in hybrid methods which seem to be the better compromise between accuracy in power system modeling and the necessity of obtaining reliable stability/instability indices [19, 20].

The name hybrid comes from the fact that it combines both the time domain and the TEF evaluation in solving stability problems and producing a stability index. "The hybrid method first computes actual system trajectory using time domain simulation, then calculates the degree of stability by evaluating the TEF index.

Security assessment consists of off-line and on-line procedures. Off-line procedures are planning tools used to verify if the system topology and the operating conditions will match the pre-defined security constraint. On-line procedures are activated during system operation aiming at verifying actual operating condition of the system.

On-line procedures have to be balanced between accuracy and short computational time. In fact, the system operator requires a fast and reliable answer to the question "secure/nonsecure" [42]. Transient stability analysis is the answer to this question.

Another very important issue in this context is the quantitative evaluation of stability/instability indices, i.e., the degree of stability. "Once the system has been evaluated in terms of stability/instability indices, a particular importance must be given to control actions aimed to improve the evaluated margins. These control actions may be defined as preventive actions or corrective actions. Examples of these actions are fast-valving, braking resistor insertion, generator re-scheduling etc" [1].

In this work, the hybrid method by means of neural networks is proposed to assess the stability of power systems. Stability analysis involves analysis of complex patterns of system behavior. Therefore, the ANN technique is used for fast pattern recognition and classification of dynamic system security status [36, 29]. The topology of the proposed neural network, the method of training, and the selection of input/output data are discussed later in this chapter.

6.1 Overview of the Implemented Hybrid Method

In this work, the concept of using neural networks is presented for power system transient stability assessment. "This concept combines the advantages of time domain simulation with capability of neural networks in fast pattern recognition to evaluate transient energy function. The level of security is calculated by using the Transient Energy Function (TEF) to evaluate energy margin (ΔV) which is called TEF index in our study. Hybrid methods can be based on:

1. Potential Energy (GPE) method [28]

2. Kinetic Energy (KE) method [27]

The hybrid method in this research is based on the generalized potential energy approach. The transient stability analysis begins with a load-flow calculation used as an initial condition followed by the dynamic simulation of the perturbed system. After the removal of the perturbation, the ANN-based procedure evaluates the Transient Energy Function (TEF) at each time sample" [1].

As explained in Chapter Five, angle and speed of the COI are used as reference for the dynamic analysis. The system instability is detected if machine angles were beyond the threshold of 180 degrees in the COI reference. The time instant that system loses stability is called critical time. The corresponding potential energy at critical time, which is assumed to be equal to the maximum of the PE, is known as V_{cr}.

The TEF index is calculated by subtracting the total transient energy function of the system at the fault clearing time from the total transient energy value at the critical clearing time, $TEF\ \ index = V_{cr} - V_{cl}$. This energy margin represents the distance of system stability from the unstable point. A low or negative value of this index indicates instability and a relatively high positive value of TEF index represents a secure condition.

Two test systems, which were explained in Chapter Two, are used in this part to validate the result of the study. The type, location, and the condition under which these perturbations were applied are discussed later for each test system separately.

6.2 The Proposed ANN Approach to TEF Evaluation

In order to achieve a neural network with transient energy approximation capability, a multi-layer feed-forward back- propagation network was used. The network consisted of three basic elements: 1) an organized topology of interconnected neurons; 2) a suitable learning algorithm, and 3) a method of recalling information.

6.2.1 Topology of the ANN

The topology of a multi-layer feed-forward ANN consisted of an input layer, one hidden layer, and an output layer.

1. The input layer

   Appropriate selection of input variables is the key to the success of ANN applications. Stability of a power system is mainly based on synchronization of all machines. Synchronism in machine speeds (also angles), (δ_i, ω_i), governs the stability of a power system. Thus, machine angle (rad) in COI reference and speed deviation (pu) of all buses were chosen as inputs to the ANN.

2. The Hidden Layer

   Computational power of the ANN is a result of the addition of hidden layers. But there are no general guidelines to determine the number of hidden layers and neurons. Many applications have proved that ANNs with one single hidden layer have sufficient capability of capturing complicated relations between input and output variables. Therefore one hidden layer with five neurons was determined. The number of neurons in the hidden layer was determined based on trial and

error.

3. The Output Layer

   Determination of the output layer is quite straight-forward. For TEF estimation, one output neuron is required. Appropriate scaling of the input and output variables was carried out and the network training set was preprocessed by normalizing the inputs and outputs so that they fall in the interval $[-1, 1]$. This preprocessing was explained in detail in Chapter Four. The input/output relation can be expressed as:

$$TEF = F(\delta_1, \omega_1, ..., \delta_n, \omega_n), \tag{6.1}$$

where n is the number of machines in the system. Sigmoid transfer function which is the most widely used function for back propagation neural networks was used for hidden and output layer neurons. Models incorporating sigmoid transfer functions often help generalized learning characteristics and yield models with improved accuracy.

6.2.2 The Back Propagation Algorithm

This algorithm is derived based on the concept of the gradient descent search to minimize the error through the adjustment of weights. The detail of this algorithm was explained in Chapter Four. A feed-forward back propagation network with Levenberg-Marquardt training algorithm was used in this section.

6.2.3 ANN Training

1. Data generation

   To develop data patterns for training and testing NNs, different cases were developed by changing the network topology, i.e., taking out one line out of

service at a time. In this work, only line-to-ground faults on all possible locations in the power system network were considered. Note that other fault types will require the same procedure as line-to-ground fault.

At first, load flow solution was taken as initial condition in each case. Then, time domain simulations were run with different fault locations. The dynamic behavior of each system was monitored following each fault. After fault removing, machine angles and speed deviations of all machines were collected at every time step for 5 seconds. The loss of synchronism usually happens within 2 to 3 seconds of the initial disturbance therefore, capturing 5 seconds seemed to be adequate. The value of TEF was calculated for every time step after fault removal. A data base was then formed by pairing the angle and speed deviation of each machine and the corresponding TEF. Accordingly, the inputs to the NN are twice the number of machines in each case and the output is the estimated TEF.

The above process was repeated with longer fault duration to cause a complete system instability in order to evaluate the critical transient energy. The instant that all machine angles were beyond 180 degrees (in COI reference) was recorded as the critical time. The transient energy function value at critical time was recorded as the critical transient energy.

2. Data preparation

The generated data of each case were normalized and shuffled several times before training the NN. This was done to enhance the randomness of the data. After the data was shuffled, it was divided into two groups, one was used for training and the other for testing. For proper NN performance, test data and

training must be different although belonging to the same statistical source. The property of being able to correctly classify previously unseen inputs is referred to as generalization.

During the training session, the NN was closely monitored to prevent network memorization or saturation. When a NN memorizes the training data, it reproduces acceptable results for patterns that have been used during the training, but unacceptable results with high errors when tested on novel patterns. There are different techniques to ensure that a NN has learned and not memorized. A properly trained NN should respond with equal error measures to both training and testing patterns. The training patterns in this study were first divided into two subsets where one subset was almost four times the size of the other subset. After the first few iterations, the NN was trained on the larger subset and tested on the smaller subset. If the errors of the larger subset and the smaller subset were comparable, the training patterns were re-shuffled and divided again into two subsets and so on.

Another problem with NN training is network saturation. This happens when the nonlinear functions of the hidden neurons reach the upper or lower saturation limits. It is common to have neurons in the saturation region, but too many of them in the saturation region would make the NN ineffective. To prevent network saturation, the hidden neurons were closely monitored and those with no contribution to the training process were eliminated.

6.3 Validation Results

Test systems in this section include the 19-machine case and the 7-machine case. The above method of generating data formed a data base consisted of 3191 data pairs for

Table 6.1: Sample Input of ANN for 7-machine case

Inputs	Angle (rad)	Speed deviation
Machine no.1	0.3941	-0.0002
Machine no.2	0.3941	-0.0002
Machine no.3	0.3941	-0.0002
Machine no.4	0.3941	-0.0002
Machine no.5	0.1713	-0.0003
Machine no.6	-0.0619	0.0017
Machine no.7	-0.3234	-0.0012

the 7-machine case and 22132 data pairs for the 19-machine case. The data was then passed to neural networks for training and testing.

In the case of 19-machine, with 38 inputs and more than 22000 data pairs, the ANN training was time-consuming. Therefore, the number of inputs were reduced to machine angles only since these variables have stronger discriminating capabilities for stability evaluation.

6.3.1 7-machine Test System

Table 6.1 shows sample input data for TEF neural networks. System specification of the 7-machine system is described in Chapter Two. The NN had $2 \times 7 = 14$ inputs which was the number of all machine angle and speed deviations.

In our study, a priori knowledge of the fault type is needed to evaluate the transient energy. The fault type under investigation was the line-to-ground fault for all possible locations. The fault was on line 11-110 which lasted for 0.08 second.

After generating and then shuffling the data pairs, 3000 of them were used to train the NN and the rest were used to test the capability of the NN to evaluate the TEF index. Table 6.2 shows the result of the TEF evaluation and the potential energy of each machine. The negative value of TEF shows the instability of the system.

Table 6.2: Output of TEF-ANN for unstable case (1)

Output	Potential Energy (pu)	TEF Index
Machine no.1	-0.0011	
Machine no.2	-0.0011	
Machine no.3	-0.0011	
Machine no.4	-0.0011	-0.3528
Machine no.5	-0.0014	
Machine no.6	-0.1368	
Machine no.7	0.0206	

Table 6.3: Output of TEF-ANN unstable case (2)

Output	Potential Energy (pu)	TEF Index
Machine no.1	-0.0083	
Machine no.2	-0.0084	
Machine no.3	-0.0084	
Machine no.4	-0.0084	-2.5176
Machine no.5	-0.0104	
Machine no.6	-0.905	
Machine no.7	0.1538	

According to one-line diagram of the system in Figure 2.14, bus 11 is the slack bus which is connected to the rest of the system via bus 110. The potential energy of machine 6, which is the slack generator, compared to other machines clarifies this point.

Table 6.3 shows another unstable case of the system. The fault was on line 120-110 which lasted for 1 second. The potential energy of machines 6 and 7 indicates that they are the most affected machines in the system.

On the other hand, Tables 6.4 and 6.5 show two stable cases for the same power system. In the first case, the fault is line-to-ground fault on line 102-10 which lasted for 0.1 second. Bus 102 which is connected to generator 2 showed a stable behavior

Table 6.4: Output of TEF-ANN for stable case (1)

Output	Potential Energy (pu)	TEF Index
Machine no.1	-0.2471	
Machine no.2	3.0382	
Machine no.3	-0.2462	
Machine no.4	-0.2462	1.8465
Machine no.5	-0.2276	
Machine no.6	0.8699	
Machine no.7	0.2944	

Table 6.5: Output of TEF-ANN for stable case (2)

Output	Potential Energy (pu) 1.0e-003	TEF Index
Machine no.1	-0.0639	
Machine no.2	-0.0639	
Machine no.3	-0.0639	
Machine no.4	0.3871	0.0029
Machine no.5	-0.0195	
Machine no.6	0.0432	
Machine no.7	0.0171	

after fault removal. This was the result of power system stabilizer on that generator.

The above argument was also true for the second stable case which was a line-to-ground fault on line 10-104. The potential energy of each machine is also presented in Tables 6.4 and 6.5 to simplify the analysis of each machine's behavior. Note that the potential energies were calculated by numerical methods and only the TEF index was the result of our neural network.

The ANN was trained with a learning rate of 0.01, momentum constant of 0.9, the maximum error tolerance of 0.5e-4, and 4400 epochs. The training algorithm was back propagation and the mean squared error as the performance function. After training the NN, a novel testing pattern was used to evaluate the accuracy of the

Figure 6.1: Error Histogram for the 7-machine NN

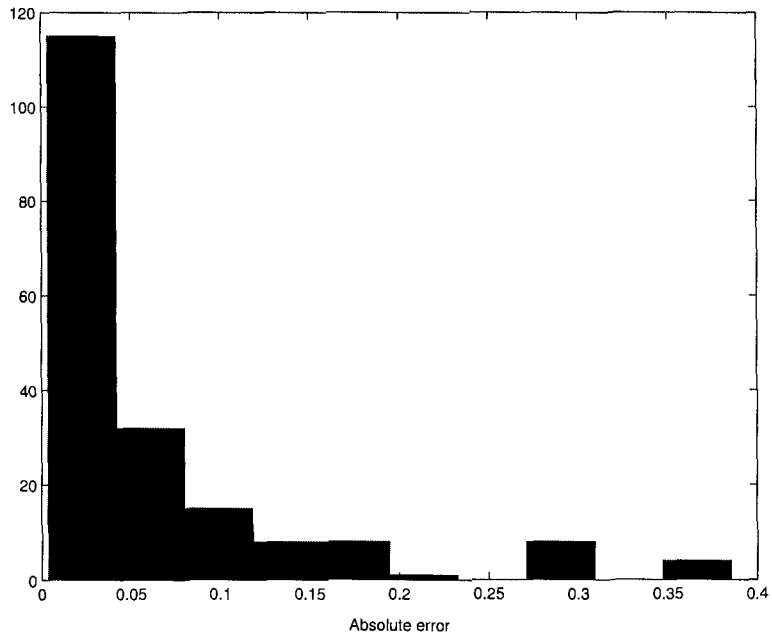

NN. To show the accuracy of obtained results, a histogram of the absolute error of all the testing pairs is shown in Figure 6.1. The absolute error is the absolute difference between the real value of TEF and the output of our neural network. The histogram shows that of 191 data points about 60% are below 0.05.

6.3.2 19-machine Test System

The same training as explained before was used to generate 22132 data pairs. Table 6.6 shows a sample generated training data. The line-to-ground fault was on line 23-7 and lasted for 0.08 second. As explained before, due to the large number of data patterns the number of inputs was reduced to 19 by only considering machine angles at the fault clearing time.

Out of these 22132 data pairs, 22000 were shuffled and then passed to the NN for training. The rest of data was used to test the capability of the NN to evaluate

Table 6.6: Sample Input of ANN for 19-machine case

Inputs	Angle (rad)	Speed deviation
Machine no.1	0.5025	-0.0002
Machine no.2	1.0157	0
Machine no.3	-0.4501	0
Machine no.4	-1.2387	0
Machine no.5	-0.6325	0
Machine no.6	0.7604	-0.0001
Machine no.7	0.8415	0.0061
Machine no.8	0.1259	-0.0001
Machine no.9	0.8335	-0.001
Machine no.10	0.3765	-0.0001
Machine no.11	-0.4795	0
Machine no.12	-0.5241	0
Machine no.13	0.9048	0
Machine no.14	-0.4756	0
Machine no.15	0.7675	-0.0002
Machine no.16	0.6219	-0.0003
Machine no.17	0.3906	-0.0002
Machine no.18	-1.0122	0
Machine no.19	-1.025	0

the TEF index. The NN output in Table 6.7 shows the corresponding TEF index to Table 6.6. The potential energy gained by each machine during fault is also presented in Table 6.7. The potential energy was calculated using numerical method and is only shown to give a better understanding of dynamic behavior of each machine. The positive value of TEF index refers to the stability of power system after fault removal.

The ANN is trained with a learning rate of 0.01, momentum constant of 0.9, the maximum error tolerance 0.5e-4, and 1000 epochs. A novel testing pattern was used to evaluate the accuracy of the NN. Figure 6.2 shows the error of 80 randomly selected points from the testing pattern. The error was defined as the difference between the real value of TEF and the result from the NN.

To show the accuracy of obtained results, a histogram of the absolute error of all the testing pairs is shown in Figure 6.3. The histogram shows about 80% of error

Table 6.7: Sample Output of ANN for 19-machine case

Output	Potential Energy (pu)	TEF Index
Machine no.1	0.0003	
Machine no.2	0	
Machine no.3	0	
Machine no.4	0	
Machine no.5	0	
Machine no.6	0.0007	
Machine no.7	0.1289	
Machine no.8	0.0002	
Machine no.9	0.0065	
Machine no.10	0	
Machine no.11	0	0.1421
Machine no.12	0	
Machine no.13	0	
Machine no.14	0	
Machine no.15	0.0001	
Machine no.16	0.0002	
Machine no.17	0.0003	
Machine no.18	0	
Machine no.19	0	

points are below 0.01.

Both error histograms indicate that the ANN-architecture is able to evaluate the TEF index mostly with higher than 2% precision. That makes the proposed ANN a reliable tool to help utility operators in decision making.

Figure 6.2: Error of TEF-NN for the 19-machine system

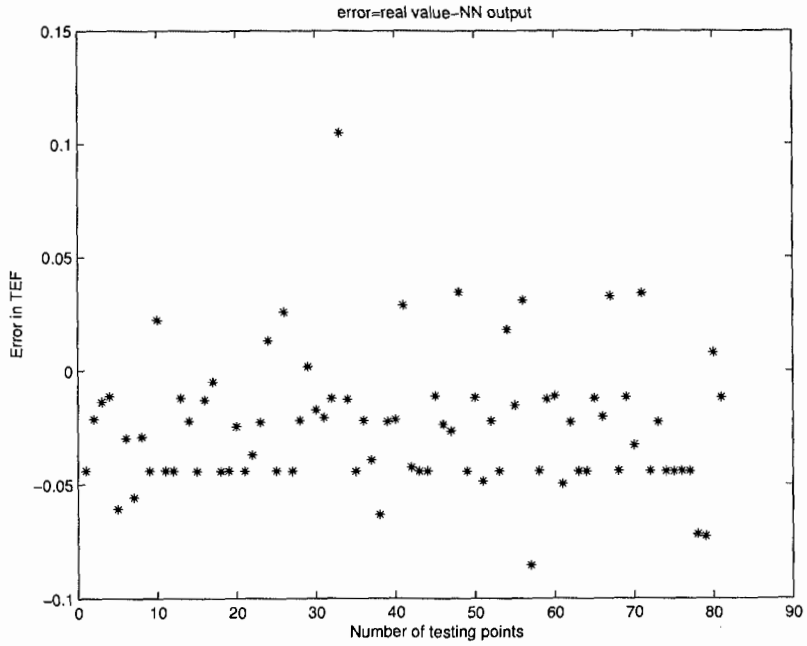

Figure 6.3: Error Histogram for the 19-machine NN

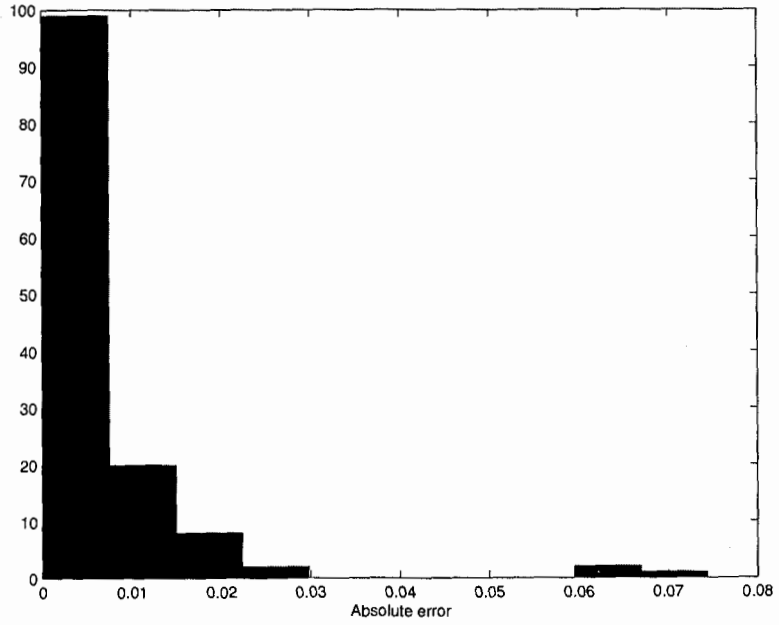

6.4 The Proposed ANN-Based Tool For Stability Analysis

In the previous section a novel neural network approach to evaluate TEF index was proposed. In this section, we proposed an ANN approach to detect whether a contingency affecting a power system can cause instability. "It is crucial for the operator to know the status of each machine in a power network after fault removal, i.e., if a machine remains stable or unstable after a particular fault.

For that purpose, an ANN-based tool was used at the fault clearing time for discriminating between stable and unstable machine clusters" [1]. The proposed ANN structure was trained and validated by simulating properly arranged scenarios from two test systems, which were used in the TEF evaluation section.

6.4.1 Topology of the ANN

The topology of a multi-layer feed-forward back-propagation ANN consisted of an input layer, one hidden layer and one output layer.

1. The input layer

   Machine angles and potential energy, evaluated at the fault clearing time for each machine, were adopted as input variables for neural networks.

2. The hidden layer

   Based on trial and error method, five neurons were considered in the hidden layer.

3. The output layer

   "The selection of output variables is defined by the recognition of the problem as

a classification one: whether a machine belongs to the stable/unstable cluster. For every single machine one neural network was adopted. A total of m neural networks was required, where m was the number of machines in each power system. The single output for each ANN was set to -1 if the corresponding generator was unstable and +1 if it was stable" [1]. Figure 6.4 shows the structure of neural network with details of each layer.

Figure 6.4: Neural network scheme for transient stability analysis

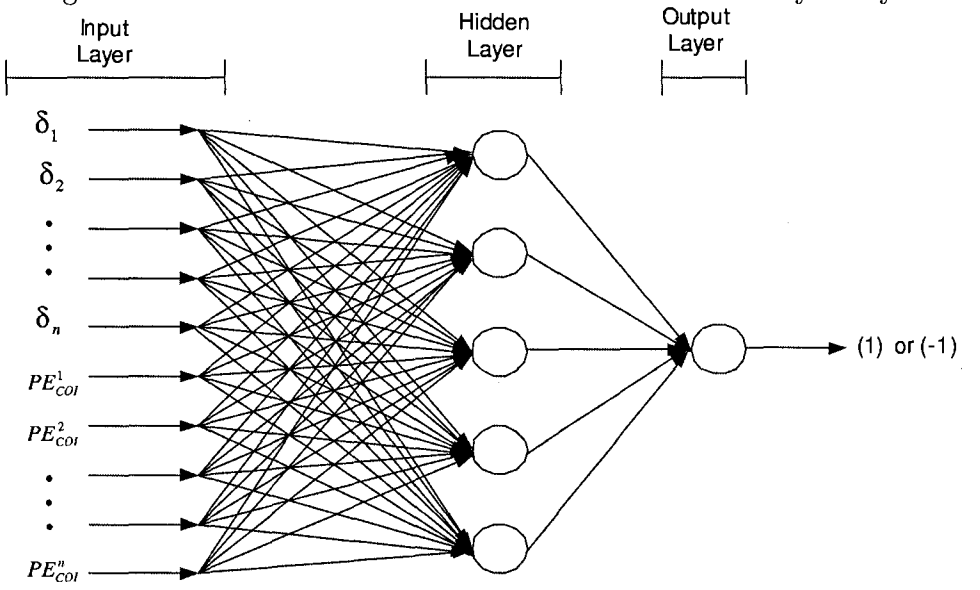

"Sigmoid" transfer function which is the most widely used function for back propagation problems was used for the hidden layer. Since the output was either 1 for stable cases and -1 for unstable cases, the "symmetric hard limit" transfer function was used for the output layer.

6.4.2 ANN Training

1. Data generation

   The simulations were performed under similar condition as explained before but this time machine angles and potential energy of each machine in COI reference were taken as inputs. Machine angles were taken as stability indicators. If the angle in COI reference was higher than 180 degrees the target output was set to -1, otherwise 1.

2. Data preparation

   "Once the training data was built, the percentage of stable/unstable cases in the data set was analyzed to make sure a sufficient number of unstable cases are present in the training set" [1].

6.5 Validation Results

The proposed framework was tested on the 19-machine case and also the 7-machine test system. The data base for the 7-machine system consisted of 3191 data patterns and 22132 data patterns for the 19-machine case. The training set was then passed to neural networks for training and testing.

6.5.1 7-machine Test System

The number of inputs was $7+7=14$, which includes machine angle and the potential energy of each machine. From the total number of 3191 simulation patterns, 2918 were used to train the ANNs and 273 were used to test them. Table 6.8 shows a representative sample of input at the fault clearing instant. The NNs performance

Table 6.8: Sample Input of ANNs

Input No.		
1	Angle of machine 1 in COI ref.	-3.2779
2	Angle of machine 2 in COI ref.	-3.2951
3	Angle of machine 3 in COI ref.	-3.2951
4	Angle of machine 4 in COI ref.	-3.2951
5	Angle of machine 5 in COI ref.	8.3477
6	Angle of machine 6 in COI ref.	-3.1129
7	Angle of machine 7 in COI ref.	-3.4476
8	Potential energy of machine 1 in COI ref.	-3.0227
9	Potential energy of machine 2 in COI ref.	-3.0367
10	Potential energy of machine 3 in COI ref.	-3.0367
11	Potential energy of machine 4 in COI ref.	-3.0367
12	Potential energy of machine 5 in COI ref.	5.0431
13	Potential energy of machine 6 in COI ref.	35.3875
14	Potential energy of machine 7 in COI ref.	10.2924

Table 6.9: Output of ANNs

Output No.	State of the i-th machine
1	-1
2	-1
3	-1
4	-1
5	-1
6	-1
7	-1

was tested by a novel input. The novel input included machine angles and potential energies of all machines after a line-to-ground fault on line 2-20. The fault lasted for about 3 seconds to make sure all the machines in the test system were gone unstable. The obtained results are shown in Table 6.9.

The NN set was also tested with the stable case (1) explained in section 6.3.1. Table 6.10 shows the result which has consistency with that obtained from the TEF index in Table 6.4. All machines in the power system remain stable after fault removal except machine 2 which was connected to bus 102. After fault removal, line 102-10

Table 6.10: Output of ANNs

Output No.	State of the i-th machine
1	1
2	-1
3	1
4	1
5	1
6	1
7	1

was out of system therefore, there is no synchronism between machine 2 and the rest of machines in the power system.

A summary of the results gained by 273 test pairs is shown in Table 6.11. As can be seen, the "False Alarm" and "Missed alarms" error indices are limited within few percent. "False Alarm" is the error in the ANN output when declared as unstable but stable by simulation and "Missed Alarm" is the error in the ANN output when declared as stable but unstable by simulation [1].

The maximum error for false alarms is 3.6% which is still considered an acceptable error rate. In case of missed alarms the error is surprisingly low thus showing that the proposed tool has a good capability in predicting the stability of machines for the line-to-ground contingency.

6.5.2 19-machine Test System

In this case again, the chosen inputs for each of neural networks were angle and potential energy of each machine therefore, $19 + 19 = 38$ inputs. From the total number of 22132 simulation patterns, 21397 were used to train the ANN set and 735 were used to test them.

Table 6.12 shows a sample of inputs at the fault clearing instant of a fault that

Table 6.11: Results of the validation data for 7-machine case

	Stable Cases	Unstable Cases	False alarms	False alarms %	Missed alarms	Missed alarms %
Machine 1	196	77	0	0.00%	0	0.00%
Machine 2	195	78	0	0.00%	0	0.00%
Machine 3	195	78	0	0.00%	0	0.00%
Machine 4	195	78	6	2.20%	0	0.00%
Machine 5	200	73	0	0.00%	0	0.00%
Machine 6	203	70	4	1.40%	0	0.00%
Machine 7	170	103	10	3.60%	0	0.00%

occurred on line 15-33. The fault lasted for about 0.05 seconds. According to simulation results, all the machines remain synchronized after fault removal except machine 15 which was disconnected from the rest of the system due to outage of line 15-33. The output of the NN, shown in Table 6.13, also confirms the simulation results.

A summary of results gained by 735 test patterns are shown in Table 6.14. The maximum error for false alarms is 4.21%. In case of missed alarms the error is very low thus showing that the proposed tool has a good capability in predicting the stability of machines.

An ANN-based contingency screening tool was proposed in this Chapter. The ANN tool makes use of the Hybrid method combining time domain simulations and energy function in transient stability analysis. The line-to-ground fault was investigated in this work but the same process can be used for other fault types.

A set of ANNs to determine the status of machines after fault removal along with an NN to evaluate the TEF index as a degree of stability was proposed. Both NNs were validated using two test power systems. The fast computation time with reliable results make the implemented ANN method an efficient on-line screening tool.

Table 6.12: Sample Input of ANN

Input No.		
1	Angle of machine 1 in COI ref.	0.2447
2	Angle of machine 2 in COI ref.	0.806
3	Angle of machine 3 in COI ref.	-0.5249
4	Angle of machine 4 in COI ref.	-1.3331
5	Angle of machine 5 in COI ref.	-0.8064
6	Angle of machine 6 in COI ref.	0.4993
7	Angle of machine 7 in COI ref.	0.5465
8	Angle of machine 8 in COI ref.	-0.0838
9	Angle of machine 9 in COI ref.	0.5788
10	Angle of machine 10 in COI ref.	0.1656
11	Angle of machine 11 in COI ref.	-0.5551
12	Angle of machine 12 in COI ref.	-0.6007
13	Angle of machine 13 in COI ref.	0.6952
14	Angle of machine 14 in COI ref.	-0.6497
15	Angle of machine 15 in COI ref.	16.1269
16	Angle of machine 16 in COI ref.	0.3604
17	Angle of machine 17 in COI ref.	0.1319
18	Angle of machine 18 in COI ref.	-1.1034
19	Angle of machine 19 in COI ref.	-1.118
20	Potential energy of machine 1 in COI ref.	-0.245
21	Potential energy of machine 2 in COI ref.	-0.2116
22	Potential energy of machine 3 in COI ref.	-0.0635
23	Potential energy of machine 4 in COI ref.	-0.0784
24	Potential energy of machine 5 in COI ref.	-0.1487
25	Potential energy of machine 6 in COI ref.	-0.256
26	Potential energy of machine 7 in COI ref.	-0.2557
27	Potential energy of machine 8 in COI ref.	-0.0794
28	Potential energy of machine 9 in COI ref.	0.4042
29	Potential energy of machine 10 in COI ref.	0.267
30	Potential energy of machine 11 in COI ref.	2.009
31	Potential energy of machine 12 in COI ref.	0.0533
32	Potential energy of machine 13 in COI ref.	2.4246
33	Potential energy of machine 14 in COI ref.	0.3024
34	Potential energy of machine 15 in COI ref.	-33.0238
35	Potential energy of machine 16 in COI ref.	0.2902
36	Potential energy of machine 17 in COI ref.	22.7351
37	Potential energy of machine 18 in COI ref.	0.1181
38	Potential energy of machine 19 in COI ref.	0.3674

Table 6.13: Output of ANNs

Output No.	State of the i-th machine
1	1
2	1
3	1
4	1
5	1
6	1
7	1
8	1
9	1
10	1
11	1
12	1
13	1
14	1
15	-1
16	1
17	1
18	1
19	1

Table 6.14: Results of the validation data for 19-machine case

	Stable Cases	Unstable Cases	False alarms	False alarms %	Missed alarms	Missed alarms %
Machine 1	651	84	21	2.80%	0	0.00%
Machine 2	672	63	0	0.00%	0	0.00%
Machine 3	714	21	0	0.00%	0	0.00%
Machine 4	632	103	2	0.27%	0	0.00%
Machine 5	651	84	0	0.00%	0	0.00%
Machine 6	672	63	0	0.00%	0	0.00%
Machine 7	630	105	10	1.37%	0	0.00%
Machine 8	714	21	31	4.21%	5	0.67%
Machine 9	630	105	5	0.67%	0	0.00%
Machine 10	651	84	21	2.80%	2	0.27%
Machine 11	672	63	0	0.00%	0	0.00%
Machine 12	672	63	0	0.00%	0	0.00%
Machine 13	630	105	1	0.13%	0	0.00%
Machine 14	609	126	5	0.67%	0	0.00%
Machine 15	630	105	0	0.00%	0	0.00%
Machine 16	630	105	0	0.00%	0	0.00%
Machine 17	662	73	11	1.50%	1	0.13%
Machine 18	609	126	0	0.00%	0	0.00%
Machine 19	609	126	7	0.95%	0	0.00%

Chapter 7

Conclusion

With the evolution of the electric power industry toward open markets over the last decade resulting in over-stressed power systems, more rigorous state estimation and security assessment are required.

State estimation is an essential monitoring tool to achieve a secure and economical operation in today's complicated power systems. Security assessment evaluates the ability of a power system to withstand a contingency.

This thesis project described implementation of artificial neural networks in state estimation of a power system by employing forecasting and filtering methods. We developed Functional Link Network to filter bad data (bad data detection) transmitted via SCADA. Time Delay Neural Network was developed to forecast the next state of the system by using the output of FLN. Two networks were validated by three power system benchmarks provided in MATLAB's Power System Toolbox (PST).

The presented results from all three test cases showed consistency in terms of accuracy and reliability. The average absolute error in forecasted voltage magnitude was about 0.001 and for phase angles less than 0.01. The satisfactory precision in results with fast computation of the implemented method established the suitability

of artificial neural networks for on-line applications in DSA.

Next, we introduced a novel approach to transient stability assessment by means of neural networks. The influencing factors in transient stability analysis were identified. Different numerical techniques as well as direct methods in Transient Energy Function (TEF) evaluation were examined.

Our study showed an effective combination of both time domain and TEF method in Hybrid Method for stability analysis. A NN-based technique to evaluate energy margin of a power system as a security index was proposed. The result obtained from the method were compared to those from MATLAB Power System Toolbox and the error histograms showed absolute error less than 0.01 for about 80% of total data.

Another ANN-based monitoring tool was also represented to identify stable and unstable machines in a power system after fault removal. The performance of the NN was verified using two test power system benchmarks. The satisfactory results in predicting stability/instability properties of a power system, along with the short computational time (a few milliseconds) made the implemented ANN method an appropriate complementary tool for contingency screening in the energy management center.

Our results show that Artificial Neural Networks are promising tools for global power system problems such as state estimation and transient stability assessment. However, as with all methods, there are some limitations too.

In our state estimation study, the TDNN failed to predict the voltage magnitude of controlled voltage buses (P-V buses). Although these buses do not affect the state estimation analysis that much, this issue should be considered in future works.

In transient stability study only line-to-ground fault was considered. We did not explore whether in the presence of multiple faults, the suggested ANN method would be suitable or not. This could also be addressed in future investigations.

Appendix A

Control Units

Figure A.1: Power system stabilizer block diagram in PST [6]

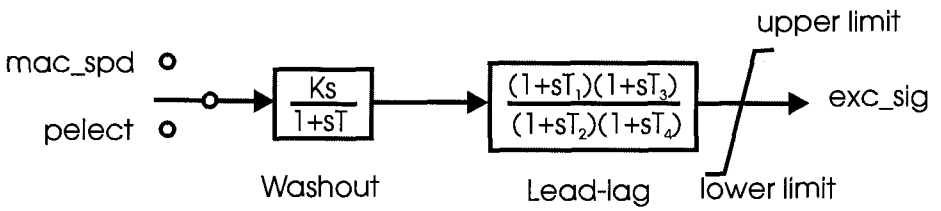

Figure A.2: ST3 Excitation System in PST [6]

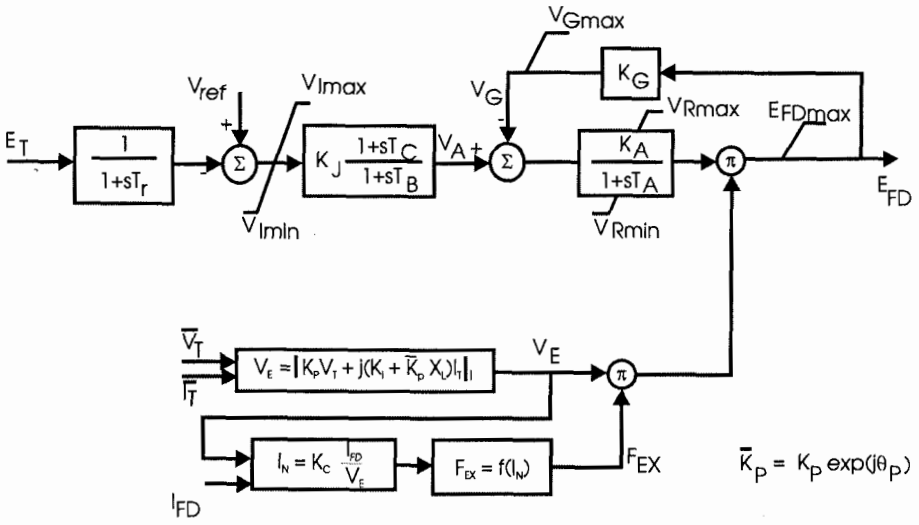

Figure A.3: Simple turbine governor model in PST [6]

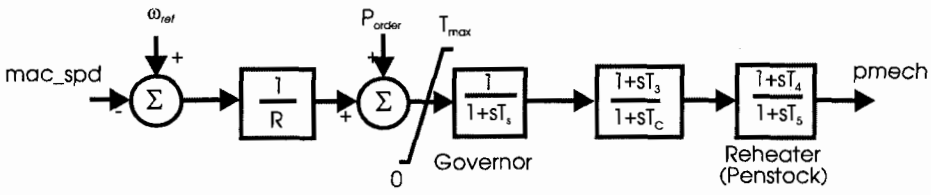

Appendix B

Specification Matrices in Power System Toolbox

Table B.1: Generator and Machine Specification Matrix Format in PST [6]

column	variable	unit
1	machine number	
2	bus number	
3	base MVA	MVA
4	leakage reactance x_l	pu
5	resistance r_a	pu
6	d-axis synchronous reactance x_d	pu
7	d-axis transient reactance x_d'	pu
8	d-axis subtransient reactance x_d''	pu
9	d-axis open circuit time constant T_{do}'	sec
10	d-axis open circuit subtransient time constant T_{do}''	sec
11	q-axis synchronous reactance x_q	pu
12	q-axis transient reactance x_q'	pu
13	q-axis subtransient reactance x_q''	pu
14	q-axis open circuit time constant T_{qo}'	sec
15	q-axis open circuit subtransient time constant T_{qo}''	sec
16	Inertia constant H	sec
17	local damping coefficient d_o	pu
18	system damping coefficient d_1	pu
19	bus number	
20	saturation factor $S(1.0)$	
21	saturation factor $S(1.2)$	
22	active power fraction	
23	reactive power fraction	

Figure B.1: Data format for induction generation in power system toolbox

column	variable	unit
1	motor number	
2	bus number	
3	motor base MVA	MVA
4	stator resistance r_s	pu
5	stator leakage reactance x_s	pu
6	magnetizing reactance X_m	pu
7	rotor resistance r_r	pu
8	rotor leakage reactance x_r	pu
9	inertia constant H	Sec
10	second cage resistance r_2	pu
11	intercage reactance x_2	pu
12	deep bar ratio	pu
13	leakage saturation current	pu
15	fraction of active bus load	

Table B.2: Exciter Specification Matrix Format in PST [6]

column	data	unit
1	exciter type	3 for ST3
2	machine number	
3	input filter time constant T_R	sec
4	voltage regulator gain K_A	
5	voltage regulator time constant T_A	sec
6	voltage regulator time constant T_B	sec
7	voltage regulator time constant T_C	sec
8	maximum voltage regulator output V_{Rmax}	pu
9	minimum voltage regulator output V_{Rmin}	pu
10	maximum internal signal V_{Imax}	pu
11	minimum internal signal V_{Imin}	pu
12	first state regulator gain K_J	
13	potential circuit gain coefficient K_P	
14	potential circuit phase angle q_P	degrees
15	current circuit gain coefficient K_I	
16	potential source reactance X_L	pu
17	rectifier loading factor K_C	
18	maximum field voltage E_{fdmax}	pu
19	inner loop feedback constant K_G	
20	maximum inner loop voltage feedback V_{Gmax}	pu

Table B.3: Governor Specification Matrix Format in PST [6]

column	variable	unit
1	turbine model number (=1)	
2	machine number	
3	speed set point ω_f	pu
4	steady state gain $1/R$	pu
5	maximum power order T_{max}	pu on generator base
6	servo time constant T_s	sec
7	HP turbine time constant T_c	sec
8	transient gain time constant T_3	sec
9	time constant to set HP ratio T_4	sec
10	reheater time constant T_5	sec

Figure B.2: Data format for power system stabilizer in PST

column	data	unit
1	type 1 speed input 2 power input	
2	machine number	
3	gain K	
4	washout time constant T	sec
5	lead time constant T_1	sec
6	lag time constant T_2	sec
7	lead time constant T_3	sec
8	lag time constant T_4	sec
9	maximum output limit	pu
10	minimum output limit	pu

Appendix C

Data Specification of the 7-machine Test System

Table C.1: Bus specification for the 7-machine test system

1	1.03	18.5	1.75	0.4	0.00	0.00	0.00	0.00
102	1.03	18.5	1.75	0.4	0.00	0.00	0.00	0.00
103	1.03	18.5	1.75	0.4	0.00	0.00	0.00	0.00
104	1.03	18.5	1.75	0.4	0.00	0.00	0.00	0.00
2	1.01	8.80	7.00	1.76	0.00	0.00	0.00	0.00
3	0.9781	-6.1	0.00	0.00	9.76	1.00	0.00	0.00
10	1.0103	12.1	0.00	0.00	0.00	0.00	0.00	0.00
11	1.03	-6.8	7.16	1.49	0.00	0.00	0.00	0.00
12	1.01	-16.9	7.00	1.39	0.00	0.00	0.00	0.00
13	0.9899	-31.8	0.00	0.00	17.67	1.00	0.00	0.00
20	0.9876	2.1	0.00	0.00	0.00	0.00	0.00	0.00
101	1.00	-19.3	0.00	1.09	0.00	0.00	0.00	0.00
110	1.0125	-13.4	0.00	0.00	0.00	0.00	0.00	0.00
120	0.9938	-23.6	0.00	0.00	0.00	0.00	0.00	0.00

Table C.2: Line specification for the 7-machine test system

1	10	0.0	0.0668	0.00	1.	0.
102	10	0.0	0.0668	0.00	1.	0.
103	10	0.0	0.0668	0.00	1.	0.
104	10	0.0	0.0668	0.00	1.	0.
2	20	0.0	0.0167	0.00	1.	0.
3	20	0.001	0.0100	0.0175	1.	0.
3	101	0.011	0.110	0.1925	1.	0.
3	101	0.011	0.110	0.1925	1.	0.
10	20	0.0025	0.025	0.0437	1.	0.
11	110	0.0	0.0167	0.0	1.	0.
12	120	0.0	0.0167	0.0	1.	0.
13	101	0.011	0.11	0.1925	1.	0.
13	101	0.011	0.11	0.1925	1.	0.
13	120	0.001	0.01	0.0175	1.	0.
110	120	0.0025	0.025	0.0437	1.	0.

Table C.3: Machine specification for the 7-machine test system

1	1	225	0.16	.00234	1.81	0.30	0.217	7.80	0.022
2	102	225	0.16	.00234	1.81	0.30	0.217	7.80	0.022
3	103	225	0.16	.00234	1.81	0.30	0.217	7.80	0.022
4	104	225	0.16	.00234	1.81	0.30	0.217	7.80	0.022
5	2	900	0.200	0.0025	1.8	0.30	0.25	8.00	0.03
6	11	900	0.200	0.0025	1.8	0.30	0.25	8.00	0.03
7	12	900	0.200	0.0025	1.8	0.30	0.25	8.00	0.03

Table C.4: Exciter specification for the 7-machine test system

0	1	0.02	200.0	0.05	0	0	5.0	-5.0
0	2	0.02	200.0	0.05	0	0	5.0	-5.0
0	3	0.02	200.0	0.05	0	0	5.0	-5.0
0	4	0.02	200.0	0.05	0	0	5.0	-5.0
0	5	0.02	200.0	0.05	0	0	5.0	-5.0
0	6	0.02	200.0	0.05	0	0	5.0	-5.0
0	7	0.02	200.0	0.05	0	0	5.0	-5.0

Appendix D

Data Specification of the 19-machine Test System

Table D.1: Bus specification for the 19-machine test system

1	1.0490	0.0000	28.3794	23.2983	0.0000	0.0000	0.00	0.00
2	1.0490	28.1220	121.0406	62.9955	0.0000	0.0000	0.00	0.00
3	1.0490	-57.8509	110.1829	70.1339	0.0000	0.0000	0.00	0.00
4	1.0490	-98.8765	74.7150	55.1440	0.0000	0.0000	0.00	0.00
5	1.0490	-63.8096	68.3083	75.4348	0.0000	0.0000	0.00	0.00
6	1.0490	8.9660	127.0900	52.5457	0.0000	0.0000	0.00	0.00
7	1.0490	16.2350	19.6897	9.1951	0.0000	0.0000	0.00	0.00
8	1.0490	-15.9550	22.6313	10.5317	0.0000	0.0000	0.00	0.00
9	1.0300	22.6917	12.2000	-0.5245	0.0000	0.0000	0.00	0.00
10	1.0400	-7.8713	16.8000	0.9749	0.0000	0.0000	0.00	0.00
11	1.0490	-56.2245	27.0400	12.2507	0.0000	0.0000	0.00	0.00
12	1.0490	-58.4070	5.6000	4.0002	0.0000	0.0000	0.00	0.00
13	1.0490	25.3923	6.0300	4.4545	0.0000	0.0000	0.00	0.00
14	1.0490	-55.9158	12.7300	4.9559	0.0000	0.0000	0.00	0.00
15	1.0490	5.7456	6.6800	5.0596	0.0000	0.0000	0.00	0.00
16	1.0490	7.4830	9.4000	4.7339	0.0000	0.0000	0.00	0.00
17	1.0490	-2.3803	11.4100	37.4331	0.0000	0.0000	0.00	0.00
18	1.0490	-86.8303	25.4000	7.0974	0.0000	0.0000	0.00	0.00
19	1.0490	-87.8436	21.7700	6.1294	0.0000	0.0000	0.00	0.00
20	1.0049	-62.0468	0.0000	0.0000	105.0300	60.0000	0.00	0.00
21	0.9957	21.4671	0.0000	0.0000	107.0400	48.0000	0.00	0.00
22	0.9928	-66.8173	0.0000	0.0000	97.1000	40.0000	0.00	10.00
23	1.0430	15.5132	0.0000	0.0000	11.6800	4.0000	0.00	0.00
24	1.0421	-16.7853	0.0000	0.0000	41.5300	15.0000	0.00	10.00

Table D.2: Bus specification for the 19-machine test system (cont)

25	1.0098	2.7673	0.0000	0.0000	80.8300	45.0000	0.00	0.00
26	1.0060	-3.0830	0.0000	0.0000	80.8300	35.0000	0.00	15.00
27	1.0050	-105.2786	0.0000	0.0000	97.0600	40.0000	0.00	59.00
28	1.0086	-102.1152	0.0000	0.0000	87.0600	32.0000	0.00	0.00
29	1.0243	-59.0441	0.0000	0.0000	0.0000	0.0000	0.00	0.00
30	1.0226	-60.4863	0.0000	0.0000	0.0000	0.0000	0.00	0.00
31	1.0153	23.1674	0.0000	0.0000	0.0000	0.0000	0.00	0.00
32	1.0243	-59.6333	0.0000	0.0000	0.0000	0.0000	0.00	0.00
33	1.0235	3.8774	0.0000	0.0000	0.0000	0.0000	0.00	0.00
34	1.0215	4.3326	0.0000	0.0000	0.0000	0.0000	0.00	0.00
35	1.0310	-2.6429	0.0000	0.0000	0.0000	0.0000	0.00	0.00
36	1.0171	-95.0157	0.0000	0.0000	0.0000	0.0000	0.00	0.00
37	1.0275	-92.4547	0.0000	0.0000	0.0000	0.0000	0.00	0.00
38	1.0347	18.7511	0.0000	0.0000	0.0000	0.0000	0.00	0.00
39	1.0378	-13.2266	0.0000	0.0000	0.0000	0.0000	0.00	0.00
40	0.9654	-55.4078	0.0000	0.0000	0.0000	0.0000	0.00	0.00
41	1.0312	10.2218	0.0000	0.0000	0.0000	0.0000	0.00	0.00
42	1.0146	-1.0369	0.0000	0.0000	0.0000	0.0000	0.00	0.00

Table D.3: Line specification for the 19-machine test system

30	12	0.00007	0.00700	0.00000	0.0	0.0	0.0	0.0	0.0
11	29	0.00010	0.00200	0.00000	0.0	0.0	0.0	0.0	0.0
27	28	0.00010	0.00075	0.04000	0.0	0.0	0.0	0.0	0.0
13	31	0.00060	0.00730	0.00000	0.0	0.0	0.0	0.0	0.0
32	14	0.00007	0.00550	0.00000	0.0	0.0	0.0	0.0	0.0
22	27	0.00350	0.02460	0.29200	0.0	0.0	0.0	0.0	0.0
41	24	0.00850	0.09950	0.50000	0.0	0.0	0.0	0.0	0.0
24	40	0.00920	0.10900	0.50000	0.0	0.0	0.0	0.0	0.0
33	15	0.00008	0.00530	0.00000	0.0	0.0	0.0	0.0	0.0
34	16	0.00007	0.00630	0.00000	0.0	0.0	0.0	0.0	0.0
25	26	0.00025	0.00282	0.01800	0.0	0.0	0.0	0.0	0.0
25	26	0.00030	0.00279	0.00900	0.0	0.0	0.0	0.0	0.0
25	23	0.00190	0.01550	0.09520	0.0	0.0	0.0	0.0	0.0
42	24	0.00800	0.08400	0.33400	0.0	0.0	0.0	0.0	0.0
35	17	0.00002	0.00050	0.00000	0.0	0.0	0.0	0.0	0.0
26	21	0.00190	0.02100	0.22000	0.0	0.0	0.0	0.0	0.0
26	22	0.00300	0.01880	0.01800	0.0	0.0	0.0	0.0	0.0
36	18	0.00007	0.00600	0.00000	0.0	0.0	0.0	0.0	0.0
37	19	0.00007	0.00400	0.00000	0.0	0.0	0.0	0.0	0.0
28	20	0.00200	0.01550	0.03200	0.0	0.0	0.0	0.0	0.0
38	9	0.00007	0.00600	0.00000	0.0	0.0	0.0	0.0	0.0
39	10	0.00007	0.00600	0.00000	0.0	0.0	0.0	0.0	0.0
20	40	0.00000	0.02000	0.00000	1.0	0.0	0.0	0.0	0.0
20	29	0.00000	0.00200	0.00000	1.0	0.0	0.0	0.0	0.0
20	30	0.00000	0.00500	0.00000	1.0	0.0	0.0	0.0	0.0
20	3	0.00000	0.00070	0.00000	1.0	0.0	0.0	0.0	0.0

Table D.4: Line specification for the 19-machine test system (cont)

21	2	0.00000	0.00100	0.00000	1.0	0.0	0.0	0.0	0.0
21	31	0.00000	0.00500	0.00000	1.0	0.0	0.0	0.0	0.0
22	32	0.00000	0.01000	0.00000	1.0	0.0	0.0	0.0	0.0
22	5	0.00000	0.00080	0.00000	1.0	0.0	0.0	0.0	0.0
23	38	0.00000	0.00500	0.00000	1.0	0.0	0.0	0.0	0.0
23	41	0.00000	0.02000	0.00000	1.0	0.0	0.0	0.0	0.0
24	39	0.00000	0.00400	0.00000	1.0	0.0	0.0	0.0	0.0
25	33	0.00000	0.00300	0.00000	1.0	0.0	0.0	0.0	0.0
25	34	0.00000	0.00300	0.00000	1.0	0.0	0.0	0.0	0.0
25	6	0.00000	0.00090	0.00000	1.0	0.0	0.0	0.0	0.0
25	42	0.00000	0.02000	0.00000	1.0	0.0	0.0	0.0	0.0
26	35	0.00000	0.00070	0.00000	1.0	0.0	0.0	0.0	0.0
26	1	0.00000	0.00200	0.00000	1.0	0.0	0.0	0.0	0.0
28	36	0.00000	0.00500	0.00000	1.0	0.0	0.0	0.0	0.0
28	37	0.00000	0.00800	0.00000	1.0	0.0	0.0	0.0	0.0
28	4	0.00000	0.00080	0.00000	1.0	0.0	0.0	0.0	0.0
23	7	0.00000	0.00070	0.00000	1.0	0.0	0.0	0.0	0.0
24	8	0.00000	0.00070	0.00000	1.0	0.0	0.0	0.0	0.0

Table D.5: Machine specification for the 19-machine test system

1	1	3000	0	0	0	0.25	0	0	1
2	2	12000	0	0	0	0.25	0	0	2
3	3	13000	0	0	0	0.37	0	0	3
4	4	9000	0	0	0	0.25	0	0	4
5	5	8000	0	0	0	0.25	0	0	5
6	6	13000	0	0	0	0.37	0	0	6
7	7	2000	0	0	0	0.25	0	0	7
8	8	6000	0	0	0	0.25	0	0	8
9	9	2392	0	0	0	0.25	0	0	9
10	10	1982	0	0	0	0.25	0	0	10
11	11	3118	0	0	0	0.25	0	0	11
12	12	640	0	0	0	0.25	0	0	12
13	13	880	0	0	0	0.25	0	0	13
14	14	1500	0	0	0	0.25	0	0	14
15	15	737	0.1	0.0	0.90	0.25	0.23	8.0	15
16	16	1137	0	0	0	0.25	0	0	16
17	17	2208	0	0	0	0.37	0	0	17
18	18	3004	0	0	0	0.25	0	0	18
19	19	2500	0	0	0	0.25	0	0	19

Bibliography

[1] R. Aresi, B. Delfino, G.B. Denegri, S. Massucco, and A. Morini, *A combined ann/simulation tool for electric power system dynamic security assessment*, IEEE Transactions on Power Systems (1999), 1303–1309.

[2] T. Athay, V.R. Sherkat, R. Podmore, S. Virmani, and C. Peuch, *System engineering for emergency operating state control.*

[3] D.S. Brereton, D.G. Lewis, and C.C. Young, *Representation of induction motor loads during power system stability studies*, AIEE Trans. **76** (1957), no. 3, 451–460.

[4] N.G. Bretas, *An iterative dynamic state estimation and bad data processing*, Int. J. Electr. Power Energy Syst. **11** (1989), no. 1, 70–74.

[5] J. Chang, G.N. Taranto, and J.H. Chow, *Dynamic state estimation in power system using a gain-scheduled nonlinear observer*, IEEE Conf. Control Application (1995), 221–226.

[6] J. Chow, *Power system toolbox dynamic tutorial and functions*, Cherry Tree Scientific Software, RR No.5 Colborne, Ontario K0K 1S0, Canada, 2 ed., 1991-2002.

[7] F.N. Chowdhury, J.P. Christensen, and J.L. Aravena, *Power system fault detection and state estimation using kalman filter with hypothesis testing*, IEEE Transactions on Power Delivery **6** (1991), 1025–1030.

[8] A.M. Leite da Silva, M.B. Do Coutto Filho, and J.F. De Querroz, *State forecasting in electric power systems*, Proc. IEE-C **130** (1983), no. 5, 237–244.

[9] K. Dèmaree, *An on-line dynamic security analysis system implementation*, A paper prepared for presentation at the IEEE Winter Meeting (1994).

[10] G.C. Ejebe, W.F. Tinney, V. Vittal, and G. Cauley, *A sparse formulation and implementation of the system transient energy function for dynamic security analysis*, Electrical Power and Energy Systems **18** (1996), no. 1, 3–9.

[11] M.A. El-Sharkawi, *Neural networks and their application to power engineering*, Control and Dynamic Systems **41** (1991).

[12] O. I. Elgerd, *Electric energy systems theory : An introduction*, McGraw-Hill, 1982.

[13] A.A. Fouad and V. Vittal, *Power system transient stability analysis using the transient energy function*, Prentice Hall, 1992.

[14] D. Hammerstrom, *Working with neural networks*, IEEE Spectrum (1993), 46–53.

[15] D.R. Hush and G. Horne, *Progress in supervised neural networks*, IEEE Signal Processing Magazine **10** (1993), no. 1, 8–37.

[16] A.B.R. Kumar, A. Ipakchi, V. Brandwajan, M.A. El-Sharkawi, and G. Cauly, *Neural networks for dynamic security assessment of large scale power systems:*

requirements overview, Proceedings 1st International forum on NNAPS (1991), 65–71.

[17] D.M. Vinod Kumar and S.C. Srivastava, *Power system state forecasting using artificial neural networks*, Electric machines and power systems **27** (1999), 653–664.

[18] D.M. Vinod Kumar, S.C. Srivastava, S. Shah, and S. Mathur, *Topology processing and static state estimation using artificial neural networks*, IEE-C Proc. **143** (1996), no. 1, 99–105.

[19] P. Kundur, *Power system stability and control*, EPRI Power System Engineering Series, McGraw-Hill, Inc., 1994.

[20] P. Kundur, J. Paserba, V. Ajjarapu, G. Andersson, A. Bose, C. Canizares, N. Hatziargyriou, D. Hill, A. Stankovic, C. Taylor, T. Van Cutsem, and V. Vittal, *Definition and classification of power system stability*, IEEE Transactions on power systems (2003), 1–15.

[21] S. Y. Kung, *Digital neural networks*, Prentice Hall Inc., Englewood Cliffs NJ, 1993.

[22] J. Lin, S. Huang, and K. Shih, *Application of sliding surface-enhanced fuzzy control for dynamic state estimation of a power system*, IEEE Transactions on power systems **18** (2003), no. 2, 570–577.

[23] A. Llamas, *Assessment of direct methods in power system transient stability analysis for on-line applications*, Ph.D. thesis, Virginia Polytechnic Institute and State University, December 1992.

[24] D. Mallieu, T.H. Vancutsem, P. Rousseaux, and M. Ribbens Pavella, *Dynamic multi level filtering for real-time estimation of electric power systems*, Control Theory and Advanced Technology **2** (1986), no. 2, 255–272.

[25] J.K. Mandal and A.K. Sinha, *Hierarchical state estimation incorporating measurment function nonlinearities*, Electrical Power and Energy Systems **19** (1997), no. 1, 57.

[26] Y. Mansour, A. Chang, J. Tamby, E. Vaahedi, B.R. Corns, and M. El-Sharkawi, *Large scale dynamic security screening and ranking using neural networks*, IEEE Transactions on power systems **12** (1997), no. 2, 954–960.

[27] Y. Mansour, E. Vaahedi, A.Y. Chang, B.R. Corns, B.W. Garrett, K. Demaree, T. Athay, and K. Cheung, *B.c. hydro's on-line transinet stability assessment model development, analysis and post-processing*, IEEE Transactions on Power Systems **10** (1995), no. 1, 241–253.

[28] G.A. Maria, C. Tang, and J. Kim, *Hybrid transient stability analysis*, IEEE Transactions on Power Systems **5** (1990), no. 2, 384–391.

[29] M. Pavella, L. Wehenkel, and Y. Zhang, *Sime: A hybrid approach to fast transient stability assessment and contingency selection*, Electric Power and Energy Systems **19** (1997), no. 3, 195–208.

[30] G.D. Prasad and S.S. Thakur, *A new approach to dynamic state estimation of power system*, Electric Power Systems Research **45** (1998), 173–180.

[31] W.W. Price, *Rapid analysis of transient stability*, Tech. Report 87/th0169-3-PWR, IEEE Task Force, September 1987.

[32] F.A. Rahimi, N.J. Balu, and M.G. Lauby, *Assessing on-line transient stability in energy management systems*, IEEE computer application in power **4** (1991), no. 3.

[33] P. Rousseaux, T.H. Van cutsem, and T.E. Dy Liacco, *Whiter dynamic state estimation*, Int. Journal of Electrical Power and Energy Systems **12** (1990), no. 2, 104–116.

[34] P. Rousseaux, D. Mallieu, T.H. Van Cutsem, and M. Ribbens-Pavella, *dynamic state prediction and hierarchical filtering for power system state estimation*, Automatica **24** (1988), no. 5, 595–618.

[35] D.E. Rumelhart, L. McClelland, and PDP research group, *Parallel distributed processing*, vol. 1, The MIT Press, Cambridge, Massachusetts, USA, 1987.

[36] P.K. Simpson, *Artificial neural systems*, Pergamon Press (1990).

[37] C.K. Tang, C.E. Graham, M. El-Kady, and R.T.H. Alden, *Transient stability index from conventional time domain simulation*, IEEE Transactions on power systems **9** (1994), no. 3, 1524–1530.

[38] G.S. Vassel, *Northeast blackout of 1965*, IEEE Power Engineering Review (1991), 4–8.

[39] A.Jr. Vidalinc, *On-line transient analysis of a multi-machine power system using the energy approach*, Master's thesis, Virginia Polytechnic Institute and State University, July 1997.

[40] Y. Xue and M. Pavella, *Extended equal area: An analytical ultra-fast method for transient stability assessment and preventive control of power systems*, International journal of electrical power and energy systems **11** (1989), no. 2, 131–149.

[41] P. Yoh-Han, *Adaptive pattern recognition and neural networks*, Addison Wesley Publishing Company Inc., 1989.

[42] Q. Zhou, J. Davidson, and A.A. Fouad, *Application of artificial neural netwroks in power system security and vulnerability assessment*, IEEE Transactions on power systems **9** (1994), no. 1, 525–532.